FUNDAMENTAL STUDIES OF SEMICONDUCTOR HETEROEPITAXY

Ralph P. Ruth, et al

North American Rockwell Corporation

Prepared for:

Advanced Research Projects Agency

January 1973

AD

FUNDAMENTAL STUDIES OF SEMICONDUCTOR HETEROEPITAXY

FIFTH SEMIANNUAL REPORT

R. P. Ruth, A. J. Hughes, J. L. Kenty, H. M. Manasevit, D. Medellin
and A. C. Thorsen

ARPA Support Office
Research, Development, Engineering and Missile Systems Laboratory
United States Army Missile Command AMSMI RND
Redstone Arsenal
Huntsville, Alabama
Contract No. DAAH01-70-C-1311

Sponsored by:
Advanced Research Projects Agency
ARPA Order No. 1585

Security Classification

DOCUMENT CONTROL DATA - R & D

(Security classification of title, body of abstract and indexing annotation must be entered when the overall report is classified)

1. ORIGINATING ACTIVITY (Corporate author)	2a. REPORT SECURITY CLASSIFICATION
North American Rockwell Corp, Electronics Group Research and Technology Division Anaheim, California	Unclassified 2b. GROUP

3. REPORT TITLE

Fundamental Studies of Semiconductor Heteroepitaxy

4. DESCRIPTIVE NOTES (Type of report and inclusive dates)

Semiannual Report, July 1972 through December 1972

5. AUTHOR(S) (First name, middle initial, last name)

Ralph P. Ruth, A. James Hughes, Joseph L. Kenty, Harold M. Manasevit, Arthur C. Thorsen, C. R. Viswanathan, Morey A. Ring

6. REPORT DATE	7a. TOTAL NO. OF PAGES	7b. NO. OF REFS
January 1973	~~105~~ 121	9 + 20 (appendices)

8a. CONTRACT OR GRANT NO.	9a. ORIGINATOR'S REPORT NUMBER(S)
DAAH01-70-C-1311 b. PROJECT NO.	C71-86.5/501
c.	9b. OTHER REPORT NO(S) (Any other numbers that may be assigned this report)
d.	

10. DISTRIBUTION STATEMENT

Distribution of this document is unlimited.

11. SUPPLEMENTARY NOTES	12. SPONSORING MILITARY ACTIVITY
Details of illustrations in this document may be better studied on microfiche	Advanced Research Projects Agency, ARPA Order No. 1585 Washington, D.C.

13. ABSTRACT

The objective of this program is to carry out a fundamental study of nucleation and film growth mechanisms in heteroepitaxial semiconductor thin films and to apply the results to the preparation of improved films and thin-film devices on insulating substrates. Both theoretical and experimental investigations are involved, with emphasis on chemical vapor deposition (CVD) techniques applied to the Si/Al_2O_3, Si/$MgAl_2O_4$, and GaAs/Al_2O_3 systems. The accomplishments of the fifth six-month period are described in terms of seven program subtasks.

The theoretical studies have concentrated on modeling the observed mobility anisotropy in the Si/Al_2O_3 and Si/$MgAl_2O_4$ systems. The investigations of (221)SiAl_2O_3 and (001)Si/Al_2O_3 were completed, extensive anisotropy calculations were made for the general (XX1)Si crystallographic orientation (which includes the major orientations of practical interest), and an emphasis was placed on understanding the (111)Si/Al_2O_3 system; calculated anisotropies based on thermally-induced stresses and resulting piezoresistance effects are too small to explain the experimental results. Experimentally observed anisotropies in this system as high as 30-40% have been observed, with an average of about 16%, while the stress model predicts values of about 6%. Residual growth stresses may be responsible for the disparity. Preliminary measurements of the variation of anisotropy in (221)Si/Al_2O_3 films as a function of thickness indicate a trend for anisotropy effects to increase for thinner films.

Studies of the basic chemistry of formation of Si and GaAs by CVD reactions have shown that Al_2O_3 surfaces do catalyze the decomposition (pyrolysis) of SiH_4 at moderate temperatures (500C), although the catalyzing action rapidly disappears upon formation of a monolayer of Si on the surface. The decomposition modes of trimethylgallium and AsH_3 have been examined, as has the thermal stability of $(CH_3GaAsH)_x$, the first apparent product of the reaction of these compounds.

Considerable effort has been devoted to attempts to prepare suitably thinned Al_2O_3 wafers for subsequent reduction to 500Å thickness by the ion-beam sputtering technique; some wafers 1-2 mils thick were produced by various polishing and/or etching procedures, and these were further thinned by the ion beam method and used in in situ CVD experiments in the electron microscope. The CVD microchamber, mounting flange, and associated gas handling system were completed and installed on the electron microscope, and focus tests and gas flow experiments were completed. Several in situ CVD experiments resulting in the growth of crystalline Si films on amorphous carbon substretes were carried out, demonstrating the feasibility of observing Si film deposition and growth (by pyrolysis of SiH_4) in the electron microscope. Additional Si CVD in situ experiments are in progress.

Measurements of electrical properties in the Si/$MgAl_2O_4$ system indicate that the carrier mobility decreases more rapidly with film thickness (for t<0.5μm) than it does in the Si/Al_2O_3 system. Studies of inhomogeneity in donor concentration in CVD films on Al_2O_3 over the film area indicate a radial concentration gradient is probably produced on the sample pedestal during deposition, either by gas flow patterns or by non-uniform temperatures in the rf-heated susceptor. Measurements of high-field transport characteristics of Si and GaAs films on Al_2O_3 have been continued, as have the investigations of photoinjected current transport through Al_2O_3 substrates.

Additional minority carrier lifetime measurements in Si heteroepitaxial films in a range of thicknesses and resistivities have indicated values ranging from 9×10^{-12} to 5×10^{-10} sec; attempts to correlate lifetimes with film resistivity and thickness have not yet been successful. Schottky-barrier diodes and FET structures have been fabricated in Si/Al_2O_3 composites, although resulting device characteristics are not yet satisfactory. Preliminary fabrication and evaluation of photovoltaic cells in Si/Al_2O_3 has also been initiated.

Other phases of the investigations are described and a summary of the work planned for the next six months is included.

DD FORM 1 NOV 68 1473

1A

Security Classification

14

KEY WORDS	LINK A		LINK B		LINK C	
	ROLE	WT	ROLE	WT	ROLE	WT
Epitaxy						
GaAs						
Si						
$A\ell_2O_3$ (sapphire)						
$MgA\ell_2O_4$ (spinel)						
Chemical vapor deposition (CVD)						
In situ film growth						
Electron microscopy						
Epitazy theory						
Heteroepitaxy						
Thin-film devices						
Semiconductors						
Film nucleation						
Transport properties						
Metalorganic compounds						
Physical vapor deposition (PVD)						
Substrate						
Polishing						
Gas-phase etching						
Anisotropy						
Thermally induced stress						
Piezoresistance						

iB

AD

FUNDAMENTAL STUDIES OF SEMICONDUCTOR HETEROEPITAXY

FIFTH SEMIANNUAL REPORT

R. P. Ruth, A. J. Hughes, J. L. Kenty, H. M. Manasevit, D. Medellin
and A. C. Thorsen

Research and Technology Division

Electronics Group

North American Rockwell Corporation

January 1973

ARPA Support Office

Research, Development, Engineering and Missile Systems Laboratory

United States Army Missile Command AMSMI RND

Redstone Arsenal

Huntsville, Alabama

Contract No. DAAH01-70-C-1311

Sponsored by:

Advanced Research Projects Agency

ARPA Order No. 1585

ABSTRACT

The objective of this program is to carry out a fundamental study of nucleation and film growth mechanisms in heteroepitaxial semiconductor thin films, and to apply the results to the preparation of improved films and thin-film devices on insulating substrates. Both theoretical and experimental investigations are involved, with emphasis on chemical vapor deposition (CVD) techniques applied to the Si/$A\ell_2O_3$, Si/$MgA\ell_2O_4$, and GaAs/$A\ell_2O_3$ systems. The accomplishments of the fifth six-month period are described in terms of seven program subtasks.

The theoretical studies have concentrated on modeling the observed mobility anisotropy in the Si/$A\ell_2O_3$ and Si/$MgA\ell_2O_4$ systems. The investigations of (221)Si/$A\ell_2O_3$ and (001)Si/$A\ell_2O_3$ were completed, extensive anisotropy calculations were made for the general (XX1)Si crystallographic orientation (which includes the major orientations of practical interest), and an emphasis was placed on understanding the (111)Si/$A\ell_2O_3$ system; calculated anisotropies based on thermally-induced stresses and resulting piezoresistance effects are too small to explain the experimental results. Experimentally observed anisotropies in this system as high as 30 to 40 percent have been observed, with an average of about 16 percent, while the stress model predicts values of about 6 percent. Residual growth stresses may be responsible for the disparity. Preliminary measurements of the variation of anisotropy in (221)Si/$A\ell_2O_3$ films as a function of thickness indicate a trend for anisotropy effects to increase for thinner films.

Studies of the basic chemistry of formation of Si and GaAs by CVD reactions have shown that $A\ell_2O_3$ surfaces do catalyze the decomposition (pyrolysis) of SiH_4 at moderate temperatures (~500 C), although the catalyzing action rapidly disappears upon formation of a monolayer of Si on the surface. The decomposition modes of trimethylgallium and AsH_3 have been examined, as has the thermal stability of $(CH_3GaAsH)_x$ - the first apparent product of the reaction of these compounds.

Considerable effort has been devoted to attempts to prepare suitably thinned $A\ell_2O_3$ wafers for subsequent reduction to 500 Å thickness by the ion-beam sputtering technique; some wafers 1 to 2 mils thick were produced by various polishing and/or etching procedures, and these were further thinned by the ion beam method and used in in situ CVD experiments in the electron microscope. The CVD microchamber, mounting flange, and associated gas handling system were completed and installed on the electron microscope, and focus tests and gas flow experiments were completed. Several in situ CVD experiments resulting in the growth of crystalline Si films on amorphous carbon substrates were carried out, demonstrating the feasibility of observing Si film deposition and growth (by pyrolysis of SiH_4) in the electron microscope. Additional Si CVD in situ experiments are in progress.

Measurements of electrical properties in the Si/$MgA\ell_2O_4$ system indicate that the carrier mobility decreases more rapidly with film thickness (for $t \leq 0.5\,\mu m$) than it does in the Si/$A\ell_2O_3$ system. Studies of inhomogeneity in donor concentration in CVD Si films on $A\ell_2O_3$ over the film area indicate a radial concentration gradient is probably produced on the sample pedestal during deposition, either by gas flow patterns or by nonuniform temperatures in the rf-heated susceptor. Measurements of high-field transport characteristics of Si and GaAs films on $A\ell_2O_3$ have been continued, as have the investigations of photoinjected current transport through $A\ell_2O_3$ substrates.

Additional minority carrier lifetime measurements in Si heteroepitaxial films in a range of thicknesses and resistivities have indicated values ranging from 9×10^{-12} to 5×10^{-10} sec; attempts to correlate lifetimes with film resistivity and thickness have not yet been successful. Schottky-barrier diodes and FET structures have been fabricated in $Si/A\ell_2O_3$ composities, although resulting device characteristics are not yet satisfactory. Preliminary fabrication and evaluation of photovoltaic cells in $Si/A\ell_2O_3$ has also been initiated.

Other phases of the investigations are described and a summary of the work planned for the next six months is included.

CONTENTS

	Page
Abstract	iii
Section I - Introduction	1
1. Program Objectives	1
2. Program Scope	2
3. Program Description by Subtask	3
Section II - Results and Discussion	5
1. Subtask 1. Theory of Epitaxy and Heteroepitaxial Interfaces	5
2. Subtask 2. Deposition Studies and Film Preparation	11
a. CVD Growth of Si on $MgAl_2O_4$	12
b. CVD Growth of Si on Al_2O_3	16
3. Subtask 3. Analysis and Purification of CVD Reactants	17
a. Analysis of CVD Reactants for Impurity Content	17
b. Study of Chemistry and Reaction Kinetics of CVD Processes	19
4. Subtask 4. Preparation and Characterization of Substrates	24
a. Polishing of Al_2O_3 Substrates	25
b. Mechanical and Chemical Thinning of Al_2O_3 Substrates	25
c. Ion Thinning of Substrates	27
d. Determination of Depth of Surface Damage in Al_2O_3	28
5. Subtask 5. Studies of in situ Film Growth in the Electron Microscope	29
a. Microchamber Testing and Gas Flow Measurements	30
b. Microchamber Operational Details	37
c. In situ CVD Experiments in the Electron Microscope	37
6. Subtask 6. Evaluation of Film Properties	43
a. Anisotropy Studies in the Si/Al_2O_3 System	45
b. $Si/MgAl_2O_4$ Studies	49
c. Studies of Homogeneity of Properties of Si/Al_2O_3 Films	49
d. Miscellaneous Film Evaluation Studies	51
7. Subtask 7. Design and Fabrication of Devices	55
a. Minority Carrier Lifetime Measurements	56
b. Miscellaneous Device Studies	58
Section III - Work Planned for Next Six Months	60
1. Subtask 1. Theory of Epitaxy and Heteroepitaxial Interfaces	60
2. Subtask 2. Deposition Studies and Film Preparation	60
3. Subtask 3. Analysis and Purification of CVD Reactants	61
4. Subtask 4. Preparation and Characterization of Substrates	62
5. Subtask 5. Studies of in situ Film Growth in the Electron Microscope	62
6. Subtask 6. Evaluation of Film Properties	63
7. Subtask 7. Design and Fabrication of Devices	63

CONTS (Cont)

Page

Section IV - Program Summary to Date 65

1. Subtask 1. Theory of Epitaxy and Heteroepitaxial Interfaces 66
2. Subtask 2. Deposition Studies and Film Preparation 67
3. Subtask 3. Analysis and Purification of CVD Reactants 69
4. Subtask 4. Preparation and Characterization of Substrates 70
5. Subtask 5. Studies of in situ Film Growth in the Electron Microscope 71
6. Subtask 6. Evaluation of Film Properties 72
7. Subtask 7. Design and Fabrication of Devices 74

References 75

Appendix A. Anisotropy in the Electrical Properties of $(001)Si/(01\bar{1}2)A\ell_2O_3$ 77

Appendix B. Preliminary EM6 Modifications for in situ Chemical Vapor Deposition 101

ILLUSTRATIONS

Figure		Page
1.	CVD Microchamber, Disassembled	31
2.	CVD Flange for Electron Microscope, with Assembled Microchamber Mounted in Place	31
3.	Electron Microscope and Gas Handling Manifold	32
4.	Schematic Diagram of Gas Handling Manifold	33
5.	Measured Pressure in Electron Microscope as Function of Microchamber Pressure	34
6.	Measured Gas Flow through Microchamber as Function of Pressure	35
7.	Electron Micrographs Showing Image Quality in CVD Microchamber at (a) 1×10^{-4} torr (Normal Microscope Vacuum) and (b) 3.5 torr (50% SiH_4 and 50% H_2)	36
8.	Elcctron Micrographs of Si Film Formed in Fourth CVD in situ Experiment (a) Bright Field and (b) Dark Field of Same Area	39
9.	Si Growth on Edges of Heating Mesh at (a) Arbitrary Time 0 sec, (b) 10 sec, (c) 20 sec	40
10.	Si Whiskers Growing on Amorphous Carbon Substrate near Heating Mesh	41
11.	Growth Sequence on Amorphous Carbon Substrate (a) 30 min, (b) 32 min, (c) 33 min after SiH_4 Was Introduced into Microchamber	42
12.	Anisotropy and Transverse-effect Coefficient for Various Film Thicknesses for (221)Si/(11$\bar{2}$2)$A\ell_2O_3$ Samples	48
13.	Hall Mobility as Function of Film Thickness for N-type (111)Si/(111)$MgA\ell_2O_4$. (Sample initially 5.4 μm thick)	50
14.	Hall Mobility as Function of Film Thickness for N-type (111)Si/(111)$MgA\ell_2O_4$. (Sample initially 1.4 μm thick.)	50
15.	Normalized Carrier Concentration as Function of Distance from Center of Susceptor (Sample Pedestal) for Pairs of Si/$A\ell_2O_3$ Samples Grown Simultaneously	52
16.	High-field i-E Characteristic of N-type (111)GaAs/(0001)$A\ell_2O_3$	54
17.	High-field i-E Characteristic of N-type (100)Si/(01$\bar{1}$2)$A\ell_2O_3$	54
18.	High-Field i-E Characteristic of Sample of Figure 17 at Various Temperatures	55
19.	Drain-to-Source I-V Characteristics of Schottky-Barrier FET in Si/$A\ell_2O_3$ Composite	59

TABLES

Table		Page
1.	Calculated Values of Anisotropy A for (XX1) Si for Various Modes of Epitaxy on Al_2O_3 and $MgAl_2O_4$ Substrates	10
2.	Comparative Electrical Properties of Si Films Grown on Polished (111) $MgAl_2O_4$ Using SiH_4 Tank C-1016 and Given $He-H_2$ Gas Atmosphere	14
3.	Effect of H_2 Etching of Substrate at 1100 C on Properties of Si Films Grown on $MgAl_2O_4$ in $He-H_2$ Atmosphere	15
4.	Mass Spectrometer Analyses of SiH_4 from Three Different Vendors	18
5.	Mass Spectrometric Analysis of AsH_3 in Carrier Gas from Three Different Vendors	20
6.	SiH_4 Pyrolysis Experiments	22
7.	Pyrolysis of Equimolar $Ga(CH_3)_3$-AsH_3 Mixtures	23
8.	Anisotropy Parameters for ~(111)Si/~$(11\bar{2}0)Al_2O_3$	46
9.	Anisotropy Parameters for (111) Si/$(10\bar{1}4)$ Al_2O_3	47

SECTION I

INTRODUCTION

This is the fifth Semiannual Technical Report for this contract. It describes work carried out during the period 1 July - 31 December 1972. Earlier semiannual reports (Refs 1-4) described work done in the first 24 months of the program.

1. PROGRAM OBJECTIVES

The overall objective of the program, as originally proposed, is to carry out a fundamental study of the nucleation and film growth mechanisms in heteroepitaxial semiconductor thin films, leading to new knowledge and understanding of these processes, and then to apply these results to the preparation of improved semiconductor thin films and thin-film devices on insulating substrates.

The specific technical objectives of the three-year program are the following:

1. Investigation of the many aspects of the mechanisms of heteroepitaxial film growth, to establish (through accumulation of basic knowledge) sets of technical guidelines for the preparation of better films which can then be applied to real situations.

2. Preparation of improved, high-quality, device-grade heteroepitaxial films of Si and GaAs on insulating substrates by chemical vapor deposition (CVD) methods.

3. Development of methods of characterizing heteroepitaxial films as to their suitability for subsequent device fabrication.

4. Design and fabrication of selected thin-film devices which take advantage of the unique properties of such films.

The general plan for accomplishing these objectives involves as the primary effort the study of the fundamentals of heteroepitaxial semiconductor film growth on insulating substrates. Specialized device fabrication is used both as a means of evaluating certain properties of the films (and thus as a measure of film quality as the program progresses) and as a means of exploiting certain unique properties of heteroepitaxial semiconductor-insulator systems. The determination of which fundamental mechanisms, properties, and processes to investigate is based on a thorough knowledge of epitaxy and its problems and on experience with thin-film device difficulties encountered over a period of several years.

The problems studied are not restricted to those identified a priori; experimental (and theoretical) attention can be shifted as the program progresses in order to achieve the goal of a better understanding of heteroepitaxial processes and the resultant improvement in thin-film active semiconductor devices.

2. PROGRAM SCOPE

The program involves both theoretical and experimental investigation of the nueleation and growth mechanisms of heteroepitaxial films in semieonductor-insulator systems, the development of improved teehniques for preparation of heteroepitaxial semiconduetor films, and the fabrieation of some devices utilizing these films, the latter primarily for the purpose of evaluating thc heteroepitaxial materials but also to exploit the special properties of such films.

The theoretieal studies consist of two types. First, there is direct interaction with the experimental program involving data analyses, suggestion of definitive experiments, and postulation of specific models to explain experimental observations. Second, there is development of original eontributions to the theory of heteroepitaxial growth.

The experimental investigations are also of two types. First, fundamental explorations are earried out to delineate meehanisms and general empirical principles of the heteroepitaxial growth proeess. Second, praetical studies aceompany the fundamental investigations so that new developments ean be immediately applied to the improvement of semieonduetor films and thin-film devices on insulating substrates.

The work has emphasized the CVD method of growing scmiconduetor thin films because of its importanee in the semiconductor industry. This emphasis on the fundamental mechanisms of CVD growth distinguishes this program from most previous fundamental studies of epitaxy, which have coneentrated upon physieal vapor deposition (PVD) methods partly beeause such studies are easier with PVD techniques.

The program emphasis is on films of Si and GaAs and substrates of sapphire ($A\ell_2O_3$) and spinel ($MgA\ell_2O_4$). The initial emphasis was on the Si-on-$A\ell_2O_3$ system, with increasing attention being given to the Si-on-$MgA\ell_2O_4$ and GaAs-on-$A\ell_2O_3$ systems. Si and GaAs have been ehosen beeause of the preeminenee of the former in the semieonductor industry and the high-frequency and high-temperature attributes of the latter; in addition, they represent the elemental and eompound semiconduetors for whieh most comparative information exists.

The program is earried on primarily at facilities of the Electronics Group of North Ameriean Roekwell Corporation (NR) by NR personnel. Parts of two of the subtasks are performed by personnel of the University of California at Los Angeles (UCLA), in the Department of Elcctrical Sciences and Engineering. Work on another of the subtasks is being done in part in the Department of Chemistry of California State University, San Diego (CSUSD). Both the UCLA and the CSUSD programs are supported by subeontracts from NR.

3. PROGRAM DESCRIPTION BY SUBTASK

The three-year program was originally divided into nine subtasks - two theoretical and seven experimental (Refs 1, 2). However, at the start of the second year it was decided, on the basis of the way in which the work of the first twelve months had developed, that the contract work would be more accurately described in terms of seven main subtasks - one theoretical and six experimental.

The seven subtasks, which will be modified as needed as the program progresses, are as follows:

Subtask 1: Theory of Epitaxy and Heteroepitaxial Interfaces. Theoretical examination of CVD kinetics and the processes of nucleation, surface migration, and film growth with emphasis on crystallographic relationships between overgrowth and substrate to attempt to identify mechanisms and establish general principles of heteroepitaxial growth; theoretical modeling of the heteroepitaxial interface using appropriate potentials to determine surface configurations and interfacial binding energies in real and/or simplified systems.

Subtask 2: Deposition Studies and Film Preparation. Investigation of the effects of various experimental parameters upon the properties of deposited semiconductor films; preparation of films for use in other parts of the program.

Subtask 3: Analysis and Purification of CVD Reactants. Analysis of the impurity content of reactant materials used in metalorganic-hydride and other CVD processes; preparation of research-sample quantities of improved-purity reactants for use in film growth experiments; investigation of the chemistry and reaction kinetics of CVD processes to improve the detailed understanding and control of the chemical reactions involved in the preparation of heteroepitaxial semiconductor films by CVD.

Subtask 4: Preparation and Characterization of Substrates. Preparation of substrate wafers and characterization of surfaces and impurity content of substrates used for semiconductor heteroepitaxy; development of reproducible new and/or improved substrate polishing, cleaning, and handling methods.

Subtask 5: Studies of *in situ* Film Growth in the Electron Microscope. *In situ* observation and study of the early stages of growth of CVD films in the electron microscope, to develop additional fundamental knowledge of the epitaxy process; results of experimental observations to be incorporated into theroetical studies wherever possible.

Subtask 6: Evaluation of Film Properties. Measurement of the electrical, optical, crystallographic, and thermal properties of heteroepitaxial semiconductor films on insulators, by a variety of measurement techniques. Standard techniques will be employed and new methods developed where required for measurement of film properties which best characterize ultimate device performance.

Subtask 7: Design and Fabrication of Devices. Design and experimental fabrication of certain types of devices, using heteroepitaxial films produced in the above studies. Some devices will be used to evaluate material properties and others to exploit semiconductor film characteristics unique to heteroepitaxial systems.

The results obtained during the fifth six-month period of the contract are discussed by subtask in Section II. An outline of the work planned for the final six months is contained in Section III, and a program summary to date is given in Section IV.

SECTION II

RESULTS AND DISCUSSION

The work of the fifth six-month period of the contract is described in detail in this section. There is extensive overlap among several of the subtasks, so the discussion in several instances involves some activities and results which are primarily part of another subtask.

1. SUBTASK 1. THEORY OF EPITAXY AND HETEROEPITAXIAL INTERFACES

Several possible approaches to the theoretical modeling of heteroepitaxial systems have been investigated under this contract. The general criteria originally adopted for determining suitability of a given technique were that the theoretical treatment and associated calculations should (1) relate explicitly to heteroepitaxy; (2) be as nearly as possible a "first-principles" approach; (3) relate as closely as possible to an actual system such as $Si/A\ell_2O_3$; and (4) represent an original contribution to the theory of heteroepitaxy.

Meeting these criteria is difficult. However, the criteria are important in providing a framework and goals for the theoretical studies. Although the $Si/A\ell_2O_3$ system is of considerable commercial and practical importance, existing theories and calculations in the literature fall drastically short in that there is no real connection with systems such as $Si/A\ell_2O_3$. The emphasis of previous theories has instead been on simple and unrealistic one- or two-dimensional cubic lattices which unfortunately cannot be applied to $Si/A\ell_2O_3$. The intent of the initial theoretical studies of this contract has been to develop an approach which relates specifically to the Si and the $A\ell_2O_3$ lattices.

During the first year of the contract a formal theoretical method of replacing overgrowth atoms on a substrate with Gaussian mass distributions was further developed for those cases where the effective interatomic potential is known. The technique, applicable to irregular-shaped islands or films of finite extent, was applied to a simplified model to determine preferred orientation relationships from calculated film-substrate interaction energies. The method was not pursued further, however, because it was not sufficiently adaptable to real systems. Several other possible approaches to the theoretical modeling of heteroepitaxial systems were critically reviewed, including the Frank-Van der Merwe model, a Green's function/Wannier-function approach, a contrived potential-energy model, and the two-body interatomic potential method. It was concluded at that time that most existing theories are inadequate for application to real systems.

The feasibility of a molecular orbital development of the heteroepitaxial interface was then investigated. However, it was determined infeasible to apply this technique in a manner directly relevant to heteroepitaxy, so the effort was terminated. The interatomic potential approach to heteroepitaxy was then reinstigated, with the goal being the computer simulation of growth of Si on $A\ell_2O_3$. Mechanical stability conditions for an $A\ell_2O_3$ lattice modeled with two-body potentials were investigated and determined to the depth required for the applications. Computer programming of the $A\ell_2O_3$ lattice energy and elastic constants was begun for use in determining appropriate empirical potentials required for modeling the $A\ell_2O_3$ lattice, a major

requirement for modeling Si growth on $A\ell_2O_3$. In addition, the application of the electron-on-network theory to the problem of determining surface configurations and interfacial binding energies in heteroepitaxial systems where the surface structure is allowed to relax was investigated and for a time appeared promising for the real systems of interest.

In the final half of the second year the theoretical studies were devoted to three main areas: (1) modeling of the $Si/A\ell_2O_3$ system by means of interatomic potentials and computer simulation; (2) use of the electron-on-network technique to calculate work functions and surface double-layer potentials of monovalent metals; and (3) calculations relating the mobility of Si films on $A\ell_2O_3$ to stress effects arising at the heteroepitaxial interface and caused by differential thermal contraction of film and substrate. The electron-on-network method has not been pursued further for possible application to heteroepitaxial systems, however, because of severe limitations of the method encountered in the preliminary studies.

The modeling of the $A\ell_2O_3$ lattice has been carried out in terms of Morse potentials; only anion-anion and cation-anion potentials have been employed. These were chosen to conform to specific constraints related to the physical lattice. Investigation of surface reconstruction in basal-plane $A\ell_2O_3$ was also initiated, using these potentials, since this phenomenon plays a major role in predicting Si film orientations on $A\ell_2O_3$. Relaxation of the four atomic planes nearest the surface was treated for the case of a surface composed of oxygen atoms with the constraints of translational symmetry in the surface and three-fold rotational symmetry normal to the surface. Programming of the case of an $A\ell$ atom surface was also begun, with the same symmetry constraints being imposed. However, the work on this aspect of the theoretical studies has not been further pursued in the past six months, as indicated below.

The theoretical studies during the past six months have concentrated exclusively on the mobility anisotropy and piezoresistance investigations in the $Si/A\ell_2O_3$ and $Si/MgA\ell_2O_4$ systems (Ref 4). The theoretical modeling of heteroepitaxial systems using interatomic potentials was deemed to be of secondary importance to the anisotropy studies at the present time, and as a consequence no further work was done on the modeling studies in this report period. However, that effort will be resumed during the next six months, with a slightly different direction and emphasis designed to illuminate some practical questions which have arisen concerning the possibility of residual growth stresses occurring in some $Si/A\ell_2O_3$ orientations.

It has long been recognized that the differential thermal contraction between a Si film and its $A\ell_2O_3$ substrate will produce substantial stress in the Si film. Through the piezoresistance effect, this stress acts to modify the electrical properties of the semiconductor, including the carrier mobility.

An assumption which is usually implicit in most semiconductor thin-film material evaluations is that the electrical properties are isotropic and thus do not depend upon orientation in the plane of the film. However, during the previous reporting period (Ref 4) it was determined experimentally that most $Si/A\ell_2O_3$ films exhibit some degree of mobility anisotropy in the plane of the film. It was recognized that a detailed theoretical investigation of this anisotropy could possibly lead to a greatly improved fundamental understanding of the mechanisms determining carrier

mobility in $Si/A\ell_2O_3$ heteroepitaxial films and thus could be of practical significance to the technology. This has been the basis for emphasizing the mobility anisotropy studies in this reporting period.

The theoretical model for the anisotropy in carrier mobility involves calculating the changes in mobility and resistivity due to the stress originating in the differential thermal contraction of film and substrate. For completeness, the difference in thermal expansion coefficients parallel and perpendicular to the c-axis in $A\ell_2O_3$ has been taken into account. The resulting theoretical model is thus the first which is valid for the case of anisotropic thermal expansion.

At the end of the previous reporting period theoretical formulas had been developed which were valid and applicable for both Si and Ge films and for $A\ell_2O_3$ and $MgAl_2O_4$ substrates (Ref 4). The (001), (110), (111) and (221) Si film orientations were treated specifically, as were some "off-orientation" cases. In the past six months publications describing the results for (221) Si (Ref 5) and (001) Si (Ref 6) were prepared. Calculations were performed for the 5 deg-off-(111) Si films investigated experimentally.

Extensive computer evaluations of theoretical formulas for the general orientation (XX1) Si were also completed. By letting X vary from zero to infinity, all Si film orientations of the form (XX1) lying along the zone defined by (001) Si, (111) Si, (221) Si, and (110) Si were treated and predicted anisotropy results obtained. Since Si film quality is usually highest for (001) and (111) types of growth, this general treatment is expected to encompass all orientations of major interest now and in the near future. In this extensive treatment, four modes of epitaxy have been considered for $Si/A\ell_2O_3$ and one mode for $Si/MgA\ell_2O_4$. The general mathematical model for the various modes of epitaxy has been completed. A basic and comprehensive account of the work is now being written for publication; it will contain fundamental information on mobility anisotropy in epitaxial Si and will constitute the first such comprehensive treatment of this subject and thus be of considerable importance.

The theoretical analysis of mobility anisotropies and the responsible physical mechanisms began as an "on-line" response to the important experimental discovery, earlier in the contract program, that an anisotropy was present in the carrier mobility in (001) Si, (221) Si and (111) Si heteroepitaxial films grown on $A\ell_2O_3$ and would probably occur in all orientations of $Si/A\ell_2O_3$. It was recognized that different physical mechanisms which could produce some form of mobility anisotropy would, in general, be expected to lead to different magnitudes of anisotropy and to different orientations for the mobility maxima and minima in the plane of the film. Thus, detailed studies of the mobility anisotropy could, in principle, provide a more powerful means than has previously been available for determining the role of various phenomena in establishing the carrier mobility in the $Si/A\ell_2O_3$ films. The anisotropy studies are therefore of great importance to this contract program and to heteroepitaxial semiconductor film technology in general.

Physical phenomena which could, in principle, lead to a mobility anisotropy in these heteroepitaxial systems include (1) surface scattering, (2) hot electron phenomena, (3) surface quantization, (4) dislocation scattering, and (5) both surface and bulk piezoresistance effects. All of these phenomena are inadequately understood

at the present time, and - with the exception of the piezoresistance studies done on this program -- all previous work that has been carried out has related to thin bulk crystals rather than to epitaxial films.

The initial theoretical work on this problem consisted of a study of the effect on carrier mobility of substrate-induced thermal contraction stresses acting through the piezoresistance effect. A theoretical model was developed which correctly predicted the magnitude of the mobility anisotropy and the angular direction in the plane of the film for which mobility maxima and minima would occur for (001) Si and (221) Si epitaxial films on $A\ell_2O_3$. Analysis of the theoretical and experimental data has shown that the model and thermal stresses do indeed largely account for the anisotropy in the mobility and the angular location of mobility maxima and minima. Thus, the anisotropy in mobility can be substantially described in terms of thermal stresses without recourse to other physical phenomena such as residual growth stresses or dislocation scattering. However, the magnitude of the overall average mobility in these films is found to be significantly lower than bulk-crystal values. This indicates that some other phenomenon, such as defect or dislocation scattering, is quite important in determining the properties of these (001) and (221) Si films.

Attention was then directed to the (111) Si case on two different $A\ell_2O_3$ substrate orientations : 5 deg off of the $(11\bar{2}0)$ plane, and $(10\bar{1}4)$. In both cases the theoretically predicted anisotropy is too small by a factor of ~3 to 6, and the predicted directions of mobility maxima and minima are rotated 90 to 100 deg away from those determined experimentally.

Extensive attempts, both theoretically and experimentally, have been made in efforts to explain the experimental (111) Si results. The experimental results show substantial data scatter and attempts have been made both to determine the origin of the scatter and to reduce its magnitude. Inhomogeneity in film properties is one potential source of both scatter and ambiguity in the experimental data. The results of experimental studies of Si film inhomogeneity are discussed in Subtask 6 of this report. While Si film inhomogeneity must be taken into account in accurately measuring mobility anisotropies, the film inhomogeneity does not itself appear to explain the large anisotropy or location of mobility maxima and minima.

A second physical mechanism -- hot electron phenomena -- has been ruled out as a likely cause of the experimental results on (111) Si since the mobility anisotropy is found to be independent of the magnitude of the electric field. Surface scattering and surface quantization are two other physical phenomena which could play a role in determining the experimentally measured anisotropy. For bulk thin films (i.e., no substrate) both these effects should lead to isotropic carrier mobilities on the basis of general symmetry arguments (Ref 6)*. The stress applied by the substrate is anisotropic and would thus be expected to lead to some anisotropy. However, intuitively this anisotropy would be expected to be of the same order as the (001) Si results -- an anisotropy of 6 to 9 percent. These phenomena appear implausible as mechanisms for producing the rather large (16 to 30 percent average) (111) Si anisotropy that has been observed.

---

*This reference is included in this report as Appendix A

A definitive interpretation or analysis of the (111) Si results can not be made at this time. Experimental efforts are underway (Subtask 6) to more adequately assess the effects of film inhomogeneity and to establish the magnitude of the contribution of possible surface effects and surface-state conductivity.

However, for purposes of discussion, suppose that the (111) Si data are shown to be correct and further that the anisotropy is substantially a bulk effect, not a surface effect. With these assumptions, it is useful to explore other potential origins for the anisotropy within the framework of a piezoresistance model. Calculations thus far have employed stresses calculated from the thermal expansion mismatch of film and substrate; it has long been recognized that lattice-constant mismatch between dissimilar materials can, in principle, lead to residual growth stresses.

In considering the possibility that residual growth stresses are responsible for the experimental results for (111) Si, the growth stresses that would be required for piezoresistance effects sufficient to produce the observed results have been calculated. In the theoretical analysis, where T_1, T_2, and T_6 are contracted-notation stress components, it is found that -- in general -- $(T_1 - T_2)$ must be substantially larger than that derived from thermal stresses, and the stress T_6 is of the opposite sign to that derived from the thermal stress and partially or totally cancels the thermal T_6.

At present there is apparently no way of deciding whether or not such growth stresses do in fact exist in Si films in the (111) orientation and--if they are important here--why such stresses do not appear to be required in the theoretical explanation for the (001) Si and (221) Si anisotropy cases. However, the possibility of a residual growth stress explanation appears plausible; this explanation would, if found to be correct, represent a major step forward in understanding some of the basic physics of heteroepitaxial Si films. Attempts are to be made in the coming reporting period, by means of either atom matching or interatomic potential modeling, to determine if growth stresses of the qualitative nature required to explain the (111) Si mobility anisotropy results in terms of a stress model are likely to occur.

During this reporting period calculations for mobility anisotropy in the general (XX1) Si orientation were carried out. Here X varies from zero to infinity to map out all orientations of the form (XX1) lying along the zone defined by (001) Si, (111) Si, (221) Si and (110) Si. These calculations have been performed for four different modes of Si/$A\ell_2O_3$ epitaxy and one mode of Si/$MgA\ell_2O_4$ epitaxy, for both n-type and p-type Si. A substantial amount of data has been generated by computer calculations.

Representative data for the anisotropy factor $A = (\mu_{max} - \mu_{min})/1/2\ (\mu_{max} + \mu_{min})$ is given in Table 1 for n-type Si. The first column contains the values of the Miller index X in the crystallographic plane (XX1) of Si. The second column shows the angle θ (in deg) of the (XX1) plane measured from the (001) plane toward the (110) plane. The remaining columns list the values of the anisotropy factor A (in percent) for various modes of epitaxy, where the modes of epitaxy are as follows:

Mode I : (001) Si//$(01\bar{1}2)\ A\ell_2O_3$
Mode II : (111) Si//$(11\bar{2}4)\ A\ell_2O_3$ and (221) Si//$(11\bar{2}2)\ A\ell_2O_3$
Mode III: (111) Si//$(11\bar{2}0)\ A\ell_2O_3$
Mode IV: (111) Si//$(10\bar{1}4)\ A\ell_2O_3$
Mode V : (111) Si//(111) $MgA\ell_2O_4$

Table 1. Calculated Values of Anisotropy A for (XX1) Si for Various Modes* of Epitaxy on $A\ell_2O_3$ and $MgA\ell_2O_4$ Substrates

X	θ (deg)	Mode I*	Mode II*	Mode III*	Mode IV*	Mode V*
0.0	0.0	6.17	0.00	4.88	0.10	0.00
0.1247	10.0	7.47	2.43	6.57	2.45	2.52
0.2573	20.0	12.25	9.11	11.90	9.20	9.44
0.4082	30.0	19.69	17.05	19.65	17.20	17.93
0.5933	40.0	21.61	18.77	21.79	19.21	21.09
0.8427	50.0	10.69	6.25	10.98	7.50	10.35
1.0	54.73	6.22	4.18	6.42	2.46	0.0
1.2247	60.0	14.36	17.05	14.54	14.91	13.80
1.943	70.0	33.12	38.99	33.76	36.63	39.72
2.0	70.529	33.93	39.94	34.59	37.60	40.91
4.010	80.0	44.26	52.66	45.36	50.81	57.45
1000.	89.96	46.92	57.17	48.27	56.24	63.51

*See text for identification of modes

Table 1 allows comparison between various modes of epitaxy with respect to the anisotropy predicted by the theory and permits some distinction to be made between the various mechanisms likely to be responsible for the anisotropy. For example, Mode V is for the Si/$MgA\ell_2O_4$ system and thus represents the case of isotropic thermal expansion. The anisotropy A in this case is thus due solely to anisotropy in the piezoresistance coefficients and in the elastic constants. On the other hand, for the (001) Si and (111) Si cases (X = 0 and X = 1, respectively) the anisotropy in mobility arises only from the anisotropy in thermal expansion.

It is of interest to note the fairly rapid increase in anisotropy values in going only 5.27 deg from the (111) Si plane toward the (110) Si plane. Also it should be pointed out that the (110) Si plane (θ = 90 deg from the (001)Si plane) probably represents the greatest anisotropy possible in this system, although this has not been rigorously proven. This fact may, however, be somewhat academic in that high quality (110) Si film growth has not yet been achieved on substrates of $A\ell_2O_3$ or $MgA\ell_2O_4$.

The anisotropy factor A of the general (XX1) Si orientation has been given in Table 1 over a wide range of angles for the sake of completeness and to illustrate how the anisotropy depends upon crystalographic orientation and mode of epitaxy. However, it should be recognized that not all of these Si orientations will be of experimental and practical significance for all epitaxy modes. In general, in proceeding away from the "natural" plane for a given mode--say (001) Si//$(01\bar{1}2)$ $A\ell_2O_3$ (Mode I)--the quality of the film growth deteriorates and may become multimoded or highly defected. The exact relationship between film quality and the number of degrees off of the orientation of a pure mode is not known in detail, although some general information has been established by earlier workers (Ref 7). The (221) Si//$(11\bar{2}2)$ $A\ell_2O_3$ is an example of an orientation that is ≈16 deg off the "natural" (111) Si // $(11\bar{2}4)$ $A\ell_2O_3$ plane and yet yields good quality films (Ref 5).

2. SUBTASK 2. DEPOSITION STUDIES AND FILM PREPARATION

During the first year of the program the emphasis on this subtask was placed on determining the effect of experimental growth parameters on the quality of Si epitaxial films grown by the CVD method of pyrolysis of SiH_4 on substrates of various orientations of $A\ell_2O_3$ and $MgA\ell_2O_4$. It was established for the growth system used that autodoping occurs in Si on $A\ell_2O_3$ at temperatures greater than about 1050 C, so a concerted study was made which considered the effects of such factors as growth temperature, growth rate, and nucleation phenomena at or below this temperature (Ref 2). It was determined that the electrical properties of undoped n-type heteroepitaxial Si films grown on various orientations of $A\ell_2O_3$ (and also $MgA\ell_2O_4$) by the CVD method of pyrolysis of SiH_4 are dominated by surface-state conduction for carrier concentrations of $\sim 10^{16}$ cm^{-3} or below. Essentially equivalent (100)- and (111)-oriented Si films were grown on $(01\bar{1}2)$ and $(10\bar{1}4)$ $A\ell_2O_3$ substrates at deposition temperatures below the autodoping range (~1050 C). $A\ell_2O_3$ orientations near the $(11\bar{2}0)$ plane, not previously used in heteroepitaxy studies, were utilized as substrates for (111) Si heteroepitaxy; this resulted in electron mobilities of 600 to 700 $cm^2/V\text{-sec}$ for carrier concentrations of 10^{15} - 10^{17} cm^{-3}, exceeding mobilities obtained on either $(01\bar{1}2)$ or $(10\bar{1}4)$ $A\ell_2O_3$ substrates.

These studies revealed the strong interrelationships that exist among the various parameters involved in optimizing Si growth on insulators. Evaluation of the electrical properties of Si films on those $A\ell_2O_3$ orientations that produce the best Si overgrowths has demonstrated that growth conditions (1) must be maximized for the particular substrate orientation chosen; (2) differ for those $A\ell_2O_3$ orientations which lead to the same Si orientation; (3) are dependent upon reactor geometry and gaseous atmosphere; and (4) must be optimized for the particular film thickness desired. Studies of Si growth by SiH_4 pyrolysis at reduced pressures (1 to 10 torr) indicated that single-crystal growth can be obtained over a fairly wide temperature range, when conditions are optimized, on both $A\ell_2O_3$ and $MgA\ell_2O_4$ substrates; these results provided necessary confirmation of the feasibility of Si film growth in the pressure range to be used in the in situ CVD experiments in the electron microscope (Subtask 5). Investigation of the growth of Si films on $A\ell_2O_3$ and $MgA\ell_2O_4$ using He as the growth atmosphere and the carrier gas showed that epitaxial growth could be achieved, although the conditions for best growth were not established at that time.

The effort on this subtask in the final half of the second year was concentrated on continuing attempts to optimize the Si deposition process for growth on $\sim(11\bar{2}0)$ and $(01\bar{1}2)$ $A\ell_2O_3$ surfaces. In the course of this work the effects of post-nucleation annealing during the deposition process on ultimate film properties were examined, but no significant improvement in overall quality of Si films resulting from these procedures was demonstrated. The effects on film growth of gas-phase etching of $A\ell_2O_3$ surfaces prior to deposition have been evaluated further; there is some indication that surface damage may not be the primary factor in determining the quality of Si overgrowths, but this question must be examined in more detail. The effect of cooled reactor chamber walls on the Si growth process was investigated further, but no significant advantage of cooled walls in the vertical reactor systems used in this work has been observed.

Considerable additional study was made of the growth and properties of Si films on Czochralski-grown stoichiometric spinel ($MgA\ell_2O_4$). This work indicated that Si films with electrical properties at least as good as those grown on $A\ell_2O_3$ can be obtained when $He-H_2$ gas mixtures are used for the growth environment. It also determined that autodoping is operative in the $Si/MgA\ell_2O_4$ system (in $He-H_2$ atmospheres) at approximately the same temperatures as for $Si/A\ell_2O_3$.

During the past six months the work of this subtask was concentrated in several areas. These include (1) the preparation of Si films on various orientations of $A\ell_2O_3$ in order to study the electrical anisotropy as a function of $A\ell_2O_3$ orientation, film thickness, and doping level (Subtask 6); (2) the preparation of samples of $GaAs/A\ell_2O_3$ and $Si/A\ell_2O_3$ for use at UCLA in the measurement of carrier lifetime and high-field transport properties and in fabrication of Schottky-barrier FET structures (Subtasks 6 and 7); (3) the preparation of samples of $Si/A\ell_2O_3$ and $GaAs/A\ell_2O_3$ for the evaluation of new tanks and sources of SiH_4 (Subtask 3); and (4) the growth of Si and GaAs films on $MgA\ell_2O_4$ and $A\ell_2O_3$ in an attempt not only to identify the preferred substrate but also to examine the effect of various substrate processing steps on film quality.

a. CVD Growth of Si on $MgA\ell_2O_4$

As indicated in the previous semiannual report (Ref 4), good quality n-type Si films have been grown on (111) $MgA\ell_2O_4$ with carrier mobilities higher than

those achieved in the $Si/A\ell_2O_3$ system. Mobilities as high as 925 cm^2/V-sec were measured in ~2 μm films, but the mobilities were influenced by the source tank of SiH_4. In fact, more recent attempts to duplicate earlier growth rate and dopant data in Si films on $MgA\ell_2O_4$ as a function of the $He-H_2$ ratio have not been successful and have indicated that even these important factors appear to be dependent on the source tank of SiH_4 used. Yet the purity of the SiH_4 as determined by growth of Si on Si in a H_2 atmosphere has been quite acceptable, with thick films (~100μm) possessing essentially bulk Si mobilities (see Subtask 3). The results seem to indicate that impurities present in the SiH_4 behave quite differently in H_2 and in $He-H_2$ mixtures. Because of these now-recognized differences only those data obtained on films grown on insulators with the same source of SiH_4 can be used for comparison purposes.

Considerable subsurface work damage has been found in (111) $MgA\ell_2O_4$ processed into polished substrates by various vendors and at NR. This damage has been revealed by etching the polished surface in hot HF or hot HBF_4 for ~45 to 90 min. A high temperature (~1500 C) anneal in air seems to reconstruct the $MgA\ell_2O_4$ surface and to minimize or remove scratches, but the electrical properties of films grown on these surfaces do not appear to be any better than those measured in films grown on those containing obvious work damage. This conclusion is based on the data shown in Table 2.

A few experiments were performed to determine the effect of heating (111) $MgA\ell_2O_4$ in H_2 at 1100 C prior to film growth at 1025 C in $He-H_2$. The electrical properties of Si films grown on these surfaces and on surfaces not treated in H_2 are not considered significantly different. The data involved are recorded in Table 3.

Most of the studies of Si growth on $MgA\ell_2O_4$ on this program have been directed to the use of (111) $MgA\ell_2O_4$, since this orientation has produced higher mobility films than have been reported in the literature for either (100) or (110) $MgA\ell_2O_4$. However, it was hoped that the process now in use for Si deposition would provide better film growth on the (110) and (100) orientations. To date the number of experiments involving these orientations has been limited.

The Si films grown on (100) $MgA\ell_2O_4$ were only partially reflective at growth temperatures of 1025 C and were slightly inferior electrically to (111) Si films grown simultaneously on (111) $MgA\ell_2O_4$ substrates. For example, a 2 μm-thick (100) film had the following properties: resistivity = 0.53 ohm-cm; carrier concentration = 3.5×10^{16} cm^{-3}; carrier mobility = 470 cm^2/V-sec. The properties of the companion (111) Si film were ρ = 0.70 ohm-cm, $n = 1.4 \times 10^{16}$ cm^{-3}, μ = 630 cm^2/V-sec. At 1050 C, essentially similar results were obtained with the (111) film being better than the (100) film.

Film growth on (110) $MgA\ell_2O_4$ appeared to improve with deposition temperature, for where only gray films were formed at growth temperatures of 1025 and 1050 C under growth conditions satisfactory for (111) substrates, somewhat reflective films were obtained at 1075 C and 1100 C. The differences in quality may be thickness-dependent rather than growth temperature-dependent, for epitaxial film quality is normally expected to improve with thickness.

Table 2. Comparative Electrical Properties of Si Films Grown on Polished (111) $MgA\ell_2O_4$ Using SiH_4 Tank C-1016 and Given He-H_2 Gas Atmosphere+

Substrate Air Annealed	Film Thickness (μm)	Resistivity (ohm-cm)	Carrier Conc. (cm^{-3})	Mobility (cm^2/V-sec)
No	2.18	0.29	3.0×10^{16}	713
No	5.43	0.12	5.6×10^{16}	910
Yes	1.36	0.29	3.0×10^{16}	740
No	1.36	0.32	3.3×10^{16}	600
Yes	1.62	0.27	3.2×10^{16}	710
No	1.68	0.21	4.1×10^{16}	710
Yes	1.82	0.56	1.5×10^{16}	750
No	1.92	0.32	2.6×10^{16}	740
No	1.88	0.29	3.2×10^{16}	670
Yes	1.73	1.2	2.0×10^{16}	270
No	1.48	0.50	2.7×10^{16}	460
No	1.34	0.44	2.3×10^{16}	630
Yes	1.52	0.40	2.7×10^{16}	580
Yes	1.61	0.22	3.8×10^{16}	760
No	1.59	0.41	3.0×10^{16}	520
No	1.71	0.24	3.5×10^{16}	740
Yes	1.61	0.33	2.9×10^{16}	650
Yes	1.55	0.53	2.7×10^{16}	440*
Yes	1.48	0.49	2.5×10^{16}	520*
Yes	1.60	0.51	2.8×10^{16}	440

+Films grouped together were grown simultaneously
*Substrates heavily etched before film growth

Table 3. Effect of H_2 Etching of Substrate at 1100 C on Properties of Si Films Grown on $MgA\ell_2O_4$ in He-H_2 Atmosphere

Growth Rate (μm/min)	Film Thickness (μm)	Resistivity (ohm-cm)	Carrier Conc (cm^{-3})	Mobility (cm^2/V-sec)	H_2 Etched
0.33	2.3	0.17	5.7×10^{16}	660	No
0.27	1.9	0.88	1.5×10^{16}	480	No
0.23	1.6	0.33	3.4×10^{16}	560	Yes
0.21	1.5	0.46	3.2×10^{16}	420	Yes
0.22	1.6	0.72	2.9×10^{16}	300	Yes

Work with $MgA\ell_2O_4$ substrates on another program at NR has led to the interesting result that (100) Si epitaxial growth also occurs on (110) $MgA\ell_2O_4$ substrates, in addition to the (110) Si growth previously observed. The orientation relationships are

$$(100)\,Si//(110)\,MgA\ell_2O_4 \text{ and } [\bar{1}10]\,Si//[0\bar{1}\bar{1}]\,MgA\ell_2O_4.$$

Thus, (110) $MgA\ell_2O_4$ is found to influence the epitaxial growth of (100) Si just as it has been shown previously to produce (100) GaAs epitaxy. This phenomenon is of sufficient interest and importance to the understanding of the mechanisms of epitaxial growth that it should be investigated further, with correlations made with surface finish, substrate composition and accuracy of orientation, and other deposition parameters.

With respect to the $MgA\ell_2O_4$ substrate surface and its effect on film quality, the following conclusions can be reached based on the results of electrical measurements on Si/$MgA\ell_2O_4$ samples:

1. When the $MgA\ell_2O_4$ substrate is properly processed (i.e., polished and cleaned) Si films grown on good quality $MgA\ell_2O_4$ from two different vendors are essentially equivalent.

2. Substrates with high-density subsurface damage but which have not been etched to remove the work-damaged surface layer can still support the growth of Si films with acceptable electrical properties.

3. Even heavily-etched scratched surfaces can permit the growth of films with good electrical properties.

4. Thicker films (~5μm) exhibit higher carrier mobilities than thinner ones (≤2μm).

5. The electrical properties of 2μm-thick films of (111) Si on $MgA\ell_2O_4$ are at least as good as those of (111) Si on $A\ell_2O_3$ and quite often better than those of (100) Si on $A\ell_2O_3$.

6. Although annealing has been found to change the $MgA\ell_2O_4$ surface in some manner, the electrical properties of Si films grown on annealed surfaces do not appear to be better than those measured in films grown on unannealed surfaces.

b. CVD Growth of Si on $A\ell_2O_3$

The preparation of Si films on $A\ell_2O_3$ for the anisotropy measurements (Subtask 6) also provided films whose properties could be used in evaluating the quality of the SiH_4 used in the deposition process. (See Subtask 3.) It was observed, in the course of those studies, that substandard properties of Si films on ~$(11\bar{2}0)$-oriented $A\ell_2O_3$ substrates (i.e., lower-than-usual carrier mobilities for a given set of deposition conditions) coincided with the use of a SiH_4 source tank which had a high level of impurities as identified by mass spectrometric analysis.

For example, as reported in Table 4 (Subtask 3), SiH_4 tank C-1016 was found to contain an unusually high H_2 and H_2O content. Film mobilities for the (111) Si films grown on ~$(11\bar{2}0)A\ell_2O_3$ using this tank were ~500 cm^2/V-sec, lower than the 600 to 800 cm^2/V-sec values previously obtained using other tanks of SiH_4, but the quality of (100) Si growth on $(01\bar{1}2)A\ell_2O_3$ did not seem to be similarly affected. Thick (111)Si films (~10μm thick) on the ~$(11\bar{2}0)A\ell_2O_3$, however, were found to possess good mobilities, a value of ~950 cm^2/V-sec having been measured in a film with a carrier concentration of 4.5×10^{16} cm^{-3}. Further consideration is being given to the possible significance of correlations of this type, as part of the attempt to identify the important controlling parameters in the Si deposition process.

3. SUBTASK 3. ANALYSIS AND PURIFICATION OF CVD REACTANTS

During the first year, techniques of gas chromatography were developed for analysis of the reactants used for semiconductor heteroepitaxy by CVD. A general-purpose gas-handling system was constructed for the highly volatile and reactive gases studied, with silicone oil and polymer columns used for the chromatography. Several extraneous impurity peaks were observed in the chromatograms of SiH_4 samples; diborane (B_2H_6) was tentatively identified as a significant impurity (~10 ppm), although not confirmed by mass spectrometer techniques. Small quantities of purified SiH_4, free of diborane, were prepared by successive injections in the chromatograph; quantities were too small, however, for use in laboratory CVD experiments.

Beginning in the second year of the program samples of SiH_4 and of trimethylgallium (TMG) used for Si and GaAs CVD experiments were analyzed for impurity content by sensitive mass spectrometric techniques. Disilane and trimethylsilane, together with several other impurities of less concern, were found in the SiH_4 samples. The analyses of TMG left some uncertainties regarding the correct impurity levels, although these were largely resolved by later analyses carried out in the final half of the second year.

Significant impurity concentrations in some of the reactants (expecially SiH_4) have severely limited the accuracy of the study of the effects of deposition parameters on Si film properties on several occasions during the contract work. Cooperative efforts with vendors for preparation and analysis of improved-purity reactants have continued.

An important study of the chemistry and reaction kinetics of CVD processes used for growing Si and GaAs films in heteroepitaxial systems was initiated late in the second year at the California State University, San Diego (CSUSD). The first experiments undertaken were directed toward determining the role of the $A\ell_2O_3$ surface in catalyzing the pyrolysis of SiH_4; experiments with the trimethylgallium (TMG)-arsine (AsH_3) reaction used for GaAs growth were also begun.

During the past six months additional analyses of reactants have been made by mass spectrometer techniques, * and the studies of CVD reaction kinetics at CSUSD have continued on both the Si and the GaAs reaction systems.

a. Analysis of CVD Reactants for Impurity Content

Four different tanks of "pure" SiH_4 were analyzed by mass spectrometry for impurity content during this reporting period, in some cases after some Si films were grown using that particular tank, The analyses are recorded in Table 4.

Cylinder C-1016 (tank DC), from Synthatron Corporation, was returned to the vendor for replacement after the high concentrations of H_2, H_2O, and Ar were found. As noted in the table, its replacement (Cylinder 6-967) was found to be of considerably higher purity.

---

* The analyses have been carried out by West Coast Technical Service, Inc., San Gabriel, CA.

Table 4. Mass Spectrometer Analyses† of SiH_4 from Three Different Vendors

Constituent	SiH_4 (DE) Cyl. RR41849 (Vendor A) ppm	SiH_4 (DI) Cyl. G170 (Vendor B) ppm	SiH_4 (DC) Cyl. C-1016 (Vendor C) ppm	SiH_4 (DM) Cyl. 6-967 (Vendor C) ppm
Hydrogen	75	10	2.49(mole %)	305
Water	<1*	<1*	690	1
Argon	250	63	220	30
Hydrocarbons	<1	<1*	<1	<1
Disilane	6	92	24	10
Boron Compounds	<1*	<1*	<1*	<1*
Carbon Dioxide	2	<1	<1	NR**
Monochlorosilane	<1*	<1*	<1*	<1*
Oxygen	<1*	<1*	<1*	<1*
Helium	<1*	<1*	<1*	<1*
Siloxanes	<1*	<1*	<1*	<1*
Silane (SiH_4)	balance	balance	balance	balance

* Limits of detection

** NR = not reported

† Analyses performed by West Coast Technical Service, Inc., San Gabriel, CA.

Vendors:

A: Will Ross, Inc., Matheson Gas Products Div., Cucamonga, CA.
B: Union Carbide Corp., Linde Div., Los Angeles, CA.
C: Synthatron Corp., Edgewater, NJ.

Both tanks DI and DM (see Table 4) have been evaluated by means of Si growth on p-type Si substrates. A 100 μm-thick film of Si grown using tank DI had the following electrical properties: $\rho = 9.3$ ohm-cm; $n = 4.8 \times 10^{14} cm^{-3}$; and $\mu = 1390$ cm^2/V-sec. A film grown using tank DM had the following properties: $\rho = 57$ ohm-cm; $n = 6 \times 10^{13} cm^{-3}$; and $\mu = 1750$ cm^2/V-sec. In both cases, the electrical characteristics are indicative of very good film quality and thus of good SiH_4 having relatively little content of impurities damaging to the properties of the Si films.

As indicated in the previous semiannual report (Ref 4), a tank of AsH_3-in-He had been returned to the vendor (Airco) because of the high content of water, O_2, CO_2, and H_2S found in the tank by mass spectrometric analysis. Its replacement was received, after many months delay, and analyzed for impurities.

The results for this tank (DP) are shown in Table 5 together with results obtained for a tank (DN) of AsH_3-in-H_2 obtained from Three-H Corporation and for tank CR, 10 percent AsH_3-in-H_2, obtained from Phoenix Research Corporation. Based on attempts to condense H_2O from the gases in tank DN, it was concluded that the mixture was quite dry. GaAs films grown using tank DN were found to have a doping level ($3 \times 10^{14} cm^{-3}$) as low as that obtained with the best gases evaluated to date, but the mobility was also quite low; therefore, this tank is to be further evaluated by growth of films with doping levels $\sim 10^{16} cm^{-3}$, which lead to higher mobilities when grown on insulators such as Al_2O_3 or $MgAl_2O_4$. Because of the long delay in the receipt of replacement tank DP, tank DN was put into use before the analysis supplied by the vendor could be verified by a local analytical service laboratory. Such a comparison is to be made in the near future.

The AsH_3-in-H_2 from Phoenix Research Corporation was found to be relatively good for GaAs growth on Al_2O_3; a doped 20 μm-thick film on (0001) Al_2O_3 had the following electrical properties: $\rho = 0.07$ ohm-cm; $n = 1.7 \times 10^{16} cm^{-3}$ and $\mu = 5470$ cm^2/V-sec. At higher doping levels ($n = 5.5 \times 10^{17}$ cm^{-3}) a 31 μm-thick GaAs film had a mobility of ~ 3900 cm^2/V-sec, also a reasonable value for a film with that doping level.

b. Study of Chemistry and Reaction Kinetics of CVD Processes

In these studies the basic chemistry involved in the formation of GaAs from the metalorganic-hydride reaction of trimethylgallium ($Ga(CH_3)_3$) and AsH_3 and in the deposition of Si by the pyrolysis of SiH_4 is being investigated experimentally.

The flow pyrolysis of trimethylgallium (TMG) with AsH_3 is being examined over an inert surface (Si mirror) to determine the requirements for the formation of pure GaAs. The parameters being varied are the pyrolysis temperature, the TMG-AsH_3 ratio, and the partial pressure of H_2. In addition, the volatile products are being determined. The decomposition modes of AsH_3 and TMG are to be examined to determine what radicals are produced in the pyrolyses of AsH_3 and of TMG and in the co-pyrolysis. The reaction of these radicals with TMG and AsH_3 will also be investigated.

Table 5. Mass Spectrometric Analysis of AsH_3 in Carrier Gas from Three Different Vendors

Constituent	AsH_3-in-He (DP)[a] Cyl. RSG-80-1889	AsH_3-in-H_2 (DN)[b] Cyl. 2264 % Vol/Vol	AsH_3-in-H_2 (CR)[c] Cyl. 16-90038
Hydrogen	<5 ppm*	90+	Balance
Methane	<1 ppm*	NR	<1 ppm
Oxygen	<1 ppm*	ND 0.001	<1 ppm
Argon	<1 ppm*	ND 0.001	NR
Hydrocarbons	<1 ppm*	NR	NR
Carbon Dioxide	<1 ppm*	ND 0.001	<1 ppm
Water	1 ppm	NR	NR
Nitrogen	2 ppm	ND 0.001	<1 ppm
Arsine	11.72(mole %)	10.1	10.1%
Helium	balance	NR	NR

* Limits of detection

NR = not reported

ND = none detected, less than 10 ppm

a Analyzed by West Coast Technical Service, Inc. San Gabriel, CA: supplier - Air Reduction Co., Inc., Airco Industrial Gases Div., Vernon, CA.

b Analyzed by Gollob Analytical Service, Berkeley Heights, NJ: supplier — Three-H Corporation, Wanamassa, NJ

c Analysis submitted by Phoenix Research Corporation, Edison, NJ: supplier - same.

The pyrolysis of SiH_4 and Si_2H_6 over $A\ell_2O_3$ has been investigated in the initial studies. The $A\ell_2O_3$ is preheated to various temperatures (400 to 1100 C) prior to each pyrolysis to determine effects due to heat treatment. The pyrolysis of Si_2H_6 over $A\ell_2O_3$ is being carried out in the presence of CH_3SiD_3 to determine whether the $A\ell_2O_3$ has changed the mechanism of decomposition from the 1, 2-hydrogen shift observed in the homogeneous decomposition

$$Si_2H_6 \rightarrow SiH_2 + SiH_4 . \qquad (1)$$

The possibility of SiH_4 decomposition initiated by H atoms from molecular hydrogen decomposition above 600 C will also be examined.

All of these reactions are carried out in flow systems with low-temperature traps which remove the heavier less stable products from the stream. This allows for the determination of the effect of pyrolysis temperature on the yield of Si_2H_6 in the pyrolysis of SiH_4:

$$2\ SiH_4 \rightarrow Si_2H_6 + H_2. \qquad (2)$$

This last point will provide some information concerning the species which are present at the point of Si deposition.

The first experiments undertaken were directed toward determining the role of the $A\ell_2O_3$ surface in catalyzing the decomposition of SiH_4 and other Si hydrides. Pyrolysis of SiH_4 was carried out in a flow system containing a Hg Toepler pump and two low-temperature traps maintained at -160C positioned beyond the heated zone. The quartz-walled heated zone (6.2 cm^3 volume) had a surface-to-volume ratio of 42.8 when packed with 3/32-in. diameter $A\ell_2O_3$ beads and 2.84 without the beads. The $A\ell_2O_3$ beads were washed in 9:2 mixture of HNO_3:HF and then rinsed with water, trichlorethylene, deionized water, and finally methanol prior to use. The results of the initial experiments were inconclusive, although SiH_4 pyrolysis appeared to take place at the same rate over a Si surface (i.e., the beads covered with a Si deposit) as over a bare $A\ell_2O_3$ surface (i.e., clean beads).

Subsequent pyrolysis experiments were carried out for 30 min each in a recirculating flow system containing a -160C cold "U" trap which condensed any Si_2H_6 formed and maintained the SiH_4 pressure at about 12 torr. In these experiments between four and six monolayers of Si or SiH_2 polymer were deposited on the test surface. The results of these experiments are given in Table 6 and show that any catalysis by $A\ell_2O_3$, SiO_2 (quartz) or pyrex is rapidly eliminated after (or possibly even before) one monolayer of Si is deposited.

To circumvent the difficulty of rapid coverage of the test surface by the depositing Si a static pyrolysis unit was constructed which consisted of a Si-mirrored pyrolysis chamber, containing cleaned $A\ell_2O_3$ beads, connected by a "U" trap to a combination Toepler pump-McLeod gage. With this apparatus it is possible to detect H_2 produced from the SiH_4 pyrolysis well before one monolayer of Si is deposited on the beads. A 13-fold increase was measured in the rate of SiH_4 decomposition over uncoated $A\ell_2O_3$ as compared with the rate over Si-mirrored beads. However, the amount of SiH_4 passing the -196C trap was about four times that of the H_2 produced in the reaction, so to correct this the "U" trap was filled with a 5Å molecular sieve. This modification decreased the background SiH_4 (due to incomplete SiH_4 condensation at -196C) by a

Table 6. SiH_4 Pyrolysis Experiments

Expt. No.	Pyrolysis Temp. (°C)	Test Surface Exposed to Pyrolysis	SiH_4 Consumed (mmol)	Si_2H_6 Produced (mmol)	H_2 Produced (mmol)
surface/volume = 2.84					
1	521	SiO_2 (quartz)	0.09	0.03	0.17
2	521	SiO_2 (quartz)	0.07	0.03	0.17
3	521	Si	0.07	0.03	0.20
4	521	Si	0.09	0.05	0.22
surface/volume = 11.9					
5	522	Pyrex	0.09	<0.01	0.29
6	522	Pyrex	0.11	<0.01	0.30
7	522	Pyrex	0.13	<0.01	0.29
8	522	Si	0.09	<0.01	0.26
9	522	Si	0.08	<0.01	0.24
surface/volume = 42.8					
10	525	Al_2O_3	0.17	0.03	0.48
11	526	Al_2O_3	0.19	0.03	0.51
12	524	Si	0.16	<0.01	0.50
13	524	Si	0.17	0.01	0.49

factor of 4. The size of the chamber was also increased so that double the number of beads could be used. In these experiments the H_2 reading was about four times the SiH_4 background. The experiments were carried out at a pressure of 100 torr at 245C. With this system the catalytic rate over Al_2O_3 was shown to be about 30 times greater than that over a Si mirror. That is, Al_2O_3 clearly does catalyze the decomposition of SiH_4. This result established the role of Al_2O_3 surfaces in the pyrolysis at moderate temperatures but leaves final delineation of this role at temperatures up to 1100C yet to be accomplished.

During this report period studies of the chemistry of the metalorganic-hydride reactions involved in the deposition of GaAs from trimethylgallium (TMG) and arsine (AsH_3) were also initiated. Pyrolyses of AsH_3, $Ga(CH_3)_3$, and AsH_3-$Ga(CH_3)_3$ equimolar mixtures were carried out in a flow system contained a pyrex turbine pump, a Si-mirrored thermal zone, and a cold "U" trap.

In control experiments, it was demonstrated that, at between 15 and 20 torr pressure, $Ga(CH_3)_3$ does not decompose below 320C while AsH_3 very slowly decomposes at 150C. The results of pyrolyses of equimolar mixtures of $Ga(CH_3)_3$ and AsH_3 are given in Table 7.

Table 7. Pyrolysis of Equimolar $Ga(CH_3)_3$-AsH_3 Mixtures

Pyrolysis Temp. (C)	Duration of Pyrolysis (hrs)	Total Non-condens. Produced (cc)	Ratio $\frac{CH_4 \text{ produced}}{H_2 \text{ produced}}$	Ratio $\frac{CH_4 \text{ produced}}{(CH_3)_3Ga \text{ consumed}}$
153	8	5.4	4.2	1.2
190	6	8.8	1.95	1.3
195	4	7.8	2.1	1.2
230	4	8.1	2.3	1.1
275	4	11.0	2.2	1.2

*No bath used on flow line.

These data suggest that $(CH_3)_3$ Ga and AsH_3 form a one-to-one complex which eliminates one CH_4. If the product $(CH_3)_2GaAsH_2$ condenses on the wall of the thermal zone a second CH_4 is apparently eliminated.

The reaction has been further examined for an equimolar mixture of AsH_3 and $Ga(CH_3)_3$ in a static system at 90-100C for 3 hr at about 250 torr total initial pressure. In this time about 25 - 30 percent reaction occurs, yielding $(CH_3GaAsH)_x$ - as the first apparent product of the reaction - and CH_4. The ratio (CH_4 produced/AsH_3 consumed) was 1.95, 2.0 and 2.1, while the ratio (CH_4 produced/$Ga(CH_3)_3$ consumed) was 1.95, 2.0 and 1.8 in the best three runs of the series.

The major problem has been the handling of $Ga(CH_3)_3$, which slowly decomposes (probably by hydrolysis) when condensed as a liquid. Frequent cleaning of the vacuum system is therefore required.

The pyrolysis of 0.12 mmoles of $(CH_3GaAsH)_x$ has been examined in recent experiments; no decomposition was noted below 360C. At 410C, 0.11 mmoles of CH_4 was produced in 4 hr. Further experiments with this compound are in progress. In addition, preliminary flow reactions of AsH_3 and CH_3SiD_3 in a 1:1 ratio at 310C were found to produce $H_2/HD/D_2$ in a ratio of 1.0:0.12:0.02. These data suggest that some H atoms were produced in the decomposition of AsH_3. These experiments also are continuing.

4. SUBTASK 4. PREPARATION AND CHARACTERIZATION OF SUBSTRATES

In the first year of the program it was demonstrated that $A\ell_2O_3$ surfaces prepared by mechanical polishing techniques and used routinely for semiconductor heteroepitaxy typically have severe surface and subsurface damage, with many scratches often several microns deep yet often rendered invisible to close inspection because of amorphous or fine-grained debris embedded in the scratches in the final polishing stages. Some improvement in mechanical polishing procedures was achieved in terms of the density and depth of such damage. Gas-phase etching/polishing procedures using SF_6 and various fluorinated halocarbons in the 1350 to 1500 C temperature range produced essentially scratch-free surfaces on $(01\bar{1}2)$ and near-$(1\bar{1}\bar{2}0)$ $A\ell_2O_3$ substrates. Extensive gas-phase etch-rate data were obtained as a function of crystallographic orientation in this temperature range.

During the first part of the second year a much improved technique for polishing $(10\bar{1}4)$ $A\ell_2O_3$ was developed, and very good surfaces in this orientation can now be obtained. Gas-phase etching/polishing techniques were further developed for (1) thinning $A\ell_2O_3$ substrates to thicknesses the order of 1 mil; (2) evaluating the effects of prolonged etching on $(01\bar{1}2)$, (0001), and ~$(11\bar{2}0)$ $A\ell_2O_3$; and (3) assessing the subsurface damage caused by various mechanical polishing procedures.

More recent work on this subtask has included verification of the polishing procedure for $(10\bar{1}4)$ $A\ell_2O_3$ as a reproducible process. Evaluation of polishing methods for $MgA\ell_2O_4$ surfaces has indicated that surface fill-in occurs for this material just as for $A\ell_2O_3$. Preliminary gas-phase etching experiments with $MgA\ell_2O_4$ surfaces were also carried out.

Ion-beam sputtering techniques have been under development for preparing ultra-thin (~200 Å) $A\ell_2O_3$ wafers for use as substrates in the in situ CVD experiments with Si (Subtask 5). Some wafers successfully thinned to ~0.002 in. by mechanical polishing techniques have been subsequently thinned by ion etching to the point of perforation in some areas, which results in adjoining regions of thickness suitable for transmission electron microscopy as applied in the in situ experiments. Typical thinning rates are 0.2 to 2.0 μm/hr. Three different $A\ell_2O_3$ orientations have been successfully thinned by this method - (0001), $(10\bar{1}4)$, and $(01\bar{1}2)$. Considerable study of properties of the resulting thinned substrates has been carried out.

The routine characterization of substrate surfaces at various stages of preparation has continued throughout the program to date, utilizing various standard techniques of X-ray and electron diffraction analysis and optical and electron (including scanning) microscopy.

During this reporting period additional $A\ell_2O_3$ substrates were prepared for epitaxial growth experiments by mechanical polishing techniques previously developed on this program (Refs 3, 4); additional effort was expended on attempts to prepare suitably thinned $A\ell_2O_3$ wafers for subsequent final thinning by the ion-beam sputtering technique; considerable further improvement in the ion-thinning process for preparing substrates for the in situ CVD experiments in the electron microscope (Subtask 5) was achieved; and etch-rate experiments to determine the depth of damage in $A\ell_2O_3$ substrate wafers at various stages of the pre-deposition preparation process were begun.

a. Polishing of $A\ell_2O_3$ Substrates

Several new sets of $A\ell_2O_3$ wafers in various orientations have been polished for use on this program. The first group consists of $(10\bar{1}4)$-oriented oval-shaped (7/16 in. x 1/2 in.) wafers finished for use as epitaxy substrates. The procedure used on these wafers was as follows: The back side was first lapped with 400-mesh boron carbide on a vibratory lapping machine. The wafers were then inverted and lapped on the second side using the same abrasive and method. After the wafers were lapped flat, the jig holding the samples was transferred to an optical polisher for further processing.

Rough polishing was continued using 5μm, 3μm, and 1μm diamond abrasive on three cast-iron laps. A brass lap was then used with a 0.5μm diamond slurry to obtain a reasonably good polished surface prior to transferring to the vibratory polisher. The wafers were then polished with 0.25μm diamond slurry on nylon cloth. After completion of this step, the samples were final-polished with 0.25μm "top" diamond using perforated Pellon cloth. This method of processing constitutes the most successful technique developed to date for this particular orientation of $A\ell_2O_3$.

Basal-plane $A\ell_2O_3$ wafers were also polished for use as substrates during this reporting period. The procedure used for polishing these substrates (~5/8-in. dia) was as follows: The as-sawed wafers were first lapped on both sides using 400-mesh boron carbide. The substrates were then rough-polished on three cast-iron laps in sequence, using diamond slurries of 5, 3, and 1μm particle size. A brass lap with 0.5μm diamond slurry was then used for the final rough polishing on the optical polisher. The wafers were then polished with a Linde "A" (0.3μm) mixture on the optical polisher using perforated Pellon cloth. Final polishing was completed on the vibratory polisher using a Linde "B" (0.05μm) mixture.

A similar procedure is being applied to a group of $(01\bar{1}2)$-oriented $A\ell_2O_3$ wafers now being prepared for a variety of experiments on this program. In all three cases the procedure being used has been largely developed in earlier studies under this contract.

b. Mechanical and Chemical Thinning of $A\ell_2O_3$ Substrates

A major effort has been expended during the past six months in an attempt to mechanically polish $A\ell_2O_3$ single-crystal wafers to 0.001-in. thickness for subsequent use in thinning to ~500Å by ion-beam sputtering (ion thinning). Such thicknesses are required for substrates that are to be used in the in situ CVD experiments in the electron microscope (Subtask 5).

It is desirable to start with crystals less than 0.001 in. thick because the ion thinning process is relatively slow (<0.5μm/hr) and surface irregularities are more likely if greater amounts of material must be removed by ion thinning. A variety of mechanical polishing techniques has been attempted, with extremely limited success: two groups of $(01\bar{1}2)$-oriented crystals were polished to thicknesses of 0.0017 in. and 0.0024 in.

The mechanical lapping and polishing procedures used in these investigations have typically started with $(01\bar{1}2)$-oriented $A\ell_2O_3$ wafers 0.010 in. thick with both sides commercially polished. The wafers are attached to a polishing jig with a low-melting-point wax and lapped on a vibratory polishing machine to ~0.006 in. thick, using 400-mesh boron carbide abrasive. The jig and mounted wafers are then transferred to an optical polishing machine and polished with successively finer diamond abrasives, beginning with 3μm particle size. The wafers processed in this way have often shattered at thicknesses of 0.005 to 0.003 in.

The following parameters were changed in various ways in attempts to produce the 0.001 in. thickness required: shape, mounting arrangement, and edge condition of wafers; size and number of wafers (hence surface area and polishing pressure); size of abrasive and wafer thickness at which the abrasive is first applied; type of slurry; size and surface configuration of lapping plate; and type of polishing motion.

With this general lapping and polishing method, only one group of wafers (which had been lightly chemically etched in H_3PO_4: H_2SO_4 (1:1) solution before lapping) was successfully polished on both sides to a thickness of 0.0017 in. This group was then successfully cut into about 0.030-in. dia disks for subsequent ion-beam thinning. Attempts to reproduce the polishing were unsuccessful. A second group of wafers, without the chemical etching, was polished to 0.0024 in. and subsequently cut into 0.030-in. dia disks. Only one side of the latter group was polished; the other side was lapped only and quite rough.

No further in-house mechanical polishing of this type is now planned. In view of the limited success and the diminishing rate of improvement, it has been decided to shift the manpower to a different facet of the program. Furthermore, wafers <0.001 in. thick are now commercially available, and these have recently been successfully cut into 0.030-in. dia disks. Actually, wafers as thin as 0.0006 in. are available,* but no technique has yet been found to cut them into small disks without shattering.

Chemical etching of $A\ell_2O_3$ in $KMnO_4$ flux at 700 to 1000C has also been attempted as a possible means of thinning substrates. $(01\bar{1}2)$-oriented wafers originally 0.010 in. thick were readily reduced to ~0.004 in. with a relatively flat and uniform surface. However, further etching to thicknesses of 0.002 in. leads to rapid edge dissolution and a corresponding large taper in thickness. As an alternate approach, samples thinned to 0.004 in. in the $KMnO_4$ flux were then etched further at ~225C in a 1:1 mixture of H_3PO_4 and H_2SO_4, which provided a much slower etching rate (0.25μm/hr). Several samples were etched to slightly less than 0.002 in. with only moderate breakage and surface faceting. One sample was further thinned to 0.0003 to 0.001 in., but severe breakage was encountered and only a few small pieces survived; those have been cut into disks for ion thinning.

---

* E.g., Insaco, Inc., Quakertown, PA.

e. Ion Thinning of Substrates

Development of the ion-beam sputtering technique as a method for thinning Al_2O_3 substrates has continued during the past six months. The operation of the ion-beam machining apparatus has been refined into a relatively routine, albeit time-consuming, operation essentially free of difficulties. The thinning rate for Al_2O_3 remains low, ~0.5μm/hr, so each sample required 2 to 5 days of operating time. Of the samples thinned to date, ~20 percent have yielded thin areas at least marginally suitable for use in the in situ studies.

A typical ion thinning procedure begins with the mounting of one or more Al_2O_3 disks 0.030 in. in diameter onto a sample holder. A beam of Ar^+ ions at 6-10 kV and ~100 μamp/cm^2 is directed at the central area (0.015 to 0.020 in. across) of the crystal at a glancing angle of 10 to 30 deg. Thinning proceeds until a perforation occurs. The area around the perforation is wedge-shaped in thickness but suitably thin for substrate use over an area ~5μm wide. The thin areas are surprisingly robust, so that the overall fabrication yield, including ion thinning and the handling involved in loading onto the heating meshes of the electron microscope microchamber (see Subtask 5), is nearly 10 percent.

The substrates that have been prepared in this manner were similar in character, the thin areas being comparable with those shown in Figures 12 and 20 in the fourth semi-annual report (Ref 4). Thickness irregularities were normally present, so that extended areas of uniformly-thin electron-transparent substrate were seldom found. The thickness gradient always present limited the usable thin region to ~5μm in width. Flux-grown (0001)-oriented Al_2O_3 crystals initially 5μm in thickness (obtained from Prof. E. White of the University of London) had thickness irregularities that were less frequent and less severe. The factor most likely responsible is the small initial thickness, but another possibility is the relatively smooth starting surface of the crystal. An improvement in thickness uniformity and the consequent enlargement of the thinned area is the strongest impetus for producing starting (pre-ion-thinning) wafers less than 0.001 in. thick. Other impetus, of course, is in the reduction of the ion-beam thinning time required.

It was shown in the previous semiannual report (Ref 4) that one apparent cause of the thickness irregularities is contamination blocking certain regions of the substrate from the ion beam. Experiments this period have shown that another causative factor is an initially rough surface. This was demonstrated by the ion-thinning of samples 0.0024 in. thick which were polished and smooth on one surface and lapped and quite rough on the other. The polished side remained smooth as a result of the sputtering action of the ion beam, with the exception of the normal formation of a few "protuberances" (Ref 4). The lapped side was made smoother by the sputtering but was still relatively rough, even when some region of the crystal first reached zero thickness. At this juncture the surface was found to consist of numerous approximately hemispherical mounds 20 to 40μm in dia. At the edges and intersections of the mounds there were numerous electron-transparent regions which had an extremely large thickness gradient and a corresponding narrow thin area. This behavior was observed for beam incidence angles of 10 and 30 deg. Thus, it is concluded that initially smooth surfaces are a necessary condition for the formation of large ion-thinned regions.

d. Determination of Depth of Surface Damage in $A\ell_2O_3$

A series of experiments designed to provide a measure of the depth of the damaged region caused by the mechanical sawing, lapping, and polishing processes used on $A\ell_2O_3$ to produce epitaxy substrates has been started, with (0001) - and $(10\bar{1}4)$-oriented slices the first to be examined. The $(01\bar{1}2)$ and the 5-deg-off-$(11\bar{2}0)$ orientations are also to be investigated.

The technique used is to observe etching rate as a function of the amount of surface material removed (based on weight-loss determination), with the appearance of a constant etch rate taken as indication that the main part of the severely damaged region has then been removed. The chemical etchant being used in these measurements is a 1:1 mixture of H_3PO_4 and H_2SO_4, with a temperature of 200 to 225C and continuous agitation of the etchant also required. Although there may be some uncertainty at this stage about the structural significance of the etch rate reaching a constant value, the technique has been found useful with other substrate materials (e.g., BeO) for indicating depths of severe damage and variations in this depth as a function of mechanical treatment and of crystallographic orientation.

Only preliminary results are available at this time, but these indicate that both orientation differences for a given mechanical surface treatment and surface processing differences for substrates of a given crystallographic orientation are being detected by this method. Results will be given in the next semiannual report.

5. SUBTASK 5. STUDIES OF IN SITU FILM GROWTH IN THE ELECTRON MICROSCOPE

In the first year of the program many of the modifications required in the electron microscope for in situ observation of the nucleation and early-stage growth of CVD semiconductor films on insulating substrates were completed. Provision for motion-picture recording of film growth was assembled and tested, and the heated specimen stage was installed and tested. The first in situ PVD experiments were also carried out near the end of the first year.

During the first six months of the second year a series of electron microscope modifications and tests was completed, culminating in the first series of successful PVD experiments inside the electron microscope. Aℓ was deposited onto a heated carbon substrate and a sequence of micrographs taken during the growth process, demonstrating the feasibility of performing in situ nucleation and growth studies in the equipment. A transmission phosphor screen (for the motion picture camera) was installed, permitting motion picture photography which does not interfere with the normal still photography. The auxiliary vacuum pumping system for the specimen chamber was fabricated, installed and tested. The basic vacuum system of the microscope itself was improved by addition of a cooled baffle, by polishing the O-ring grooves, and by thoroughly cleaning the microscope interior. A PVD source assembly was fabricated, installed and used in conjunction with the specimen heater to perform the PVD experiments.

Calculations and design for the CVD microchamber were also completed, and the fabrication of the microchamber and the differential pumping apertures was begun. At the end of the second year a modified design of the CVD microchamber and associated hardware was developed and fabrication nearly completed. Numerous additional in situ PVD experiments were carried out, with both Aℓ and Au deposited onto amorphous carbon substrates to delineate further the required techniques and experimental problems to be encountered in the CVD experiments.

During the past six months, the fabrication of the CVD microchamber and its mounting flange has been completed. A gas handling manifold has been installed on the electron microscope and connected to the CVD flange. Focus tests of the microchamber were completed satisfactorily. Gas flow experiments were performed to determine the flow rate of gas through the microchamber as a function of pressure and to determine the maximum pressure attainable in the microchamber. Constructional details of the microchamber were described in a brief technical paper (Ref 8) during this period; the paper is included in this report as Appendix B.

Several in situ CVD experiments have now been performed, resulting in the successful growth of Si films on amorphous carbon substrates. Although the experiments were preliminary in nature, several important features have been demonstrated:

1. The pyrolysis of SiH_4 to form Si inside the electron microscope is feasible.

2. Crystalline Si can be grown on amorphous carbon substrates.

3. The pyrolysis reaction appears to have an "incubation period."

4. Nucleation of Si on amorphous carbon is relatively slow, with subsequent growth rapid.

5. The Si islands formed are three-dimensional, angular in nature, and do not change significantly during coalescence.

a. Microchamber Testing and Gas Flow Measurements

Fabrication of the CVD microchamber and CVD flange was completed early in this reporting period; they are shown in Figures 1 and 2, respectively. Beam focus tests were satisfactory, with the substrate in proper focus at all magnifications from 1500X to 100,000X.

With the removable aperture and aperture cap of the microchamber (Figure 1 of Ref 8 — see Appendix B) in place, the objective aperture of the electron microscope must be withdrawn and cannot be used. The removable aperture is used in its place, with the resulting image quality a function of the aperture size, being better the smaller the aperture size. Currently a 100 μm dia removable aperture is used in place of the normal 25 μm objective aperture, with a consequent slight reduction in image quality. (This appears as a loss in contrast and an increase in overall background intensity, which is visible to the experienced observer in Figure 7a.) As more experience is gained in aligning the removable aperture, a smaller aperture size will be used and no loss in image quality will be present.

A gas-handling manifold and metering system has been installed on the microscope. It is shown in the photograph in Figure 3 and schematically in Figure 4. The manifold is of stainless steel tubing (1/4 in. dia) connected to the microchamber through the CVD flange, which fits in the right-hand side of the microscope specimen chamber.* Gas is bled into the microchamber through a Whitey 22RS4-A metering valve, and the microchamber pressure is measured with a Leybold-Heraeus TM202 thermocouple gauge.

The gas flow tests conducted with the microchamber and gas handling manifold were of two types: (1) the gas pressure in the electron microscope was measured as a function of the microchamber gas pressure, and (2) the flow rate of gas through the microchamber was measured as a function of pressure. The tests were conducted as follows. The gas pressure in the electron microscope was measured by an ionization gauge mounted on the left-hand side of the specimen chamber. The microchamber pressure was measured by the thermocouple gauge mounted between the microchamber and the metering valve, so the measured pressure may be somewhat greater than the actual pressure in the substrate region. Both apertures were 0.004 in. in diameter.

Results of the pressure tests with only the normal microscope pumping system in operation are shown in Figure 5. The maximum pressure permissible in the electron microscope is 1×10^{-4} torr, which corresponds to a maximum permissible microchamber pressure of approximately 1500 millitorr. The maximum permissible

*The term "specimen chamber" refers to that relatively large portion of the electron optical column of the microscope containing the CVD microchamber and the specimen holder stage with its associated control mechanisms for translation. With a conventional electron microscope specimen holder in position, the specimen chamber would also contain a specimen holder exchange and an airlock mechanism.

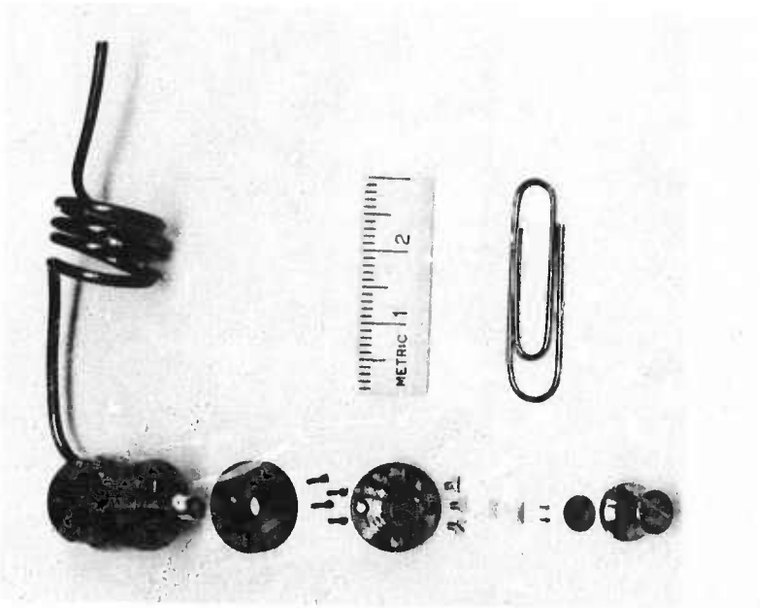

Figure 1. CVD Microchamber, Disass .bled

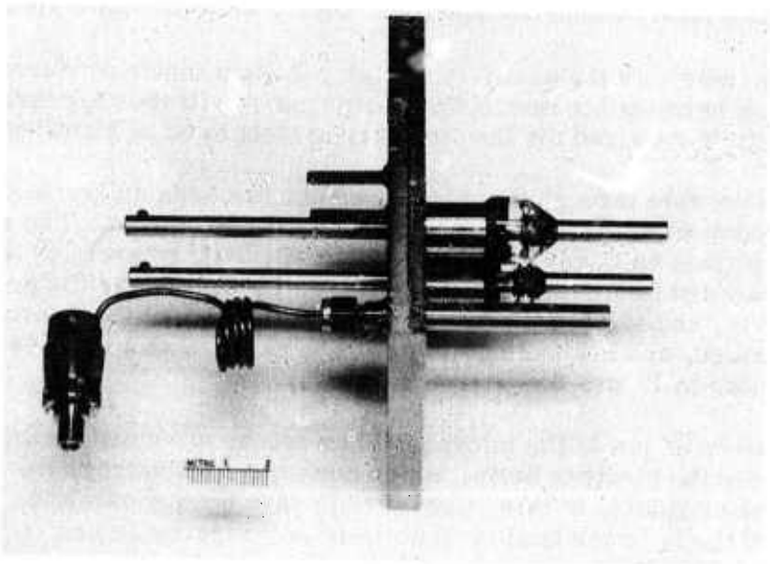

Figure 2. CVD Flange for Electron Microscope, with Assembled Microchamber Mounted in Place

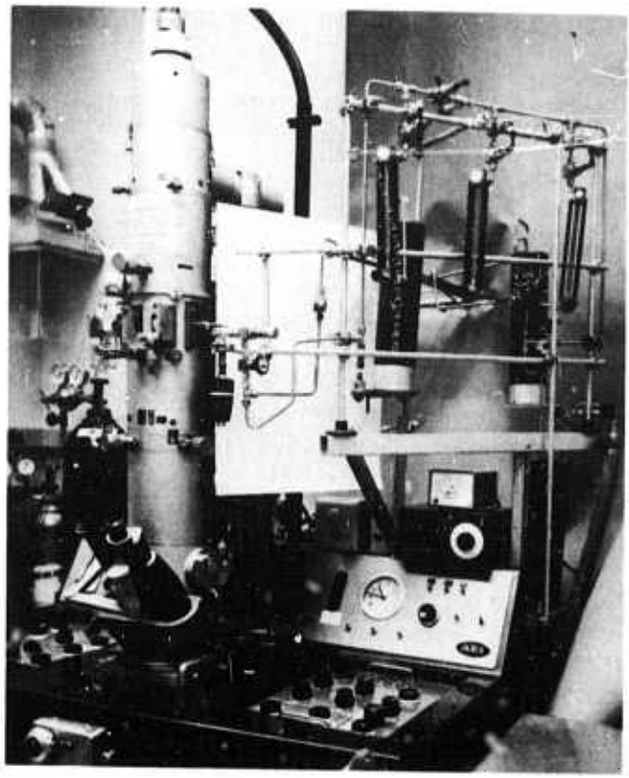

Figure 3. Electron Microscope and Gas Handling Manifold

microchamber pressure will vary from one run to another, as shown by the four tests of Figure 5, presumably dependent upon how tightly the removable aperture is reinstalled.

Pressure tests with the auxiliary pumping system installed showed only a slightly higher maximum permissible microchamber pressure. It thus appears that a larger pumping capacity is required for the auxiliary system to be of significant value.

The gas flow rate through the microchamber has been determined by measuring the pressure decay when the metering valve is suddenly closed. The rate at which gas flows out is given by $G = [VP_1/760(t_2-t_1)]\ell n\ (P_1/P_2)$, where G is the flow in cm^3/min corrected to standard temperature and pressure, P_1 and P_2 are the pressures in torr at times t_1 and t_2, and $V = 9.7\ cm^3$ is the internal volume of the microchamber, thermocouple gauge, and connecting tubing. The gas flow was found to vary with pressure as shown in Figure 6.

The presence of gas in the microchamber causes unwanted multiple scattering of many electrons in the electron beam, which consequently destroys the image quality. Estimates of the magnitude of this effect (Ref 2) have been shown to be correct, as only a slight change in image quality is noticeable. Figures 7a and 7b illustrate the loss of image quality visible in a network of cellulose acetate (a processing residue) on an amorphous carbon substrate, with the microchamber containing 50 percent SiH_4 and 50 percent H_2 at a pressure of 3.5 torr.

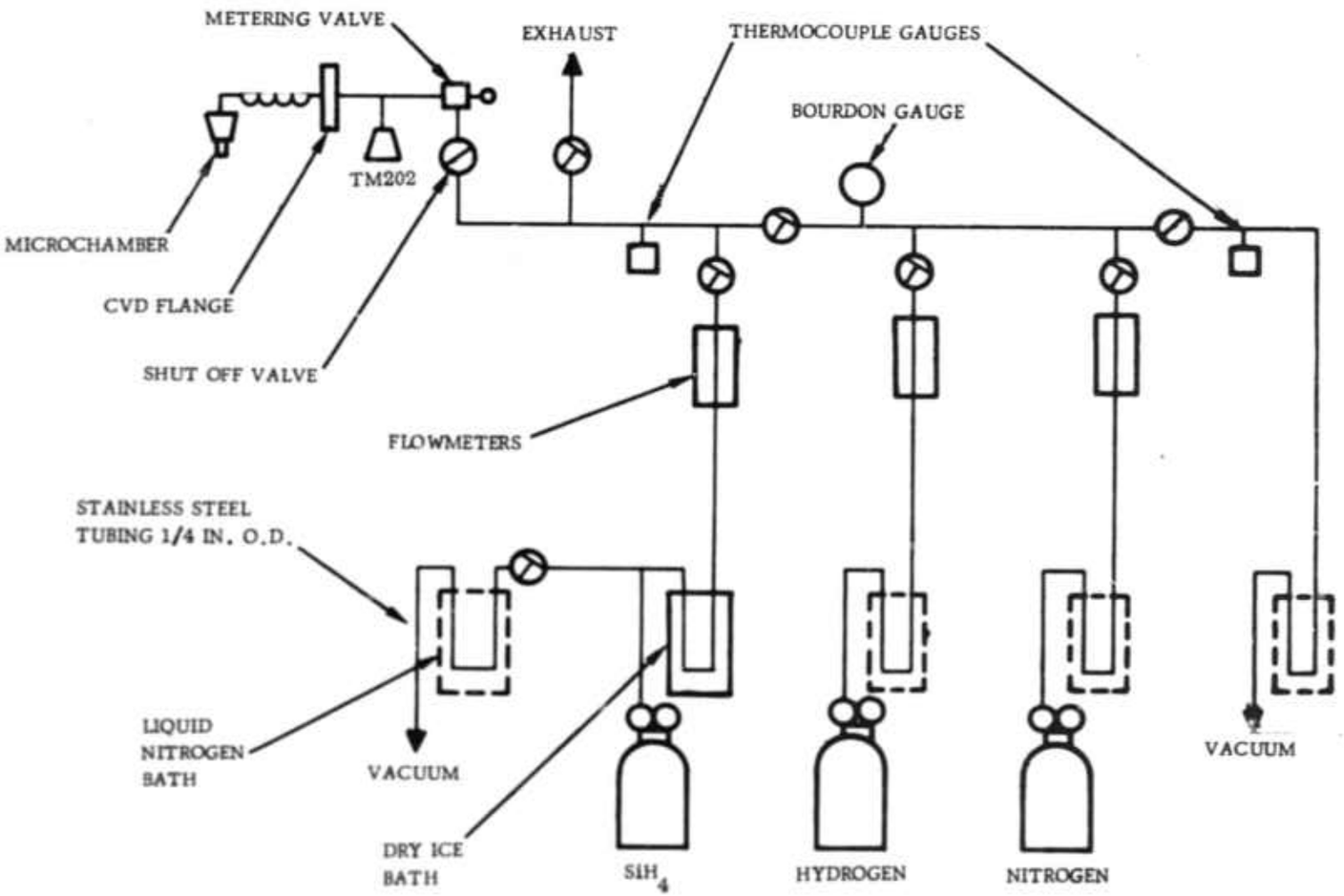

Figure 4. Schematic Diagram of Gas Handling Manifold

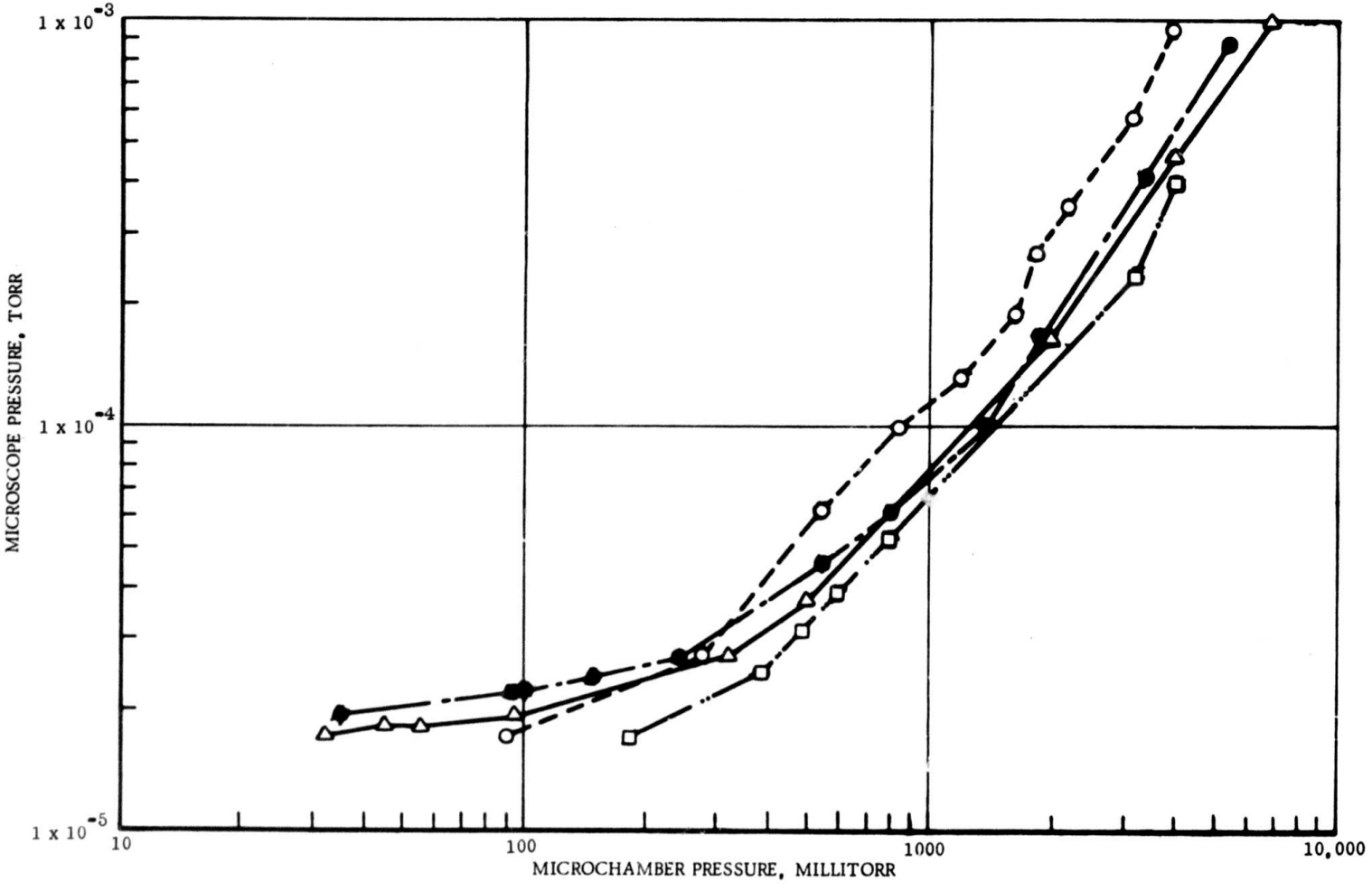

Figure 5. Measured Pressure in Electron Microscope as Function of Microchamber Pressure

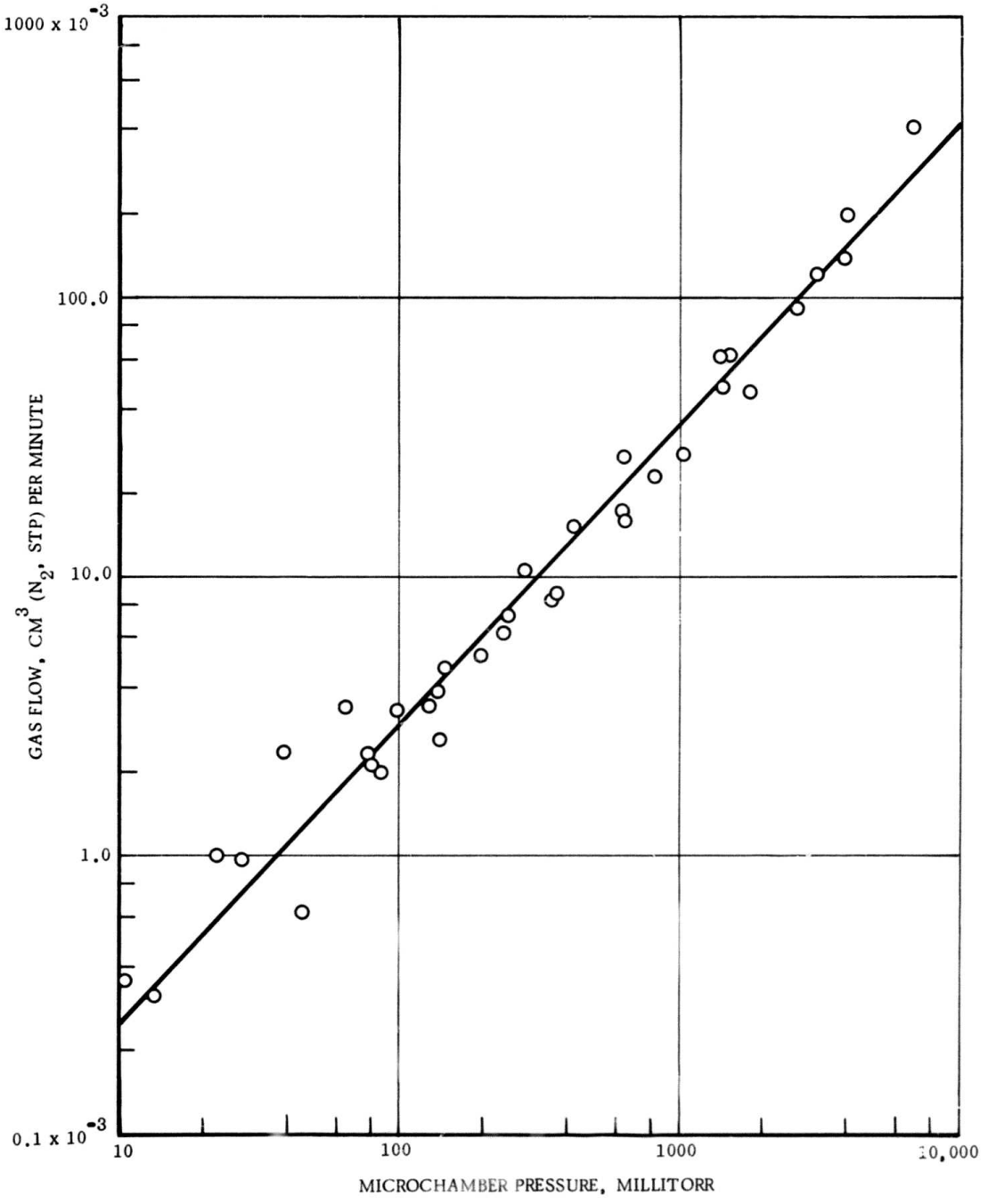

Figure 6. Measured Gas Flow through Microchamber as Function of Pressure

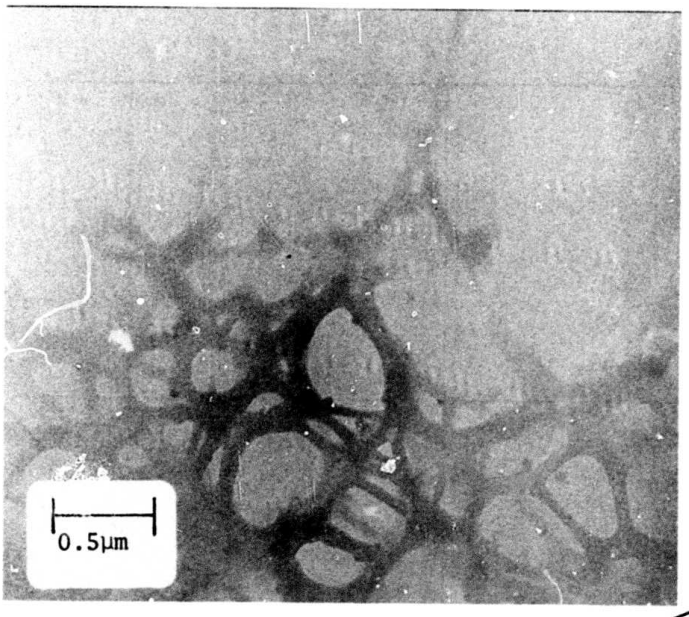

(a)

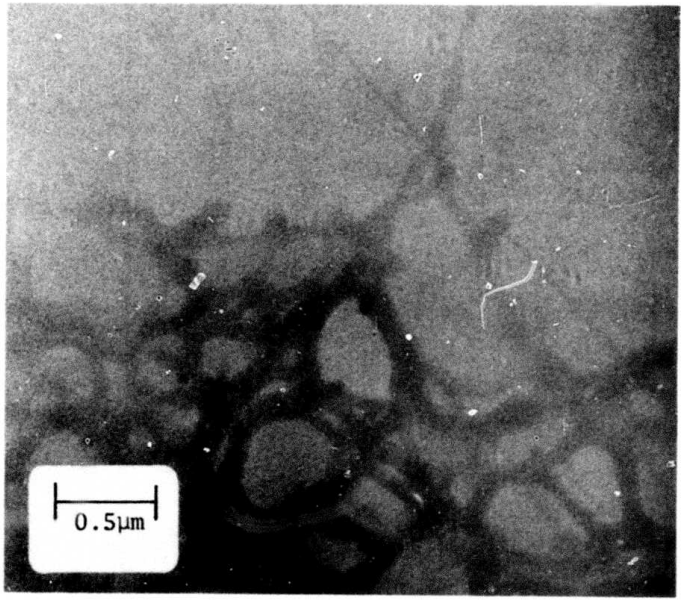

(b)

Figure 7. Electron Micrographs Showing Image Quality in CVD Microchamber at (a) 1×10^{-4} torr (Normal Microscope Vacuum) and (b) 3.5 torr (50% SiH_4 and 50% H_2).
(The image is cellulose acetate network (a processing residue) on amorphous carbon substrate)

b. Microchamber Operational Details

During this report period considerable effort was spent on developing a technique for loading and unloading the CVD microchamber to properly align a selected thin area in a given $A\ell_2O_3$ substrate. This loading and alignment procedure is more lengthy than anticipated because the suitable electron-transparent regions in the $A\ell_2O_3$ substrates are smaller than desired.

An appreciation of the loading time required and the necessity for large, thin areas of $A\ell_2O_3$ substrates can be obtained from a consideration of the requirements for successful loading and of the dimensions involved. Open areas 100 μm sq in the two substrate heating meshes must first be aligned with each other, then with a thin region in the $A\ell_2O_3$ substrate, and then with the center electrode aperture of 100 μm dia (Figure 1 of Appendix B), all of which in turn must be aligned with the 100 μm-dia removable aperture. All work must be performed under a 50X stereo microscope.

The probability of achieving successful alignment can be estimated as follows. In the best case, open areas in the two heating meshes are perfectly aligned with each other, and can also be aligned exactly with one aperture so that 100 percent of the area is open. In the worst case, however, the two heating meshes will be completely misaligned with each other, and with the aperture, and only 9.4 percent of the area is open. Experimentally, careful alignment has produced an average of about 80 percent open area at this stage of the procedure. The probability of aligning the second aperture with the first is a function of how accurately the removable aperture is machined. In the one aperture used to date the best alignment attainable produces only ~25 percent open area. The overall probability of aligning both meshes and both apertures thus results in from 2.7 to 25 percent open area, with experimentally the average being ~20 percent. This figure must in turn be multiplied by the percentage of the area on the $A\ell_2O_3$ substrate which is suitably thin for use, typically 2 to 3 percent. (This is an area ~5 μm wide and ~400 μm total length in a circular disk 0.030 in. in dia.) Thus, the overall chance of a suitably thin region of the $A\ell_2O_3$ substrate being located in the open area of the apertures and heating meshes is about 0.5 percent, or 1 in 200.

To date there have been 12 attempts to load and align a substrate, each attempt requiring approximately four hours time. Eleven attempts were completely unsuccessful and one was only marginal, in that the $A\ell_2O_3$ region located was considerably thicker than optimum but did permit some electron transparency; it consequently was utilized for a CVD in situ experiment, described in the next section. Experience in loading is likely to reduce somewhat the time required per experiment, but the largest improvement will clearly come from increasing the size and uniformity of the thin areas in the $A\ell_2O_3$ substrates.

c. In situ CVD Experiments in the Electron Microscope

After completion of the gas handling manifold, a number of experiments were performed to ensure that gas handling procedures used were completely safe. (SiH_4 explodes spontaneously upon contact with air.)

Toward the end of the report period five in situ Si CVD experiments were performed. In two of the experiments a Si film was formed, demonstrating that SiH_4 pyrolysis inside the microscope is feasible.

The first three in situ CVD experiments utilized an Al_2O_3 substrate in which a thicker than optimum region was aligned with the apertures. The procedure was first to turn on the electron beam, then bleed gas into the microchamber to the desired total pressure (1.2 and 1.5 torr for the first two experiments), and then heat the substrate by gradually increasing the current through the heating grids. In the first two experiments, no Si deposition was observed. It is believed that the SiH_4 flow utilized was too low (0.4 percent SiH_4 in H_2). In the third CVD experiment the concentration was raised to 40 percent SiH_4 in H_2 at a total pressure of 2.5 torr. Again no Si deposition was observed, even though the substrate heater current was 1.0 amp. (It has been previously found that 1.25 amp is normally sufficient to evaporate Cr from the stainless steel grid.) This strongly suggested that the Al_2O_3 substrate was not being heated properly, a problem which had occurred repeatedly in the earlier PVD experiments.

The next CVD experiments were conducted with amorphous carbon substrates, which generally cause no substrate heating problems. The gas mixture for the fourth experiment was ~25 percent SiH_4 in H_2 at a total pressure of 3.5 torr. The image quality of the carbon substrate was slightly degraded as a result of gas admission, but otherwise unchanged. Upon heating the substrate no change occurred until a heating current of 1.4 amps was attained, at which time the electron microscope screen rapidly darkened as a Si film several microns thick formed within ~2 sec. Since the thickness limit for electron transparency in Si is ~800Å, no details of the film were visible. The experiment was terminated, and the substrate and heating grid removed and inserted into a conventional specimen holder.

Examination in the electron microscope revealed a thin region in the CVD Si film that had been formed on a cooler substrate region near one edge of the grid heater. The film gave a typical Si electron diffraction pattern. The film was crystalline and fine-grained, as can be seen in Figure 8a (bright field) and in the dark-field micrograph of Figure 8b. For the dark-field mode of operation the objective aperture was displaced so that only the Si grains which contribute to one quadrant of the (111) diffraction ring appear bright.

The fifth CVD experiment was performed by first heating the amorphous carbon substrate (heater current 1.25 amp) to the desired temperature. While at this temperature, but prior to SiH_4 introduction, large numbers of small nuclei or particles appeared on the substrate surface. Although small and somewhat indistinct, these particles exhibited growth and coalescence phenomena. Their origin is uncertain but presumably they are Cr or an unknown contaminant evaporated from the grid. (They appear as small particles in the background in Figures 9 and 11.)

After 40 min at the elevated temperature a 13 percent SiH_4-in-H_2 mixture at 1.0 torr was admitted to the microchamber. After 2 min, Si growth was visible on the heating grid, forming large irregular masses which moved about considerably during growth. A typical growth sequence is shown in Figures 9a through 9c.

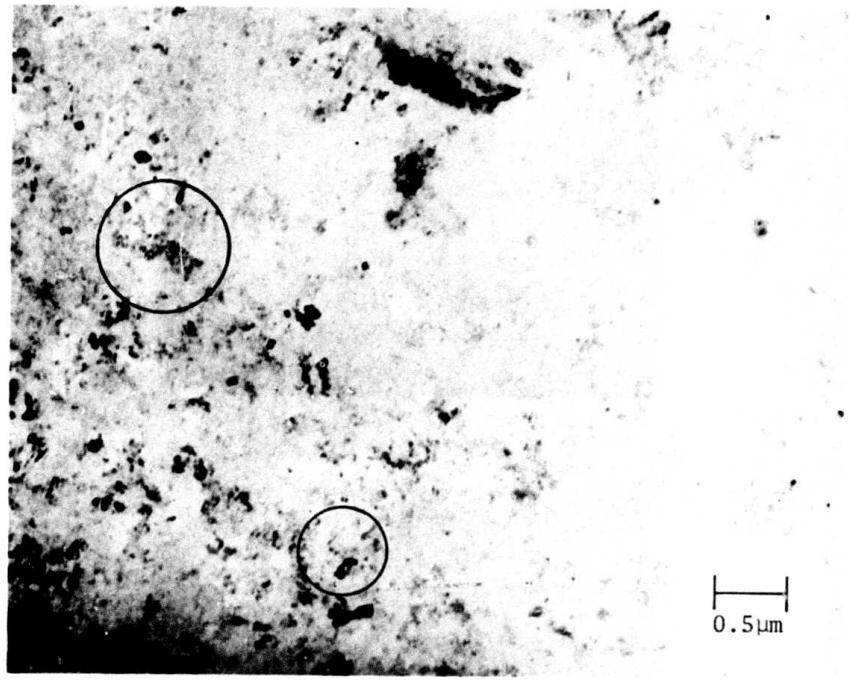

(a)

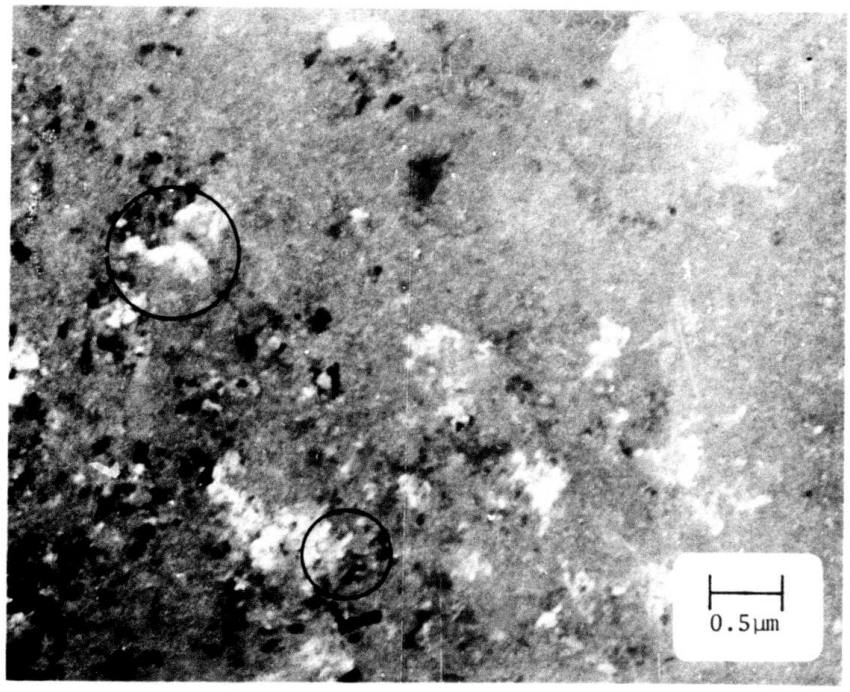

(b)

r igure 8. Electron Micrographs of Si Film Formed in Fourth CVD in situ Experiment. (a) Bright Field and (b) Dark Field of Same Area. (In b, Si grains which contribute to one quadrant of (111) diffraction ring appear bright.)

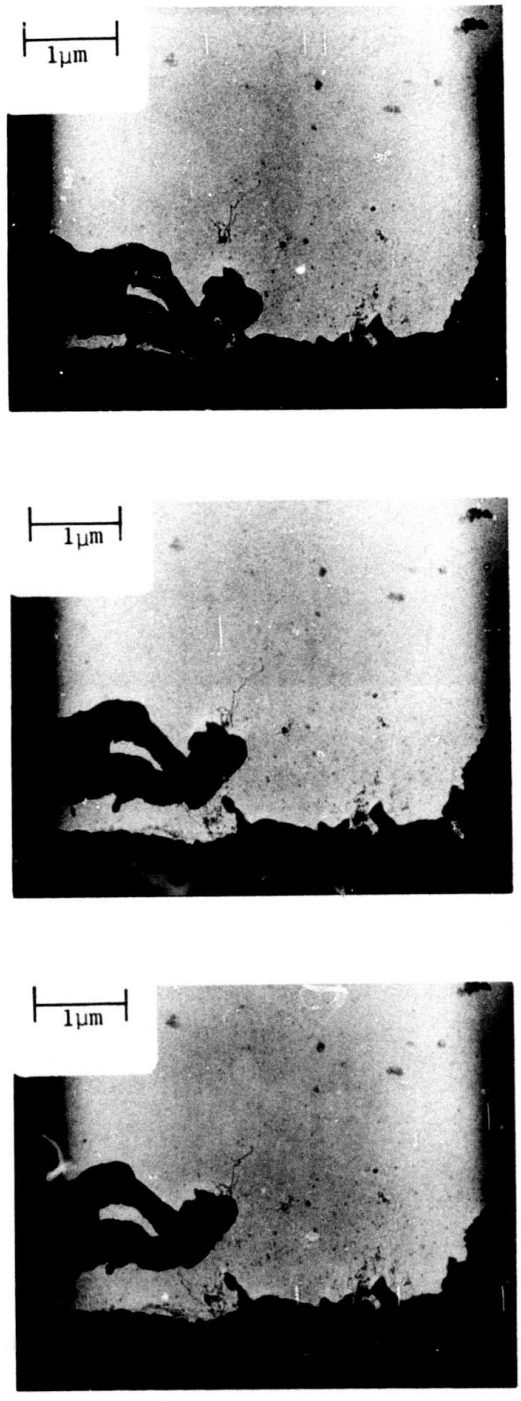

(c)

Figure 9. Si Growth on Edges of Heating Mesh at (a) Arbitrary Time 0 sec, (b) 10 sec, (c) 20 sec.

Si whiskers, shown in Figure 10, became visible on the carbon substrate after ~10 min. The Si whiskers grew by the vapor-liquid-solid (VLS) mechanism, as evidenced by the small liquid droplets visible on the tips of the whiskers. The whisker growth was more prominent near the heating grid (the source of the liquid contaminant) and quite sparse in the central substrate regions.

Conventional Si nucleation, growth, and coalescence were observed on the substrate after 30 min. These phases of the development of the deposit are shown in Figures 11a through 11c. Although the original negatives were overexposed, a considerable amount of information concerning the growth mechanism can be obtained from photographs made during the growth process. Perhaps the most significant feature is that the nucleation of Si on amorphous carbon is slow compared with the subsequent growth of the deposit. There appears to be an incubation period, ~30 min in the experiment described here, during which no nuclei form on the substrate. Once nucleated, however, the Si grows relatively rapidly and no further nucleation occurs.

Another growth feature of interest is that the Si formed is three dimensional, as are the nuclei in most thin-film growth processes. Different, however, is the shape of the particles, the Si being considerably more angular in nature than most other nuclei that have been directly observed during film growth. The growth sequence shown here (Figure 11) is also different in that the Si islands are quite large at the time of coalescence, with very little shape change occurring at the point where two islands coalesce. This suggests a low surface diffusion coefficient for the Si/carbon system.

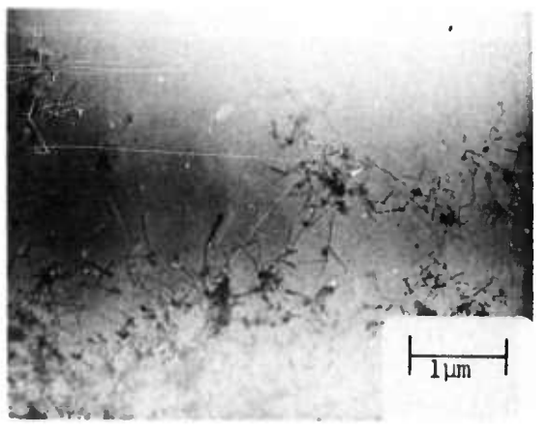

Figure 10. Si Whiskers Growing on Amorphous Carbon Substrate near Heating Mesh.

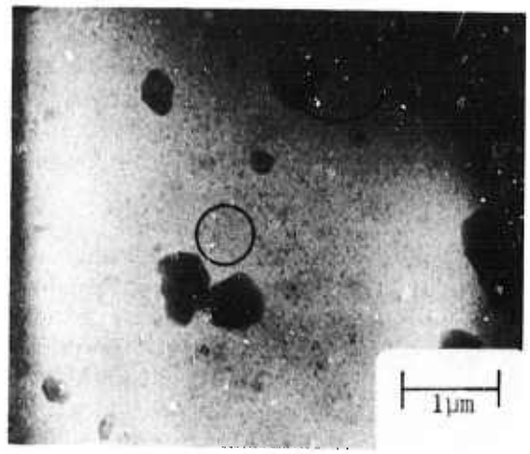

(a)

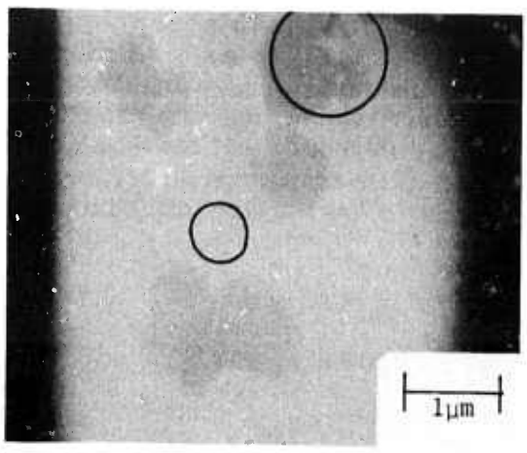

(b)

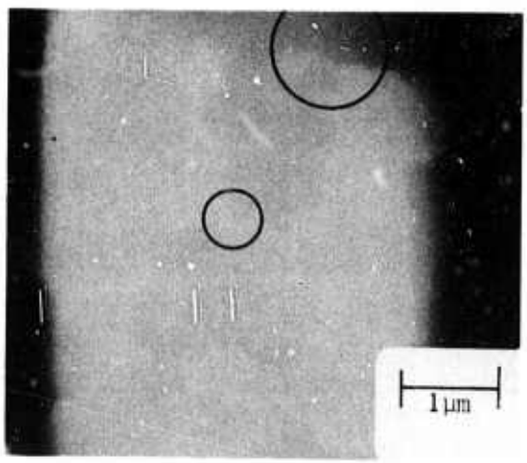

(c)

Figure 11. Growth Sequence on Amorphous Carbon Substrate (a) 30 min, (b) 32 min, (c) 33 min after SiH_4 Was Introduced into Microchamber.

The growth phenomena shown in this experiment, if truly characteristic of Si CVD growth from the pyrolysis of SiH_4, are significantly different from conventional thin-film growth and thus warrant considerable study. The conclusions stated above are, of course, preliminary in nature and must be verified by further experimentation.

6. SUBTASK 6. EVALUATION OF FILM PROPERTIES

During the first year, the routine evaluation of film properties was carried out by established methods of X-ray and electron diffraction analysis, metallographic analysis, and electrical measurements of transport properties. In addition, a new technique for evaluating the characteristics of the interfacial region of heteroepitaxial films was developed, involving measurement of the photoelectron emission from monochromatically-illuminated films in the MIS configuration on insulating (viz., Al_2O_3) sustrates. Relatively large photocurrents due to electron transport through thick (~10 mils) single-crystal Al_2O_3 substrates were measured as a function of photon energy. Photoelectric threshold energies, escape length (mean free path) of excited electrons, and band bending in the semiconductor film adjoining the interface were determined in the Si/Al_2O_3 and $GaAs/Al_2O_3$ systems. Observation of the energy spectrum of back-scattered proton or alpha-particle beams injected in channeling directions in heteroepitaxial semiconductor films was also investigated as a means of measuring the density and the location of structural defects in the films. Experiments indicated that Si/insulator films have less imperfect interfacial regions than do GaAs/insulator films. The best structures of those examined were found in (100) Si films on $(01\bar{1}2)$ Al_2O_3 substrates and in (111) Si films grown on near-$(11\bar{2}0)$ Al_2O_3 substrates.

In the first part of the second year the study of the effects of changes in deposition parameters on Si/Al_2O_3 film properties continued. Those studies provided considerable insight into the factors which most strongly influence film quality, so that identification of some of the conditions for optimized film growth on various Al_2O_3 orientations could be made. The importance of reactor geometry was recognized and demonstrated; the extent of Al autodoping from the substrate was established, and appropriate annealing procedures for minimizing the effects were determined. The use of previously unused Al_2O_3 substrate orientations (e.g., near the $(11\bar{2}0)$ plane) for Si growth led to epitaxial films as good as or better than those previously reported.

The measurements of photoemission of electrons from heteroepitaxial semiconductor films and of the transport of electrons in Al_2O_3 were carried further. Work functions of additional metals were determined, and the mechanism of electron transport through the insulator was studied further. Measurements of high-field transport properties of Si and GaAs heteroepitaxial films were also initiated.

The evaluation work in the final months of the second year included (1) study of the variation of the electrical properties of Si/Al_2O_3 with temperature, in which some effects attributed to high defect densities or inhomogeneous strains were observed; (2) the first stages of an extensive experimental study of the anisotropy of the electrical properties in Si/Al_2O_3; (3) evaluation of the electrical properties of Si films on $MgAl_2O_4$, with evidence that n-type films with mobilities higher than those obtained in the Si/Al_2O_3 system can be obtained; (4) additional measurements of the electrical properties of Si/Al_2O_3 to establish parametric relationships among temperature, growth rate, and substrate orientation; (5) further study of the photoelectric effects

observed in the $Si/A\ell_2O_3$ system, including verification that the observed phenomena do result from photoinjection of electrons from metal films into $A\ell_2O_3$ and determination of the work functions of additional metals and the heights of the metal-$A\ell_2O_3$ interface barriers; and (6) additional measurements of the high-field transport properties of heteroepitaxial films.

The anisotropy studies were concentrated in the $(221)Si/(11\bar{2}2)A\ell_2O_3$ and the $(100)Si/(01\bar{1}2)A\ell_2O_3$ systems. These two Si planes are basically different in that the anisotropy in the (221) plane can be expected for any Si heteroepitaxial system, while that in the (100) Si plane results from the anisotropic thermal contraction of $A\ell_2O_3$ and would not be present, e.g., in the $Si/MgA\ell_2O_4$ system. The mobility anisotropy factor A, defined as the ratio of the difference between the maximum and minimum values of carrier mobility in the plane of the film to the average value of the mobility in that plane, was found to be about 40 percent for the (221) plane and about 9 percent for the (100) plane. Results of calculations (Subtask 1) based on the piezoresistance effect in Si resulting from the difference in the thermal expansion coefficients for Si and $A\ell_2O_3$ agreed well with the experimental data. The calculations and the experimental results also indicate that (221) Si probably exhibits higher electron mobilities than other more commonly used orientations.

In the past six months further experimental studies of anisotropy in the electrical properties of $(111)Si/A\ell_2O_3$ have been in progress, using both $(10\bar{1}4)$- and $(11\bar{2}0)$-oriented $A\ell_2O_3$ substrates. The observed anisotropies have not agreed with the predictions of the piezoresistance model for this Si orientation, for reasons which have not yet been established (Subtask 1); anisotropies as high as 30 to 40 percent have been observed, while the stress model predicts values the order of 6 percent. These discrepancies are still under investigation because the anisotropy effects which have been discovered and largely explained by the stress model are highly significant to the entire technology of heteroepitaxial semiconductor devices.

During this same period the electrical evaluation of (111) Si films on $MgA\ell_2O_4$ has continued, with some evidence that the mobility decreases much more rapidly with film thickness (for thicknesses less than ~0.5 μm) than it does in the $Si/A\ell_2O_3$ system. This indicates a need for a comparative study of early stages of film growth in the two systems to assist in identifying the preferred substrate material for Si heteroepitaxial devices.

Recently, the experimentally observed inhomogeneity in the donor concentration in a CVD $Si/A\ell_2O_3$ film from point-to-point over the film area has been investigated in an attempt to identify and correct the cause.

In other recent evaluation work some additional attempts have been made to obtain high-field transport characteristics of Si and GaAs films on $A\ell_2O_3$; although contact problems have continued to be troublesome, high-field data have been obtained (including some at 77K) with good consistency among the samples measured. The study of photoelectric properties of $A\ell_2O_3$-based systems has concentrated on attempting to determine the nature of the dependence of the photoinjected current upon the condition and method of preparation of the $A\ell_2O_3$ surface.

a. Anisotropy Studies in the Si/$A\ell_2O_3$ System

Experimental studies of the anisotropy in the electrical properties of (111)Si/~$(11\bar{2}0)A\ell_2O_3$ have been nearly completed during this report period. This particular orientation of $A\ell_2O_3$ has been explored in detail during the past year since it yields high quality nominally (111)-oriented Si epitaxial films. The specific orientation of the substrate that has been used (5 deg from the $(11\bar{2}0)$ plane) is found to result in a Si film whose orientation is 4 deg off the (111) Si plane.

The anisotropy effects observed have not agreed with the piezoresistance calculations previously carried out for the (111)Si/$(11\bar{2}0)$ $A\ell_2O_3$ system. These calculations predict a mobility anisotropy, described by an anisotropy factor A (Ref 4) of 6.4 percent with a maximum mobility occurring parallel to one of the $A\ell_2O_3<1\bar{1}00>$ directions in the plane of the substrate. In contrast, the experimental data indicate that a mobility maximum occurs approximately 50 deg from the $[1\bar{1}00]$ axis. The magnitude of the anisotropy varies considerably for the samples measured but averages ~16 percent. Table 8 shows the pertinent results obtained from a computer fit of the data on various samples. As in previous planes analyzed, a fit is made to the equation $\mu/\mu_o = (B + C \cos 2\theta)^{-1}$, where B and C are constants.

The transverse effect, given theoretically by an equation of the form $E_T/j\rho_o = D \sin 2\theta$, where E_T is the transverse electric field, has also been examined experimentally. The coefficient D, deduced from a computer fit to the data, is also given for various samples in Table 8. The experimental curve for the transverse effect is found to result in $E_T = 0$ at approximately 50 deg from the $[1\bar{1}00]$ axis. The theoretical treatment for the "on-axis" case predicts a zero transverse field for $j//[1\bar{1}00]$. Thus, the experimental results for the transverse effect are displaced the same amount from the theoretically predicted direction as they are for the longitudinal effect.

Calculations for the off-axis case (5 deg from the $(11\bar{2}0)$ plane) have been completed (see Subtask 1). Both the location of the mobility maximum and the magnitude of the anisotropy calculated from the thermal stress model do not appear to agree with the experimental results discussed above.

Studies of the electrical anisotropy in $(\bar{1}11)$Si/$(10\bar{1}4)A\ell_2O_3$ have also been continued during this report period. Detailed data on six films grown in a vertical reactor and three films grown in a horizontal reactor have been obtained. Those grown in the vertical reactor were found to have considerable scatter in the mobility data, probably a result of inhomogeneities in donor concentration in different regions of the film. Estimates indicate that the anisotropy factor (a computer fit has not yet been carried out) for these films is ~30 percent. The three films grown in the horizontal reactor showed relatively homogeneous properties and little scatter in the mobility, although the mobilities were quite low. The latter films yield an anisotropy factor of ~40 percent.

A summary of the data obtained on these samples is shown in Table 9. The coefficient D of the transverse effect for this orientation averages 0.17, compared with the theoretically predicted value of 0.012. Also shown in the table is the maximum variation in carrier concentration (Δn) measured on the different legs of a given sample. It can be seen that the homogeneity in film properties (represented by a small Δn) is much better for the films grown in the horizontal system, although the average mobilities of the films are lower.

Table 8. Anisotropy Parameters for ~(111)Si/~(11$\bar{2}$0)Al_2O_3

Sample No.	μ_A (cm^2/V-sec)	A (Percent)	Angle of μ_{max} from [1$\bar{1}$00] (deg)	D	Angle of Zero Transverse Effect (deg)
LM-71	489	32.5	42	0.158	42
LM-67	578	14.6	47	0.153	45
LM-83	557	6.9	55	0.091	51
LM-91	587	11.0	63	0.046	71
LM-105	570	15.8	55	0.077	55
LM-109	527	21.5	44	0.13	50
LM-110	594	10.8	41	0.17	45
Averages		16	50	0.12	51

It is evident that the anisotropy in mobility and the associated transverse effect in the (111)Si/(10$\bar{1}$4)Al_2O_3 system are much larger than the values predicted (~4 percent and 0.012, respectively) by the stress model heretofore applied. Further studies of the (111)Si system are clearly necessary before an understanding of the origin of the discrepancies between theory and experiment can be acquired.

Attempts have been made recently to examine the variation of the anisotropy factor in (221)Si/(11$\bar{2}$2)Al_2O_3 films as a function of film thickness. It is hoped that such data may provide information of the variation of stress in heteroepitaxial films with film thickness. The results of this preliminary study are shown in Figure 12, where the measured anisotropy factor A and transverse-effect coefficient D are plotted versus film thickness. Although there is considerable scatter in the data, there does appear to be a trend for the anisotropy effects to increase for the thinner films. At the present time, however, there is still some question as to whether the anisotropy is a function of the average mobility in the film. Such a dependence of anisotropy upon mobility would also lead to the results shown in Figure 12, since the mobility decreases with decreasing film thickness. Further experiments now being planned should provide more insight into this question.

In order to rule out surface conduction effects as a significant contributor to the observed anisotropy in Si/Al_2O_3 films, a set of photolithographic masks has been designed to allow measurement of transport properties under flat-band conditions. Using this technique, the anisotropy bridge pattern will be covered with an oxide and the active portion of the bridge will in turn be covered with an Al film. This structure will then form an MOS device, and the transport properties will be measured as a function of gate voltage.

Table 9. Anisotropy Parameters for (111) Si/(10$\bar{1}$4) $A\ell_2O_3$

Sample	Thickness (μm)	Carrier Conc. (cm^{-3})	Anisotropy Factor A (percent)	Transverse Effect D	Mobility μ_A ($cm^2/V\text{-sec}$)	Variation in Carrier Conc. (Δn)	Comments
LG-92	1.95	3.54×10^{16}	-28	-0.12	-440	26	Vertical Reactor
LG-98	2.01	3.86×10^{16}	24 • / 33 •	0.16 • / 0.18 •	437 • / 485 •	18	Vertical Reactor
JP-48	1.68	2.39×10^{16}	36	0.199	445	25	Vertical Reactor
LG-79	1.82	3.86×10^{16}	30	0.078	460	21	Vertical Reactor
LG-77	1.84	4.08×10^{16}	24	0.103	455	17	Vertical Reactor
LG-100	1.83	3.8×10^{16}	18	0.127	450	26	Vertical Reactor
LG-111	2.08	5.57×10^{16}	44	0.220	328	7	Horizontal Reactor
LG-105	2.05	5.71×10^{16}	41	0.271	320	13	Horizontal Reactor
LG-109	1.99	4.99×10^{16}	39	0.270	297	7	Horizontal Reactor

• Separate numbers deduced from the two bridge patterns on this sample.

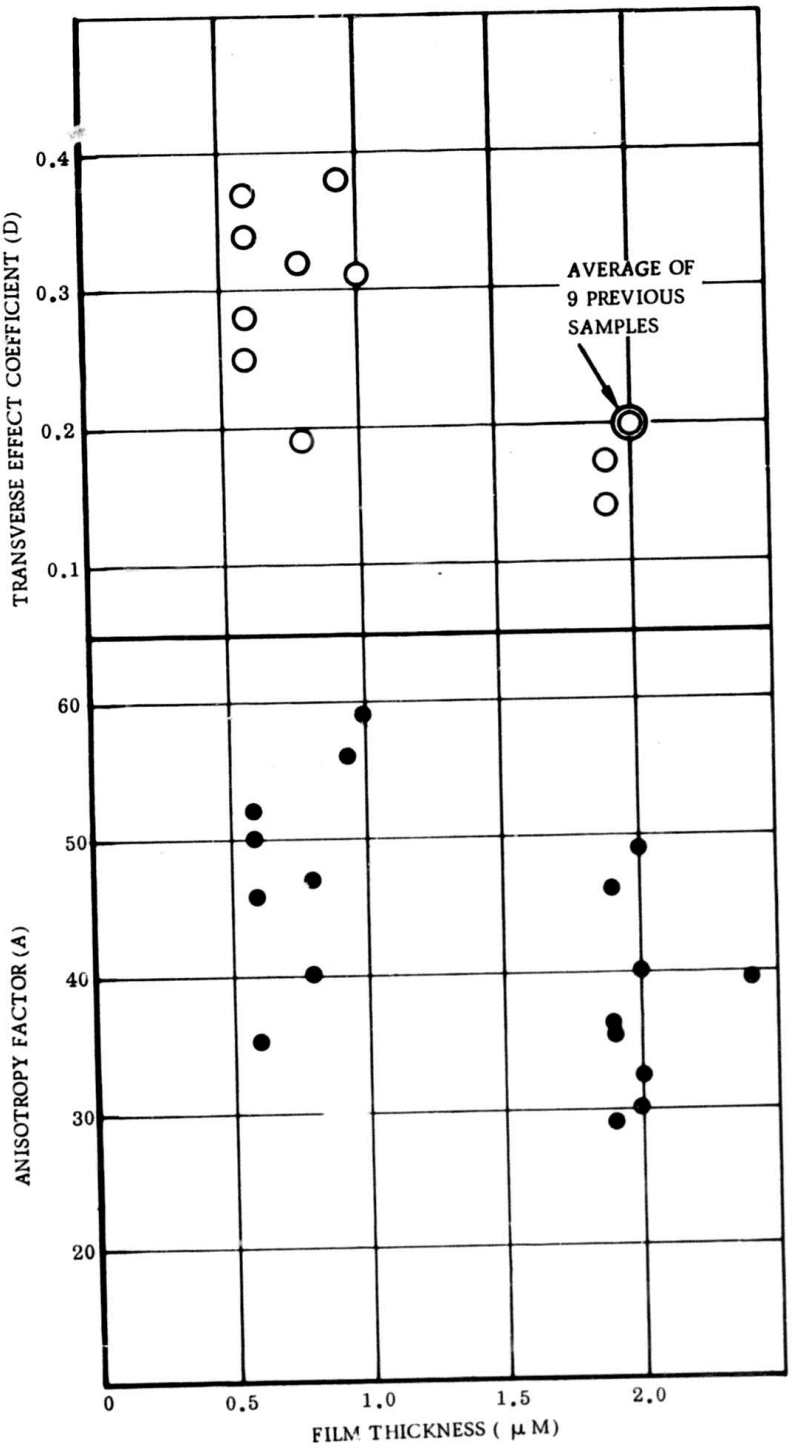

Figure 12. Anisotropy and Transverse-effect Coefficient for Various Film Thicknesses for (221)Si/(11$\bar{2}$2)Aℓ_2O_3 Samples

In order to rule out the possibility that anisotropic effects may be associated with "warm-electron" conduction (i.e., nonohmic behavior) the current-voltage relationship was examined over two orders of magnitude of current in several anisotropy samples. The results showed ohmic behavior over the whole range of currents (and electric fields), indicating that this effect is not pertinent to the present anisotropy results. (See also Subtask 1.)

b. $Si/MgAl_2O_4$ Studies

The apparent nonreproducibility of the electrical properties of Si films grown on $MgAl_2O_4$ substrates over a considerable period of time has suggested that substrate crystal origin and surface preparation may have more significant influence on film quality than in the Si/Al_2O_3 system. Accordingly, preliminary experiments have been undertaken to evaluate the growth of $Si/MgAl_2O_4$ using substrates of various origins with growth surfaces prepared and treated in a variety of ways.

The Si films were grown under nominally the same growth conditions which have previously yielded good quality Si on Al_2O_3 substrates. The preliminary results indicate that no firm conclusions can yet be drawn: Hall mobility variations from approximately 400 to about 750 cm^2/V-sec showed no definite trends relating to substrate origin and/or preparation. This suggests that an additional factor or factors may be controlling the Si film quality on $MgAl_2O_4$ substrates. Further experiments pursuing this problem will be undertaken during the last six months of the program.

The electrical properties as a function of film thickness have been examined in two n-type $Si/(111)MgAl_2O_4$ films. Data were obtained by successively thinning the films and remeasuring the electrical properties. The mobilities of the as-grown films were greater than those obtained for Si/Al_2O_3 films of approximately the same thickness and studied in the same way (Ref 3).

Data on a 5.4 μm-thick sample are shown in Figure 13 and similar data on a 1.4 μm-thick sample are shown in Figure 14. The mobilities were found to decrease much more rapidly with film thickness for thicknesses less than ~0.5 μm than was the case for the Si/Al_2O_3 films. This result is rather surprising and suggests that additional comparisons between the early stages of growth of (111)Si on Al_2O_3 and on $MgAl_2O_4$ substrates should be undertaken. If consistent results were to be obtained verifying the behavior described above it could be a significant factor in the choice of substrate for device applications using films ~1 μm thick.

c. Studies of Homogeneity of Properties of Si/Al_2O_3 Films

The problem of inhomogeneous donor concentrations in different regions of Si/Al_2O_3 films, which has seriously complicated the analysis of electrical anisotropy in these films, has been under investigation during the past several months. In an attempt to produce films with more uniform doping impurity distributions, a number of films were grown with only one substrate in the reactor for each run. (Most often, two or three substrates are employed simultaneously.) Anisotropy measurements on these samples generally did not show enough of an improvement in homogeneity for this technique to be considered a solution. For example, two $(221)Si/(1\bar{1}\bar{2}2)Al_2O_3$ samples still showed an average of 29 percent variation in carrier concentration in different regions of the film, compared with an average of 35 percent obtained on nine previous samples.

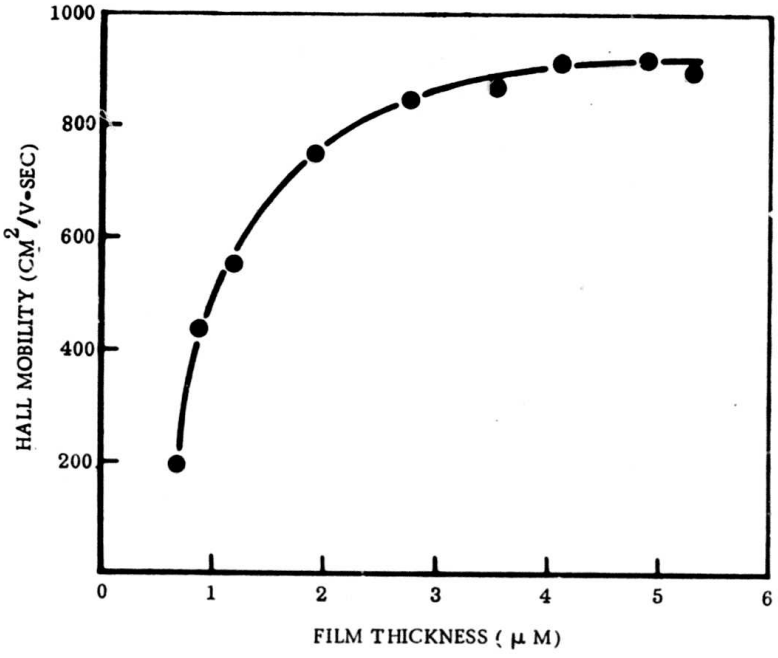

Figure 13. Hall Mobility as Function of Film Thickness for N-type (111)Si/(111)$MgAl_2O_4$. (Sample initially 5.4 μm thick.)

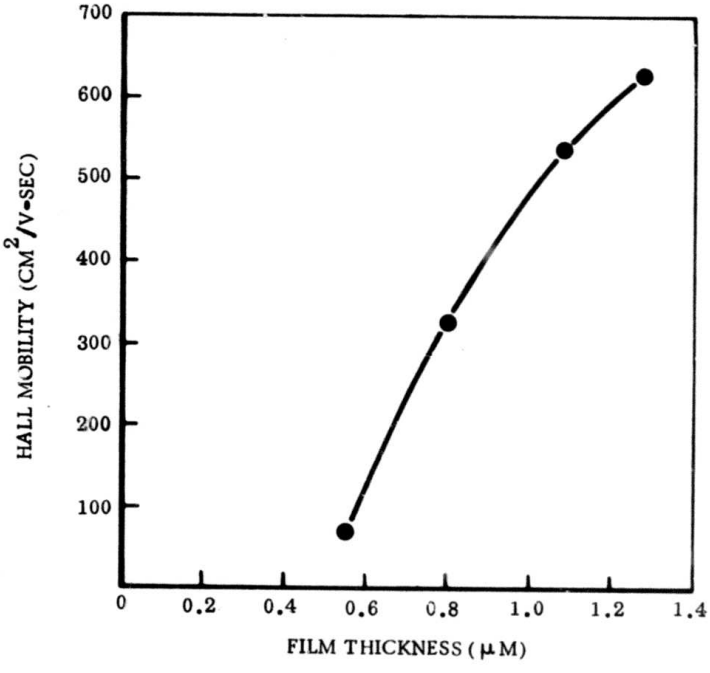

Figure 14. Hall Mobility as Function of Film Thickness for N-type (111)Si/(111)$MgAl_2O_4$. (Sample initially 1.4 μm thick.)

In order to quantify the extent of dopant variation across a given Si film, carrier concentration data from anisotropy samples formed in films grown simultaneously were correlated with their position on the rf-heated susceptor during growth. Since the exact positioning of the samples on the susceptor was not known, it was assumed that there is a radial gradient of carrier concentration such that the maximum concentration in the films would be obtained in the region grown at the center of the susceptor. The position of each leg of the anisotropy pattern on the susceptor could then be deduced so that a plot of the carrier concentration N_D versus distance from the center of the susceptor could be made.

Such a plot is shown in Figure 15; the carrier concentration has been normalized to the value of carrier concentration at the center of the susceptor (N_D^c). Each curve represents data for two anisotropy samples grown at the same time. (Each sample yields 10 data points corresponding to the 10 legs of the anisotropy bridge pattern.) The results of three runs are plotted in the figure; one shows a minimum variation in carrier concentration (~10 percent), one shows a maximum variation (~45 percent, and one is between the other two. The closeness of the data points to a smooth curve lends confidence to the validity of the assumption that a radial concentration gradient does indeed exist.

The reasons for the variations are not known at this time, but may relate to gas flow characteristics in the reactor. This is suggested by the fact that growth in a horizontal reactor (where presumably the gas flow is more laminar in nature) has consistently yielded more homogeneous films. Alternatively, the variation in temperature across the susceptor due to inhomogeneous heating by the rf coils has been examined. Preliminary measurements of the variation in temperature as a function of position on the susceptor indicate that temperature gradients of as much as 5-20C over a distance of 0.5 in. may exist at the growth temperatures (1000-1100C). Although the exact profiles are not known at this time, if a temperature gradient of 20C in 0.5 in. is assumed it is possible to use previous data to estimate the variation of carrier concentration to be the order of 30 percent. Such a large temperature gradient may well account for the observed film inhomogeneities.

d. Miscellaneous Film Evaluation Studies

Profiling studies have been carried out on several p-type $Si/A\ell_2O_3$ samples. The films were grown with no intentional dopants added; the acceptor impurities that were present resulted from $A\ell$ autodoping from the substrate. Measurements of electrical properties were made after successively reducing the film thickness by polishing techniques; the results indicate a slight decrease in acceptor concentration as the $Si\text{-}A\ell_2O_3$ interface is approached.

This demonstrates that the electrically active $A\ell$ does not increase in concentration near the interface, as might be expected. Presumably some of the $A\ell$ nearer the interface forms neutral complexes with the higher concentrations of defects and/or impurities which may be present in the film near the $A\ell_2O_3$.

The design of photolithographic masks for the fabrication of MOS transistors to examine field-effect mobility as a function of channel orientation in the plane of $Si/A\ell_2O_3$ films has been completed. The masks for these studies should be available early in the next report period.

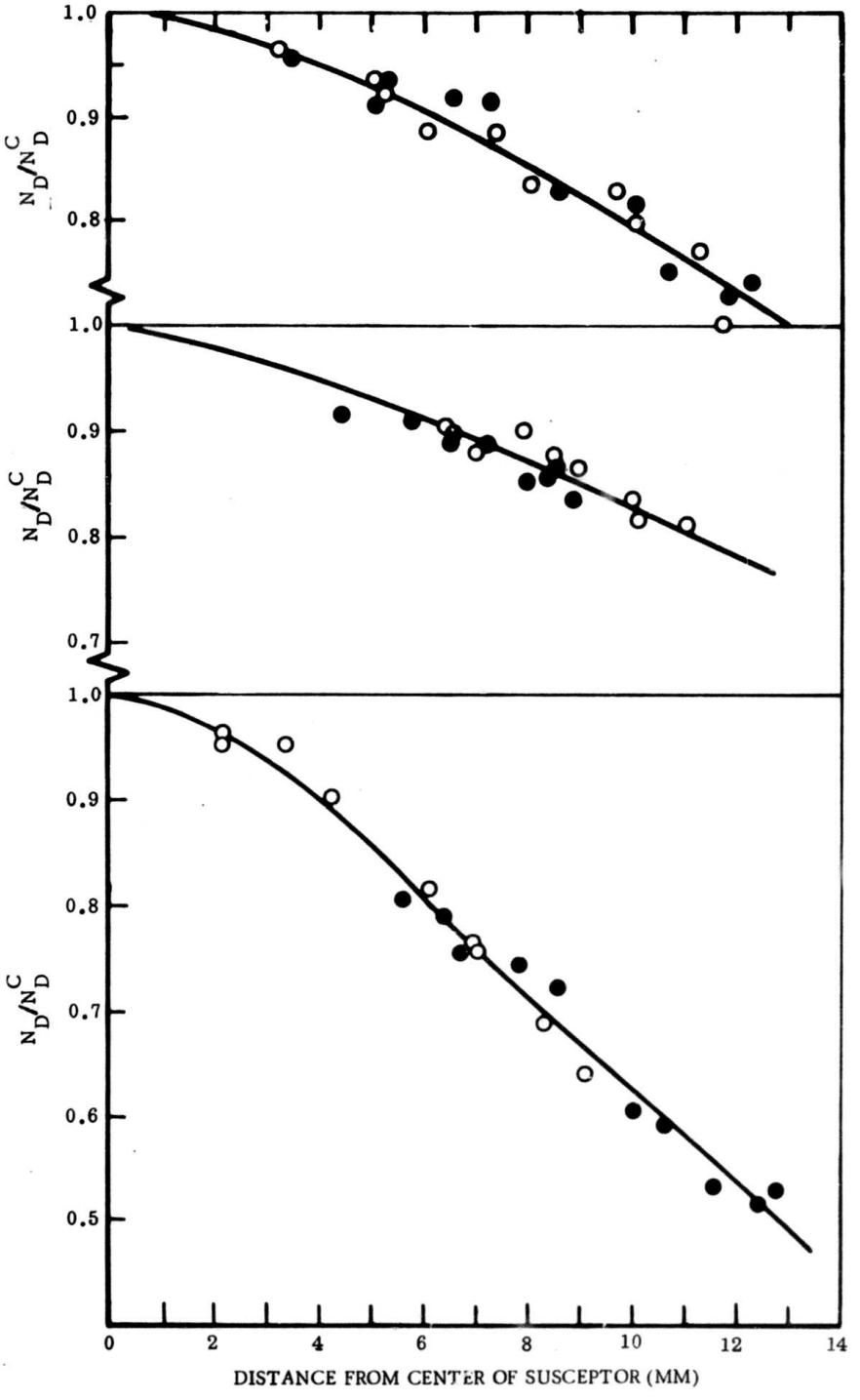

Figure 15. Normalized Carrier Concentration as Function of Distance from Center of Susceptor (Sample Pedestal) for Pairs of $Si/A\ell_2O_3$ Samples Grown Simultaneously. (See text.)

In previous reports (Refs 3, 4) experiments at UCLA using the photoelectric technique to study the characteristics of $A\ell_2O_3$ films have been described. These measurements have been continued during this six-month period. Attempts are still being made to perfect the experimental conditions for the study of transport properties of electrons injected into the $A\ell_2O_3$ substrates by the time-of-flight measurement method. In these experiments a light chopper is used to pulse the light beam, and the pulsed light beam (with a rise time the order of 0.1 msec) is incident on the metal electrode of the MIM sandwich. A 1-megohm resistor is connected in series with the bias voltage supply and the sample. An oscilloscope measures the voltage due to the photocurrent pulse across the 1-megohm resistor. The difficulty, however, is in having the input-circuit time constant low enough while still being sufficiently sensitive to measure very low current levels the order of 10^{-10} amp.

In the transient measurements, some ionization effects were also observed which interfered with the photocurrent measurements. This emphasized the need for ensuring that the incident UV light falls only on the center of the metal electrode a d not anywhere else. The steady-state photocurrent-voltage characteristics are also being measured, and it is hoped that an understanding of the mechanism for transport of injected electrons in the $A\ell_2O_3$ substrates can be acquired thereby.

The high-field transport properties of heteroepitaxial Si and GaAs films are still under study at UCLA. The experimental arrangement was described in an earlier report (Ref 3). As indicated in the last semiannual report (Ref 4), ohmic contact to n-type GaAs films was achieved using a Ag-Ge-In alloy.

Ohmic contact to the Si samples has also been obtained; a 5000Å-thick SiO_2 layer was deposited on the n-type Si wafer using the "silox" process. Windows were then cut in the oxide, using a photolithographic technique, in the region where the ohmic contact was required. Phosphorus was next deposited in the window at 950C for 5 to 10 min. $A\ell$ was evaporated over the entire sample, and then the excess was removed by photolithography. The $A\ell$ remaining on the contact window was sintered at 530C for 3 min, resulting in ohmic contact to the n-type Si.

Results of measurements on a GaAs film sample and three different regions of a Si film sample, both on $A\ell_2O_3$ substrates, are shown in Figures 16 and 17, respectively. Both films are n-type. The data for GaAs are similar in general behavior to that previously reported (Figure 42, Ref 4), with a deviation from linear behavior for fields beyond about 1.7kV/cm and a "peak" at about 3kV/cm, and with a subsequent current increase at higher fields due to specimen heating. The data for Si are similar but with no evidence of the heating effect at higher fields.

In order to interpret these data properly it is necessary to obtain supplementary measurements on these samples as a function of temperature and also on films in several different crystallographic orientations. For this purpose two sample chambers - one for low-temperature measurements and one for use at elevated temperatures - were fabricated so that measurements could be made throughout a wide range of temperatures. A new mask set was made to permit measurement of the i-E characteristics as a function of direction of applied field in the plane of the sample, to allow for possible anisotropy of the effects. Figure 18 shows the i-E data for the n-type Si sample of Figure 17, taken at three different temperatures. The functional dependence is seen to remain linear for fields up to nearly 5kV/cm at 77K, with evidence of increased resistivity in the vicinity of room temperature, as expected for Si. Additional data of this type are being obtained, with a summary of results to be given in a future report.

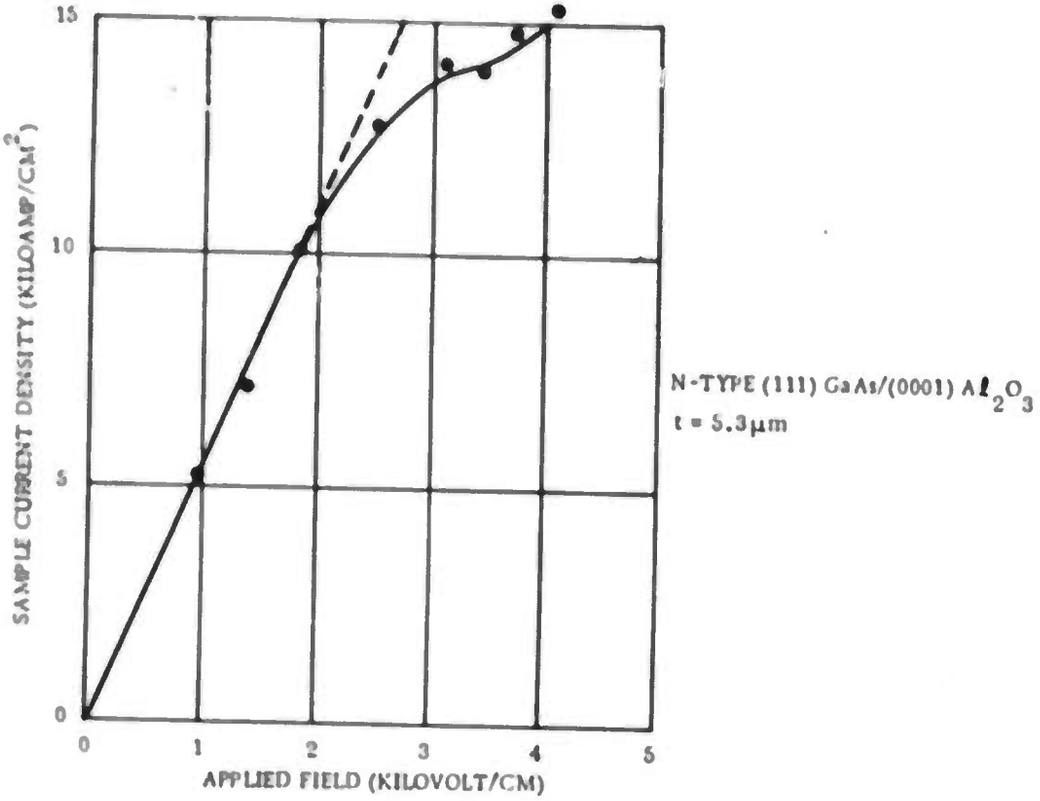

Figure 16. High-field I-E Characteristic of N-type (111)GaAs/(0001)Al_2O_3

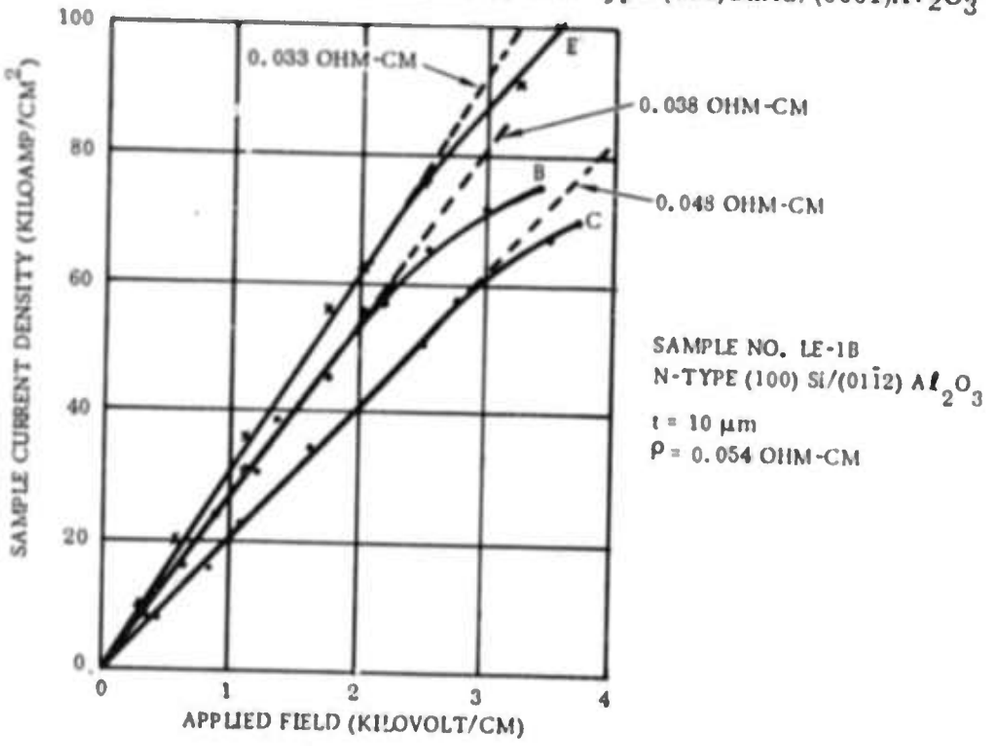

Figure 17. High-field I-E Characteristic of N-type (100)Si/(01$\bar{1}$2)Al_2O_3

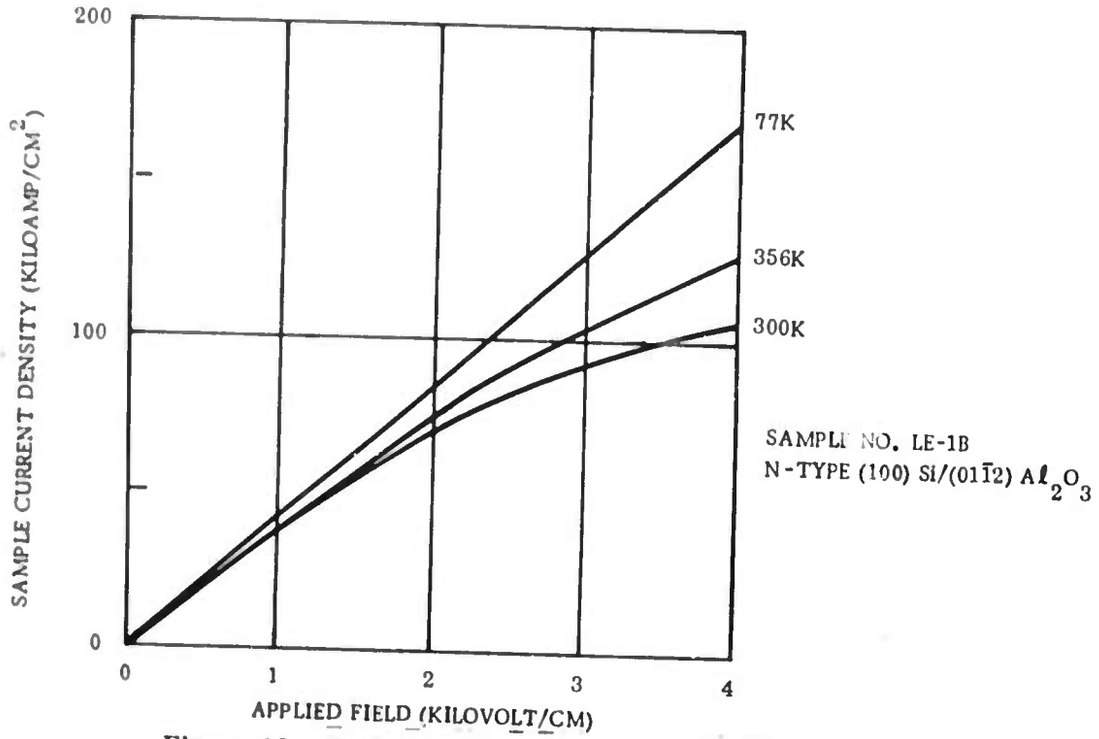

Figure 18. High-Field i-E Characteristic of Sample of Figure 17 at Various Temperatures

7. SUBTASK 7. DESIGN AND FABRICATION OF DEVICES

In the first year of the contract apparatus for determining carrier lifetime by C-V measurement in MOS structures was designed and constructed, and tests were begun. A special MOS structure was designed for measurement of channel conductance, high- and low-field transport properties, and various interface characteristics of heteroepitaxial films. Initial attempts to fabricate Schottky-barrier diodes in $Si/A\ell_2O_3$ films as a means of evaluating their electrical properties were not successful.

In the first half of the second year the preliminary design of a Schottky-barrier type of FET was completed for use in fabricating experimental FET structures in GaAs/insulator films for operation at 1 GHz. Preliminary results on carrier lifetime in $Si/A\ell_2O_3$ films were obtained, after initial development of the measurement technique on bulk single-crystal Si samples was completed and after impurity contamination problems encountered in the oxide growth process were solved.

During the second six months of the second year the device-oriented effort centered about the determination of carrier lifetimes using the MOS-pulsed-capacitance technique and attempts to fabricate a Schottky-barrier FET in $GaAs/A\ell_2O_3$. Numerous processing difficulties were encountered in both of these investigations. An analysis was made to evaluate the effect of the impurity redistribution in the Si in the region near the oxide interface (resulting from the oxidation process used for making the MOS structures) on the interpretation of lifetime data obtained by this technique.

Lifetime measurements in both Si and GaAs films as a function of film thickness, carrier concentration, and crystallographic orientation were obtained on numerous samples, with thicknesses ranging from ~1 to ~10μm and resistivities from ~0.01 to ~1 ohm-cm. Analysis of the data for Si films indicated values ranging from 9×10^{-12} to $\sim 5 \times 10^{-10}$ sec. Attempts were made to find correlations between carrier lifetime and film resistivity and thickness but those studies have not been completed. Similar measurements were begun on GaAs films on $A\ell_2O_3$ substrates.

In the past six months an analysis of surface effects on the results of the lifetime measurements was carried out. Recent device efforts have produced Schottky-barrier diodes (in n-type $Si/A\ell_2O_3$ samples) having good reverse but unsatisfactory forward characteristics, so further improvements are being sought. The Schottky-barrier FET structures that have been made are still not satisfactory, with further work still in progress. Plans have also been made to adapt surface charge transport techniques developed with bulk single-crystal Si at NR (to facilitate fabrication of a variety of memory, shift register, analog delay line, and optical imaging devices) to $Si/A\ell_2O_3$ or $Si/MgA\ell_2O_4$ to produce charge-coupled devices (CCD). Observation of CCD operation will give information about the density of trap states at the Si-oxide interface, the rate of generation of minority carriers in the Si film, and the effects of various processing steps on these characteristics. An existing set of masks and an already-developed process will be used initially; tolerant specifications will permit a minimum of experimental effort being spent studying charge transfer itself. The Si to be used must have carrier concentrations $<10^{16}cm^{-3}$ and preferably be n-type; film thickness should exceed ~3μm to accommodate the gate depletion regions.

a. Minority Carrier Lifetime Measurements

The pulsed-capacitance MOS technique used at UCLA for measurement of minority carrier lifetimes in the heteroepitaxial films has been described in previous reports (Refs 3, 4). This technique has been used to provide data on both the minority carrier lifetime τ_g and the surface recombination velocity s in $Si/A\ell_2O_3$ films of thicknesses ranging from 1.4 to 9.0μm and of various resistivities in the (100) and (111) orientations. The following analysis of the pulsed-capacitance MOS technique has been performed in order to establish the effects of surface phenomena on the lifetime measurements.

Let D be the diameter of the gate electrode of the n-type MOS capacitor. (The following analysis is valid for $D \geq 20\mu m$.) When a negative voltage is applied on the gate electrode a space-charge region (SCR) is formed in the semiconductor. The value of s is a maximum immediately after the application of the voltage step (depleted surface) but decreases rapidly as the minority carrier concentration increases throughout the transient. If the MOS capacitor is pre-biased into inversion prior to the depleting voltage step, then the surface recombination velocity in the region of the surface directly beneath the gate electrode will remain at a very low value throughout the transient.

Due to impurity redistribution effects the SCR width y_d along the Si surface will differ from the SCR width x_d perpendicular to the gate electrode. For a boron-doped Si sample oxidized in steam at 900C typically $y_d = 2.7\ x_d$. For a phosphorus-doped Si sample oxidized under identical conditions $y_d = 0.5x_d$. With the surface generation currents being reduced to an edge effect when pre-biased into inversion and with impurity redistribution effects being considered, the MOS transient is now described by the equation

$$-\frac{d}{dt}\left(\frac{C_o}{C}\right)^2 = \frac{n_i C_o \left(\frac{C_F}{C} - 1\right)}{C_F N_B \left[1+\left(\frac{N_S}{N_B} - 1\right) \exp\left(-\left\{\frac{C_1}{C} - \frac{C_1}{C_o}\right\}\right)\right]} \cdot \frac{1}{\tau_{g_{eff}}}, \qquad (3)$$

where C = MOS capacitance per unit area,

C_o = oxide capacitance per unit area,

C_F = MOS capacitance per unit area at end of transient,

N_B = Si bulk doping concentration,

N_S = Si surface doping concentration,

n_i = intrinsic carrier concentration, and

$$C_1 = \frac{\epsilon_s}{x_1}.$$

In the last term ϵ_s = Si permittivity, x_1 is a parameter that defines the extent of the impurity redistribution (Ref 4), and $\tau_{g_{eff}}$ is an "effective" thermal generation lifetime given by

$$\frac{1}{\tau_{g_{eff}}} = \frac{1}{\tau_g} + \frac{4as}{D}, \qquad (4)$$

where τ_g = actual bulk thermal generation lifetime, D = gate diameter, and $a \equiv \sqrt{\frac{N_B}{N_S}}$.

The s value in Eq (4) is the value of the surface recombination velocity for the depleted lateral SCR and so should represent the maximum surface recombination velocity of the Si sample. The effect of the surface on the MOS transient has now been reduced to that of an edge effect. Schroder and Nathanson (Ref 9) first noted this effect on pulsing from accumulation to inversion. With the capacitor pre-biased into inversion, however, the surface effects are essentially eliminated.

The maximum possible value of s is given by $s_{max} = \frac{\bar{v}}{2}$, where $\bar{v}$ is the thermal velocity of the minority carriers. For holes with $\bar{v} = 5 \times 10^6$ cm/sec the maximum possible value of the surface term $\frac{4as}{D}$ is, for a = 0.5 and D = 5×10^{-2}cm, equal to 10^8 sec^{-1}. For bulk thermal generation lifetime values of $\tau_g \leq 10^{-9}$ sec the surface generation term becomes negligible in comparision with the bulk generation term. For all of the Si/Al_2O_3 samples measured thus far $\tau_{g_{eff}}$ was found to be $\leq 5 \times 10^{-10}$sec, so that it may be concluded that the generation-recombination mechanisms are bulk - rather than surface-dominated in these samples.

One further feature of Eq (4) is that a plot of $1/\tau_{g_{eff}}$ versus 1/D should yield a straight line whose intercept on the $1/\tau_{g_{eff}}$ axis is proportional to $1/\tau_g$ and whose slope is proportional to s.

No correlation has been found between τ_g and the Si resistivity in these $Si/A\ell_2O_3$ samples for resistivity values between 0.018 and 0.3 ohm-cm. Values from 2×10^{-11} to 5×10^{-10} sec were observed for τ_g. The Si film thicknesses ranged from 1.4 to 9.0μm in the samples studied. Lifetime values of 6×10^{-11} sec were observed in the thinnest (1.4μm) films and values of 5×10^{-10} sec in the thickest (9.0μm) films. In general, the thicker films exhibited the larger τ_g values, but much scatter in the data is evident. All of the samples have been pulsed at several pulse amplitudes in order to investigate the variation in lifetime with depth below the top surface of each film; these data are presently being analyzed. Low temperature measurements are also being performed on Si and GaAs films on $A\ell_2O_3$ in an attempt to establish the effective energy level of the traps involved.

b. Miscellaneous Device Studies

The attempts to develop a Schottky-barrier FET in heteroepitaxial film structures have been continued at UCLA. The main difficulty encountered in this work to date has been in obtaining good ohmic contact to the source and drain regions of the FET structure. The method finally found successful has been described in the discussion of high-field transport property measurement (Subtask 6).

In order to obtain a good Schottky-barrier exhibiting low leakage current several alterations in the masks and the associated processing steps were made; these resulted in fabrication of devices considerably improved over those made previously. However, Schottky-barrier diodes in these samples still exhibited leakage currents higher than desired.

Despite this continuing problem, such Schottky-barrier diodes have been used as the basis for Schottky-barrier FET structures fabricated in the composites. The drain-to-source current-voltage behavior of one of these FET's in $Si/A\ell_2O_3$ is shown in Figure 19. The principal feature of the data shown is the domination by leakage currents in the low current-voltage region. Further attempts to improve the FET characteristics are in progress.

Preliminary studies of the properties of photovoltaic cells fabricated in $Si/A\ell_2O_3$ samples, designed to exploit some of the unique features of these composites, have been undertaken. Both a p-n function cell and a Schottky-barrier cell have been designed, although only the latter has been fabricated to date. A p-type $Si/A\ell_2O_3$ film 1μm thick was used for deposition of Aℓ contacts, after the usual buffer etching and predeposition cleaning of the Si surface. The Aℓ electrodes were sintered at 500C in a N_2 atmosphere, and Cr-doped Au was deposited to form the Schottky-barrier electrodes on the composite sample. This and similar devices are now under test for photovoltaic response; results will be described in a later report.

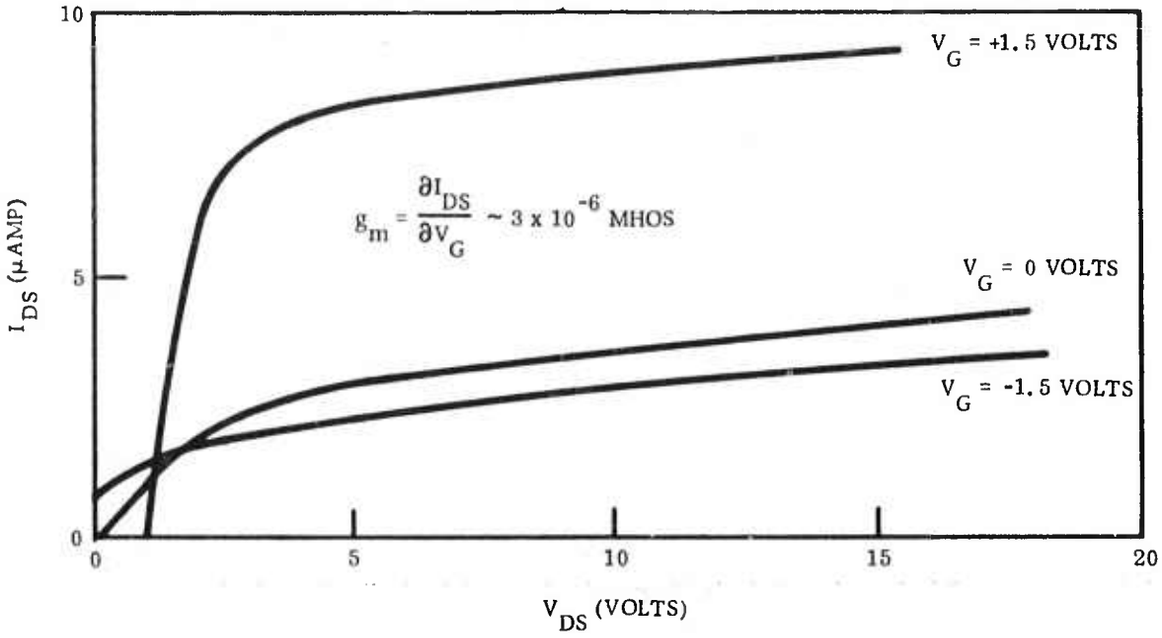

Figure 19. Drain-to-Source I-V Characteristics of Schottky-Barrier FET in $Si/A\ell_2O_3$ Composite

SECTION III

WORK PLANNED FOR NEXT SIX MONTHS

The planned effort for the next six months in the seven subtasks of the program will include the following. There will be increased emphasis on device work in this period. Because this will be the final six-month period of the originally planned program it is anticipated that various changes will be made during the conduct of the work to ensure that the subtasks will all be advanced to the required level of accomplishment by the end of the contract performance period.

1. SUBTASK 1. THEORY OF EPITAXY AND HETEROEPITAXIAL INTERFACES

The theoretical activities will be of two types and will include (1) additional studies of the piezoresistance effect and mobility anisotropy for certain orientations of $Si/A\ell_2O_3$ films and (2) completion of the computer simulation of Si growth on $A\ell_2O_3$ by pairwise-potential modeling.

The comprehensive description of the mathematical framework of the $Si/A\ell_2O_3$ piezoresistance - mobility studies will be completed and will be published. Attempts will be made to resolve the current difficulties in assessing and interpreting the experimental results for ~(111) Si films on various substrates. The current anisotropy studies have suggested that lattice constant mismatch stresses should be examined qualitatively as a function of film/substrate orientations; an attempt will be made in terms of an atom-matching model and/or an interatomic potential model to determine if the qualitative and semiquantitative features of such stresses can explain the (111) Si results within the framework of a piezoresistance - stress model.

The interatomic potential modeling of the $Si/A\ell_2O_3$ system will also be resumed, initially for the case of Si on basal-plane $A\ell_2O_3$. The atomic configuration of a small cluster of Si atoms will be determined under the constraint of minimum energy. The end result sought is determination of the relative orientation between film and substrate in the $Si/A\ell_2O_3$ system. It is also intended that a second substrate orientation (perhaps $(01\bar{1}2)A\ell_2O_3$, which produces the (100) Si orientation) will be examined theoretically if time permits, with surface reconstruction and computer-simulated Si growth again attempted.

2. SUBTASK 2. DEPOSITION STUDIES AND FILM PREPARATION

The work of this subtask will explore further the conditions required to obtain optimized single-crystal Si growth on $A\ell_2O_3$ and $MgA\ell_2O_4$ of various crystallographic orientations in order to identify the preferred substrate for Si device applications. Particular attention will be paid to the use of $He-H_2$ carrier-gas mixtures in the growth process for Si and the effect of such mixtures on minimizing the autodoping phenomenon. The nature of the autodoping mechanism will be explored further, using bulk Si wafers and $A\ell_2O_3$ and $MgA\ell_2O_4$ substrates as sources of dopant in various gaseous atmospheres. The effects of gas flow rates and patterns, reactor and pedestal geometries, and temperature on film properties will also be examined. P-type doping techniques for Si films on insulators will be developed so as to permit the growth and study of multilayer structures and the accompanying film interfaces and permit the fabrication and evaluation of such devices as bipolar transistors. Achievement of higher mobilities in heteroepitaxial Si films has renewed the possibility that bipolar transistors may now be feasible in the Si/insulator system.

Experiments will also be performed to determine the properties of GaAs films grown on GaAs substrates and on Al_2O_3 and $MgAl_2O_4$ substrates which already contain high resistivity layers. Additional experiments with nucleation and early stage film growth behavior in the Si/insulator and GaAs/insulator systems will also be carried out in terms of the dependence of film electrical properties and structural characteristics on the method of preparation of the substrate. Multilayer films of GaAs of alternating conductivity type will be prepared on both Al_2O_3 and $MgAl_2O_4$ both for study of the interface problem and for fabrication of experimental device structures.

3. SUBTASK 3. ANALYSIS AND PURIFICATION OF CVD REACTANTS

The studies of the chemistry and reaction kinetics involved in the formation of Si films by SiH_4 pyrolysis and of GaAs films by the trimethylgallium (TMG)-arsine (AsH_3) reaction will be continued. Three main investigations will be undertaken.

The first is based on the data obtained to date for the TMG-AsH_3 reaction. These data suggest that the reaction of TMG with AsH_3 below 275C generates $(CH_3)_2GaAsH_2$ and $(CH_3GaAsH_2)_x$ as intermediates in the formation of GaAs. Experiments to isolate these compounds and examine their thermal decompositions will be continued. It is also planned that the reaction of $(CH_3)_3Ga$ with AsH_3 above 320C, where $(CH_3)_3Ga$ decomposes, will be investigated further.

The second series of experiments is the study of the pyrolysis of SiH_4 over Al_2O_3 prior to the deposition of one monolayer of Si, to clarify more exactly the role played by Al_2O_3 surfaces. The catalytic effect after the Al_2O_3 is preheated will be examined, and the observations will be carried out over a range of temperatures to establish the nature of the reaction in the Si deposition temperature region.

The third investiation will be an examination of the suggestion that the rate of SiH_4 pyrolysis should increase at temperatures above ~700C in the presence of H_2. Experimental data in the standard CVD reactors at NR indicate an increase in the "efficiency" of the pyrolysis reaction as H_2 is added to a He carrier gas and also an increase, for a given carrier gas, with temperature. The extent to which the pyrolysis reaction can be enhanced by temperature increase and by H_2 partial pressure increase in the range up to ~1000C will be examined carefully in these studies.

In addition to the chemical kinetics studies, the analysis of CVD reactants, primarily by mass spectrometric techniques, will be continued, as will collaborative efforts with various vendors to obtain reactants of improved purity. At the present time there is no plan to initiate the synthesis of any of the reactants at NR laboratories. However, long-planned experiments to determine impurity content (and identification) of a series of Si and GaAs heteroepitaxial films as a function of distance from the film-substrate interface will probably be carried out during this period utilizing new Auger electron spectroscopy apparatus; these data can provide an indirect measure of the purity of the reactants used. Growth conditions and the electrical properties of films will continue to be correlated with the results of reactant impurity analyses to attempt to identify the primary sources of the properties observed in these films.

4. SUBTASK 4. PREPARATION AND CHARACTERIZATION OF SUBSTRATES

A major part of the effort of this subtask consists of routinely preparing and characterizing substrates of $A\ell_2O_3$ and $MgA\ell_2O_4$ for use in growing Si and GaAs films for other parts of the program. In addition to this activity, however, the development of improved substrate surface preparation methods will continue to be a significant part of the subtask effort. Mechanical and chemical-mechanical polishing methods, gas-phase etching-polishing procedures, ion-beam sputtering methods, liquid-phase etching methods, and annealing cycles at various elevated temperatures, as well as various combinations of these procedures, will be further evaluated for the purpose of finding the best available procedure for producing surfaces for heteroepitaxy.

The preparation of ultra-thin (~200Å) substrates of $A\ell_2O_3$ for the in situ CVD experiments in the electron microscope (Subtask 5) will continue. The thinning technique now employed — mechanical polishing to 0.001 — 0.002 in. and subsequent ion-beam sputtering to ~200Å — will still be used. The alternative approach of chemically etching from ~0.004 in. thickness down to ~0.001 in. followed by ion-beam sputtering to ~200Å will be further investigated as a possible means of obtaining these substrates. Considerable effort will be placed on developing a technique for producing larger and more uniform thinned regions.

The depth-of-damage studies, initiated in the past six months using etch-rate methods, will be extended to other substrate orientations at various stages of surface preparation. Other specialized techniques of material evaluation, such as reflection electron diffraction, replica and scanning electron microscopy, X-ray topography, backscattering of charged-particle beams, and Auger electron spectroscopy will be further exploited in order to find correlations between the initial properties of the substrate surfaces and the eventual properties of the Si and/or GaAs films grown on these surfaces.

5. SUBTASK 5. STUDIES OF IN SITU FILM GROWTH IN THE ELECTRON MICROSCOPE

The initial work in the next six months will concentrate on determining the reproducibility of substrate heating and on calibrating the substrate temperature versus the grid heating current. If necessary in order to attain a higher temperature, tungsten grids will be substituted for the present stainless steel and a higher current substrate power supply installed.

In situ CVD experiments will be performed on $(01\bar{1}2)$-oriented $A\ell_2O_3$ substrates, with later experiments on (0001) and/or $(10\bar{1}4)$ orientations. The nucleation, growth, and coalescence process will be studied primarily as a function of temperature to determine the mechanism whereby structural defects (e.g., stacking faults and grain boundaries) are incorporated into the growing film. The effect of substrate surface defects, such as etch pits and scratches, on the film nucleation rate and the orientation of nuclei pinned at such defects will be examined and compared with nucleation phenomena on defect-free regions of the surface. All variables will be examined with particular emphasis on the differences, if any, between the nucleation and growth mechanisms observed in a CVD system and those known to exist for PVD systems. Both bright-field and dark-field transmission electron microscopy as well as electron diffraction analysis will be used in these investigations.

The effects of SiH_4/H_2 ratio and the total gas pressure will be examined experimentally later in the program. Further improvements in the motion picture recording system will also be made, if needed.

6. SUBTASK 6. EVALUATION OF FILM PROPERTIES

The routine evaluation of the structural and electrical properties of Si and GaAs heteroepitaxial films will be continued by means of various methods of X-ray and electron diffraction analysis, metallographic analysis, and measurement of both fundamental and device-related electrical properties. Experiments using backscattering analysis of charged particle beams will be resumed for establishing the depth and density of defects in the films, with the results to be correlated with characteristics of the substrates used to grow the films. Efforts to select the preferred substrate material in the Si/insulator system will continue, based on comparative measurements of film characteristics on $A\ell_2O_3$ and $MgA\ell_2O_4$ substrates.

It is anticipated that new analytical equipment soon to be available will permit successive Auger electron analysis and removal of thin layers of the semiconductor film by ion-beam sputtering to be repeated sequentially, thus making possible the investigation of the variation of film properties as a function of depth into the film. In addition, surface examination of both films and substrates will be carried out by techniques of scanning electron microscopy.

Studies of the anisotropy in electrical properties in the $Si/A\ell2O_3$ system will be continued with emphasis on determining the reasons for the anomalously large effects observed in Si films on or near the (111) orientation. Similar studies will be undertaken on the $Si/MgA\ell_2O_4$ system. Studies of the variation of electrical properties with temperature for $Si/A\ell_2O_3$ and $Si/MgA\ell2O_4$ films will be continued, with emphasis placed on isolation of those effects associated with thermally-induced stress. The $(221)Si/(11\bar{2}2)A\ell_2O_3$ system will be used primarily for this work, since recent study has shown that there are current directions in these films for which the stress effects produce either (1) mobility degradation, (2) mobility enhancement, or (3) no effect on mobility. Selection of the appropriate current direction thus will permit study of a variety of electrical properties. These measurements will be supplemented by studies of anisotropic effects in the field-effect mobility in MOS devices, of particular importance for potential device applications.

The measurements of high-field transport properties of Si and GaAs as a function of temperature, film resistivity, film thickness, and crystallographic orientation will be concluded. The studies of internal photoemission in $A\ell_2O_3$ at various temperatures will be continued to help to characterize $A\ell_2O_3$ substrate surface conditions; the effects of various annealing treatments on the photoemission characteristics will be explored. Measurements will be made of the current-voltage characteristics and of the quantum efficiency of the process in an attempt to model the charge transport mechanisms in $A\ell_2O_3$.

7. SUBTASK 7. DESIGN AND FABRICATION OF DEVICES

There will be an emphasis in the final six months of the program on the design and fabrication of experimental devices in both Si and GaAs films on $A\ell_2O_3$ and $MgA\ell_2O_4$ substrates. Some multilayer device structures will be grown directly (Subtask 2) by means of appropriate doping changes, but most devices will be fabricated by conventional post-growth processing.

Measurement of the properties of MOS devices will be used as a means for evaluating the characteristics of the $Si/A\ell_2O_3$ and $Si/MgA\ell_2O_4$ systems. Comparison of devices formed in Si on various orientations of $A\ell_2O_3$ and $MgA\ell_2O_4$ will be continued so that the goal of selecting a preferred substrate for the growth of Si on insulators can be realized. Attention will be given to the effects of stress on device performance, so that optimized device operation can be achieved.

Existing surface charge transport techniques developed with bulk Si will be adapted to the $Si/A\ell_2O_3$ and $Si/MgA\ell_2O_4$ systems to produce charge-coupled devices; observation of device operation will provide information on the density of trap states at the Si-oxide interface, the rate of generation of minority carriers in the film, and the effects of various processing steps on these characteristics. The fabrication and evaluation of both junction-type and Schottky-barrier photovoltaic cells will be continued, with cell performance characterized by current-voltage and quantum efficiency measurements under various conditions. The measurement of carrier lifetimes will be continued on both Si and GaAs heteroepitaxial films on $A\ell_2O_3$ and $MgA\ell_2O_4$ substrates by the MOS pulsed C-V technique. These measurements will be made as a function of film thickness, orientation and resistivity throughout a range of sample temperatures. Modifications now being made in the measuring equipment will permit measurement of lifetimes as low as 10^{-12} sec. Analysis of the defect and impurity levels in Si and GaAs heteroepitaxial films using pulsed Schottky-barrier diode measurements will also be undertaken.

In addition to fabricating, testing, and evaluating Schottky-barrier diodes and FET's in both Si and GaAs films on $A\ell_2O_3$ and $MgA\ell_2O_4$ substrates, some bipolar devices will be made in which carrier lifetime will be improved by $HC\ell$ gettering during the oxidation process. Attempts will also be made to fabricate, test and evaluate a solid state photomultiplier using heteroepitaxial films. Other optical device applications involving the unique optical transparency of the insulator substrate will also be examined if time permits.

SECTION IV

PROGRAM SUMMARY TO DATE

The overall objective of the program, for which this is the Fifth Semiannual Report, is to carry out a fundamental study of the nucleation and film growth mechanisms in heteroepitaxial semiconductor thin films, leading to new knowledge and understanding of these processes, and then to apply these results to the preparation of improved semiconductor thin films and thin-film devices on insulating substrates.

The specific technical objectives of the three-year program are the following:

1. Investigation of the many aspects of the mechanisms of heteroepitaxial film growth, to establish (through accumulation of basic knowledge) sets of technical guidelines for the preparation of better films which can then be applied to real situations.

2. Preparation of improved, high-quality, device-grade heteroepitaxial films of Si and GaAs on insulating substrates by chemical vapor deposition (CVD) methods.

3. Development of methods of characterizing heteroepitaxial films as to their suitability for subsequent device fabrication.

4. Design and fabrication of selected thin-film devices which take advantage of the unique properties of such films.

The general plan for accomplishing these objectives involves the study of the fundamentals of heteroepitaxial semiconductor film growth on insulating substrates, with specialized device fabrication used as a means of evaluating certain film properties (and thus as a measure of film quality as the program progresses) and as a means of exploiting those properties unique to heteroepitaxial semiconductor-insulator systems.

The determination of the fundamental mechanisms, properties, and processes to be investigated is based on extensive background knowledge of epitaxy and thin-film device difficulties encountered for many years in many laboratories. The problems under study are not restricted to those identified a priori; experimental and theoretical attention is shifted as needed as the program progresses.

The program involves both theoretical and experimental investigation of the nucleation and growth mechanisms of heteroepitaxial films in semiconductor-insulator systems. The theoretical studies consist of two types of activity: (1) direct interaction with the experimental program involving data analyses, suggestion of definitive experiments, and postulation of specific models to explain experimental observations, and (2) development of original contributions to the theory of heteroepitaxial growth, with the goal of generating significant advances in fundamental epitaxy theory.

The experimental investigations are also of two types: (1) fundamental explorations to delineate mechanisms and general empirical principles of the heteroepitaxial growth process, and (2) practical studies that accompany the fundamental investigations so that any new developments can be immediately applied to the improvement of semiconductor films and thin-film devices on insulating substrates.

The work has emphasized the CVD method of growing semiconductor thin films because of its importance in the semiconductor industry. Specifically, the program emphasis is on films of Si and GaAs and substrates of sapphire ($A\ell_2O_3$) and spinel ($MgA\ell_2O_4$). The initial emphasis has been on the Si-on-$A\ell_2O_3$ system, with increasing attention being given to the Si-on-$MgA\ell_2O_4$ and GaAs-on-$A\ell_2O_3$ systems. Si and GaAs have been chosen because of the preeminence of the former in the semiconductor industry and the high-frequency and high-temperature attributes of the latter.

The program is carried on primarily at the facilities of the North American Rockwell (NR) Electronics Group in Anaheim. Parts of three of the subtasks have been performed by personnel of the University of California at Los Angeles (UCLA), in the Department of Electrical Sciences and Engineering, and by personnel of the California State University, San Diego (CSUSD), by means of subcontracts from NR.

The accomplishments of the contract program to date are summarized by subtask as follows.

1. SUBTASK 1. THEORY OF EPITAXY AND HETEROEPITAXIAL INTERFACES

During the first year a formal theoretical method of replacing overgrowth atoms on a substrate with Gaussian mass distributions was further developed for those cases where the effective interatomic potential is known. The technique, applicable to irregular-shaped islands or films of finite extent, was applied to a simplified model to determine preferred orientation relationships from calculated film-substrate interaction energies. The method was not pursued further, however, because it was not sufficiently adaptable to real systems. Several other possible approaches to the theoretical modeling of heteroepitaxial systems were critically reviewed, including the Frank-Van der Merwe model, a Green's function/Wannier-function approach, a contrived potential-energy model, and the two-body interatomic potential method. It was concluded that the existing theories are inadequate for application to real systems such as those of interest in this program.

The feasibility of a molecular orbital development of the heteroepitaxial interface was then investigated. However, it was determined infeasible to apply this technique in a manner directly relevant to heteroepitaxy, so the effort was terminated. The interatomic potential approach to heteroepitaxy was then reinstigated, with the goal being the computer simulation of growth of Si on $A\ell_2O_3$. Mechanical stability conditions for an $A\ell_2O_3$ lattice modeled with two-body potentials were investigated and determined to the depth required for the application. Computer programming of the $A\ell_2O_3$ lattice energy and elastic constants was begun for use in determining appropriate empirical potentials required for modeling the $A\ell_2O_3$ lattice, a major requirement for modeling Si growth on $A\ell_2O_3$. In addition, the application of the electron-on-network theory to the problem of determining surface configurations and interfacial binding energies in heteroepitaxial systems where the surface structure is allowed to relax was investigated, and for a time it appeared promising for the real systems of interest.

In the second half of the second year the theoretical studies were devoted to three main areas: (1) modeling of the Si/$A\ell_2O_3$ system by means of interatomic potentials and computer simulation; (2) use of the electron-on-network technique to calculate work functions and surface double-layer potentials of monovalent metals

(although this method has not been pursued further for application to heteroepitaxial systems because of severe limitations encountered in the preliminary studies); and (3) calculations relating the mobility of Si films on Al_2O_3 to stress effects arising at the heteroepitaxial interface and caused by differential thermal contraction of film and substrate. The modeling of the Al_2O_3 lattice was carried out in terms of Morse potentials; only anion-anion and cation-anion potentials were employed. These were chosen to conform to specific constraints related to the physical lattice. Investigation of surface reconstruction in basal-plane Al_2O_3 was also initiated, using these potentials, since this phenomenon plays a major role in predicting Si film orientations on Al_2O_3. Relaxation of the four atomic planes nearest the surface was treated for the case of a surface composed of oxygen atoms with the constraints of translational symmetry in the surface and three-fold rotational symmetry normal to the surface. Programming of the case of an Al atom surface was also begun, with the same symmetry constraints being imposed. (This aspect of the theoretical studies has not been further pursued in the past six months, however.)

The theoretically calculated changes in mibility and resistivity in the plane of the film in the Si/Al_2O_3 system caused by thermally induced stresses and the piezoresistance effect were found in excellent agreement with experimental results. Theoretical formulas were developed for both Si and Ge and for Al_2O_3 and $MgAl_2O_4$ substrates and for a variety of crystallographic orientations. Detailed calculations were combined with experimental observations (Subtask 6) for the (001)Si/(0112) Al_2O_3 and (221) Si/(11$\bar{2}$2) Al_2O_3 systems, and investigation of the (111) Si/Al_2O_3 system began. These theoretical and experimental results have emerged as the most significant contribution of this contract program to date; the results are of major importance to the entire technology of heteroepitaxial semiconductor films and devices.

Theoretical studies in the past six months have concentrated exclusively on the mobility anisotropy in Si/Al_2O_3 and $Si/MgAl_2O_4$ hetero-systems. During this period the investigation of (221) Si/Al_2O_3 was completed and the results published, and the (001) Si investigation was also completed and has been accepted for publication in May of 1973. Considerable additional effort was devoted to the case of (111) Si growth on two different Al_2O_3 substrate orientations. Anisotropies calculated on the basis of thermal expansion stress were found to be too small to explain the experimental (111) Si results. Definitive resolution of this disparity has not yet been achieved. The possibility that residual growth stresses are responsible has been explored and represents a plausible but as yet unproven explanation. If found to be correct, this interpretation would add to the basic understanding of heteroepitaxial Si films. Extensive mobility anisotropy calculations have also been made for the general (XX1) Si orientation for four modes of Si/Al_2O_3 epitaxy and one mode of $Si/MgAl_2O_4$ epitaxy. These calculations encompass all the modes of major interest and include (001), (111), (221), and (110) Si orientations. A comprehensive description of the theoretical models developed, the mathematical formalism employed, and the numerical results obtained is in preparation for publication.

2. SUBTASK 2. DEPOSITION STUDIES AND FILM PREPARATION

During the first year of the program the emphasis on this subtask was placed on determining the effect of experimental growth parameters on the quality of Si epitaxial films grown by the CVD method of pyrolysis of SiH_4 on substrates of various orientations of Al_2O_3 and $MgAl_2O_4$. It was established for the growth system used that autodoping

occurs in Si on $A\ell_2O_3$ at temperatures greater than about 1050 C, so a concerted study was made which considered the effects of such factors as growth temperature, growth rate, and nucleation phenomena at or below this temperature. It was determined that the electrical properties of undoped n-type heteroepitaxial Si films grown on various orientations of $A\ell_2O_3$ (and also $MgA\ell_2O_4$) by the CVD method of pyrolysis of SiH_4 are dominated by surface-state conduction for carrier concentrations of $\sim 10^{16}$ cm^{-3} or below. Essentially equivalent (100)- and (111)-oriented Si films were grown on $(01\bar{1}2)$ and $(10\bar{1}4)$ $A\ell_2O_3$ substrates at deposition temperatures below the autodoping range (~1050 C). $A\ell_2O_3$ orientations near the $(11\bar{2}0)$ plane, not previously used in heteroepitaxy studies, were utilized as substrates for (111) Si heteroepitaxy; this resulted in electron mobilities of 600 to 700 $cm^2/V\text{-sec}$ for carrier concentrations of 10^{15} - 10^{17} cm^{-3}, exceeding mobilities obtained on either $(01\bar{1}2)$ or $(10\bar{1}4)$ $A\ell_2O_3$ substrates.

These studies revealed the strong interrelationships that exist among the various parameters involved in optimizing Si growth on insulators. Evaluation of the electrical properties of Si films on those $A\ell_2O_3$ orientations that produce the best Si overgrowths has demonstrated that growth conditions (1) must be optimized for the particular substrate orientation chosen; (2) differ for those $A\ell_2O_3$ orientations which lead to the same Si orientation; (3) are dependent upon reactor geometry and gaseous atmosphere; and (4) must be optimized for the particular film thickness desired. Studies of Si growth by SiH_4 pyrolysis at reduced pressures (1 to 10 torr) indicated that single-crystal growth can be obtained over a fairly wide temperature range, when conditions are optimized, on both $A\ell_2O_3$ and $MgA\ell_2O_4$ substrates; these results provided necessary confirmation of the feasibility of Si film growth in the pressure range to be used in the in situ CVD experiments in the electron microscope (Subtask 5). Investigation of the growth of Si films on $A\ell_2O_3$ and $MgA\ell_2O_4$ using He as the growth atmosphere and the carrier gas showed that epitaxial growth could be achieved, although the conditions for best growth were not established at that time.

The effort on this subtask in the final half of the second year was concentrated on continuing attempts to optimize the Si deposition process for growth on $\sim(11\bar{2}0)$ and $(01\bar{1}2)$ $A\ell_2O_3$ surfaces. In the course of this work the effects of post-nucleation annealing during the deposition process on ultimate film properties were examined, but no significant improvement in overall quality of Si films resulting from these procedures was demonstrated. The effects on film growth of gas-phase etching of $A\ell_2O_3$ surfaces prior to deposition were evaluated further; there is some indication that surface damage may not be the primary factor in determining the quality of Si over-growths, but this question must be examined in more detail. The effect of cooled reactor chamber walls on the Si growth process was investigated further, but no significant advantage of cooled walls in the vertical reactor systems used in this work has been observed.

Considerable additional study was made of the growth and properties of Si films on Czochralski-grown stoichiometric spinel ($MgA\ell_2O_4$). This work indicated that Si films with electrical properties at least as good as those grown on $A\ell_2O_3$ can be obtained when $He\text{-}H_2$ gas mixtures are used for the growth environment. It was also determined that autodoping is operative in the $Si/MgA\ell_2O_4$ system (in $He\text{-}H_2$ atmospheres) at approximately the same temperatures as for $Si/A\ell_2O_3$.

During the past six months the work of this subtask was concentrated on studies relating to the growth of Si on $MgA\ell_2O_4$ and to the support of other phases of the program by preparation of $Si/A\ell_2O_3$ and $GaAs/A\ell_2O_3$ films. These were prepared for

further studies in anisotropy, lifetime measurements, fabrication of Schottky-barrier FET structures, high-field transport measurements, and for the evaluation of new tanks and sources of SiH_4 and AsH_3. The Si/$MgAl_2O_4$ studies again indicated that good quality films could be grown on $MgAl_2O_4$ but that the Si growth conditions and film mobility are affected by the tank of SiH_4 in use.

3. SUBTASK 3. ANALYSIS AND PURIFICATION OF CVD REACTANTS

During the first year, techniques of gas chromatography were developed for analysis of the reactants used for semiconductor heteroepitaxy by CVD. A general-purpose gas-handling system was constructed for the highly volatile and reactive gases studied, with silicone oil and polymer columns used for the chromatography. Several extraneous impurity peaks were observed in the chromatograms of SiH_4 samples; diborane (B_2H_6) was tentatively identified as a significant impurity (~10 ppm), although not confirmed by mass spectrometer techniques. Small quantities of purified SiH_4, free of diborane, were prepared by successive injections in the chromatograph; quantities were too small, however, for use in laboratory CVD experiments.

Beginning in the second year of the program samples of SiH_4 and of trimethylgallium (TMG) used for Si and GaAs CVD experiments were analyzed for impurity content by sensitive mass spectrometric techniques. Disilane and trimethylsilane, together with several other impurities of less concern, were found in the SiH_4 samples. The analyses of TMG left some uncertainties regarding the correct impurity levels, although these were largely resolved by later analyses carried out in the final half of the second year.

Significant impurity concentrations in some of the reactants (especially SiH_4) have severely limited the accuracy of the study of the effects of deposition parameters on Si film properties on several occasions during the contract work. Cooperative efforts with vendors for preparation and analysis of improved-purity reactants have continued.

An important study of the chemistry and reaction kinetics of CVD processes used for growing Si and GaAs films in heteroepitaxial systems was initiated late in the second year at the California State University, San Diego (CSUSD). The first experiments undertaken were directed toward determining the role of the Al_2O_3 surface in catalyzing the pyrolysis of SiH_4; experiments with the trimethylgallium (TMG)-arsine (AsH_3) reaction used for GaAs growth were also begun.

During the past six months additional analyses of reactants have been made by mass spectrometer techniques, and the studies of CVD reaction kinetics have continued on both the Si and the GaAs reaction systems. Four different tanks of SiH_4 were analyzed by mass spectrometry for impurity content and evaluated by means of Si film growth on p-type Si substrates. Two of the tanks were found to be of high quality, producing Si films with $n \sim 10^{14}cm^{-3}$ and high mobility. Two tanks of AsH_3-in-He were similarly found to be of high purity, producing undoped GaAs films of low donor-impurity carrier concentration ($\sim 10^{14}cm^{-3}$).

The studies of the basic chemistry of formation of Si and of GaAs by CVD reactions have continued, using both flow and static pyrolysis systems. Initial experiments undertaken to determine the role of the Al_2O_3 surface in the pyrolytic decomposition of SiH_4 demonstrated that any catalysis by Al_2O_3 surfaces (or by SiO_2 or pyrex surfaces) rapidly disappears with the formation of a monolayer of Si on the surface. Subsequent experiments with improved (static pyrolysis) apparatus clearly demonstrated that Al_2O_3 does act as a catalyst in the decomposition of SiH_4 at moderate temperatures (~500 C) but leaves determination of the catalyst role at Si deposition temperatures yet

to be determined. Studies of the deposits of GaAs from trimethylgallium (TMG) and AsH_3 were also begun, with the decomposition modes of both TMG and AsH_3 being examined. Pyrolysis of TMG, AsH_3, and equimolar TMG-AsH_3 mixtures were carried out. TMG apparently does not decompose below 320 C; AsH_3 slowly decomposes at 150 C. The first apparent product of the TMG-AsH_3 reaction — $(CH_3\,GaAs\,H)_x$ — is apparently stable below 360 C. Further experiments on the stability of this compound at other temperatures are in progress, and additional studies of the decomposition of AsH_3 have also been initiated.

4. SUBTASK 4. PREPARATION AND CHARACTERIZATION OF SUBSTRATES

In the first year of the program it was demonstrated that $A\ell_2O_3$ surfaces prepared by mechanical polishing techniques and used routinely for semiconductor heteroepitaxy typically have severe surface and subsurface damage, with many scratches often several microns deep yet often rendered invisible to close inspection because of amorphous or fine-grained debris embedded in the scratches in the final polishing stages. Some improvement in mechanical polishing procedures was achieved in terms of the density and depth of such damage. Gas-phase etching/polishing procedures using SF_6 and various fluorinated halocarbons in the 1350 to 1500 C temperature range produced essentially scratch-free surfaces on $(01\bar{1}2)$ and near-$(11\bar{2}0)$ $A\ell_2O_3$ substrates. Extensive gas-phase etch-rate data were obtained as a function of crystallographic orientation in this temperature range.

During the first part of the second year a much improved technique for polishing $(10\bar{1}4)$ $A\ell_2O_3$ was developed, and very good surfaces in this orientation can now be obtained. Gas-phase etching/polishing techniques were further developed for (1) thinning $A\ell_2O_3$ substrates to thicknesses the order of 1 mil; (2) evaluating the effects of prolonged etching on $(01\bar{1}2)$, (0001), and ~$(11\bar{2}0)$ $A\ell_2O_3$; and (3) assessing the subsurface damage caused by various mechanical polishing procedures.

More recent work on this subtask has included verification of the polishing procedure for $(10\bar{1}4)$ $A\ell_2O_3$ as a reproducible process. Evaluation of polishing methods for $MgA\ell_2O_4$ surfaces has indicated that surface fill-in occurs for this material just as for $A\ell_2O_3$. Preliminary gas-phase etching experiments with $MgA\ell_2O_4$ surfaces were also carried out.

Ion-beam sputtering techniques have been under development for preparing ultrathin (~200Å) $A\ell_2O_3$ wafers for use as substrates in the in situ CVD experiments with Si (Subtask 5). Some wafers successfully thinned to ~0.002 in. by mechanical polishing techniques have been subsequently thinned by ion etching to the point of perforation in some areas, which results in adjoining regions of thicknesses suitable for transmission electron microscopy as applied in the in situ experiments. Typical thinning rates are 0.2 to 2.0 μm/hr. Three different $A\ell_2O_3$ orientations have been successfully thinned by this method — (0001), $(10\bar{1}4)$, and $(01\bar{1}2)$. Considerable study of properties of the resulting thinned substrates has been carried out.

The routine characterization of substrate surfaces at various stages of preparation has continued throughout the program to date, utilizing various standard techniques of X-ray and electron diffraction analysis and optical and electron (including scanning) microscopy.

During this reporting period additional $A\ell_2O_3$ substrates were prepared for epitaxial growth experiments by mechanical polishing techniques previously developed on this program. Additional effort was expended on attempts to prepare suitably thinned $A\ell_2O_3$ wafers for subsequent final thinning by the ion-beam sputtering technique; con-

siderable further improvement in the ion-thinning process for preparing substrates for the in situ CVD experiments in the electron microscope (Subtask 5) was achieved; and etch-rate experiments to determine the depth of damage in $A\ell_2O_3$ substrate wafers at various stages of the pre-deposition preparation process were begun. $A\ell_2O_3$ wafers 0.001-0.002 in. thick were produced by mechanical polishing, by chemical etching, and by a commercial vendor using an undisclosed mechanical polishing method, but the yield was very low in all three cases. Efforts to thin the $A\ell_2O_3$ chemically were marginally successful, but this work will continue. The thin wafers were further thinned by the ion-beam sputtering technique to ~500Å for use as CVD substrates, although the thickness uniformity was not further improved beyond that reported previously.

5. SUBTASK 5. STUDIES OF IN SITU FILM GROWTH IN THE ELECTRON MICROSCOPE

In the first year of the program many of the modifications required in the electron microscope for in situ observation of the nucleation and early-stage growth of CVD semiconductor films on insulating substrates were completed. Provision for motion-picture recording of film growth was assembled and tested, and the heated specimen stage was installed and tested. The first in situ PVD experiments were also carried out near the end of the first year.

During the first six months of the second year a series of electron microscope modifications and tests was completed, culminating in the first series of successful PVD experiments inside the electron microscope. Aℓ was deposited onto a heated carbon substrate and a sequence of micrographs taken during the growth process, demonstrating the feasibility of performing in situ nucleation and growth studies in the equipment. A transmission phosphor screen (for the motion picture camera) was installed, permitting motion picture photography which does not interfere with the normal still photography. The auxiliary vacuum pumping system for the specimen chamber was fabricated, installed, and tested. The basic vacuum system of the microscope itself was improved by addition of a cooled baffle, by polishing the O-ring grooves, and by thoroughly cleaning the microscope interior. A PVD source assembly was fabricated, installed, and used in conjunction with the specimen heater to perform the PVD experiments.

Calculations and design for the CVD microchamber were also completed, and the fabrication of the microchamber and the differential pumping apertures was begun. At the end of the second year a modified design of the CVD microchamber and associated hardware was developed and fabrication nearly completed. Numerous additional in situ PVD experiments were carried out, with both Aℓ and Au deposited onto amorphous carbon substrates to delineate further the required techniques and experimental problems to be encountered in the CVD experiments.

During the past six months, the fabrication of the CVD microchamber and its mounting flange has been completed. A gas handling manifold has been installed on the electron microscope and connected to the CVD flange. Focus tests of the microchamber and the gas-handling manifold were completed satisfactorily. Gas flow experiments were performed to determine the flow rate of gas through the microchamber as a function of pressure and to determine the maximum pressure attainable in the microchamber before the performance of the microscope becomes impeded by the pressure rise. Constructional details of the microchamber were described in a technical paper given during the report period.

Several in situ CVD experiments were performed, resulting in the successful growth of crystalline Si films on amorphous carbon substrates. It has now been demonstrated that the pyrolysis of SiH_4 to form crystalline Si films inside the electron microscope is feasible. Although the observations are preliminary in nature, several growth features have been observed, including an apparent incubation period and a growth morphology different from that of physically vapor deposited (PVD) films.

6. SUBTASK 6. EVALUATION OF FILM PROPERTIES

During the first year, the routine evaluation of film properties was carried out by established methods of X-ray and electron diffraction analysis, metallographic analysis, and electrical measurements of transport properties. In addition, a new technique for evaluating the characteristics of the interfacial region of heteroepitaxial films was developed, involving measurement of the photoelectron emission from monochromatically-illuminated films in the MIS configuration on insulating (viz., $A\ell_2O_3$) substrates. Relatively large photocurrents due to electron transport through thick (~10 mils) single-crystal $A\ell_2O_3$ substrates were measured as a function of photon energy. Photoelectric threshold energies, escape length (mean free path) of excited electrons, and band bending in the semiconductor film adjoining the interface were determined in the $Si/A\ell_2O_3$ and $GaAs/A\ell_2O_3$ systems. Determination of the energy spectrum of back-scattered proton or alpha-particle beams injected in channeling directions in heteroepitaxial semiconductor films was also investigated as a means of measuring the density and the location of structural defects in the films. Experiments indicated that Si/insulator films have less imperfect interfacial regions than do GaAs/insulator films. The best structures of those examined were found in (100) Si films on $(01\bar{1}2)$ $A\ell_2O_3$ substrates and in (111)Si films grown on near-$(11\bar{2}0)$ $A\ell_2O_3$ substrates.

In the first part of the second year the study of the effects of changes in deposition parameters on $Si/A\ell_2O_3$ film properties continued. Those studies provided considerable insight into the factors which most strongly influence film quality, so that identification of some of the conditions for optimized film growth on various $A\ell_2O_3$ orientations could be made. The importance of reactor geometry was recognized and demonstrated; the extent of $A\ell$ autodoping from the substrate was established and appropriate annealing procedures for minimizing the effects were determined. The use of previously unused $A\ell_2O_3$ substrate orientations (e.g., near the $(11\bar{2}0)$ plane) for Si growth led to epitaxial films as good as or better than those previously reported.

The measurements of photoemission of electrons from heteroepitaxial semiconductor films and of the transport of electrons in $A\ell_2O_3$ were carried further. Work functions of additional metals were determined, and the mechanism of electron transport through the insulator was studied further. Measurements of high-field transport properties of Si and GaAs heteroepitaxial films were also initiated.

The evaluation work in the final months of the second year included (1) study of the variation of the electrical properties of $Si/A\ell_2O_3$ with temperature, in which some effects attributed to high defect densities or inhomogeneous strains were observed; (2) the first stages of an extensive experimental study of the anisotropy of

the electrical properties in $Si/A\ell_2O_3$; (3) evaluation of the electrical properties of Si films on $MgA\ell_2O_4$, with evidence that n-type films with mobilities higher than those obtained in the $Si/A\ell_2O_3$ system can be obtained; (4) additional measurements of the electrical properties of $Si/A\ell_2O_3$ to establish parametric relationships among temperature, growth rate, and substrate orientation; (5) further study of the photoelectric effects observed in the $Si/A\ell_2O_3$ system, including verification that the observed phenomena do result from photoinjection of electrons from metal films into $A\ell_2O_3$, and determination of the work functions of additional metals and the heights of the metal-$A\ell_2O_3$ interface barriers; and (6) additional measurements of the high-field transport properties of heteroepitaxial films.

The anisotropy studies were concentrated in the $(221)Si/(11\bar{2}2)A\ell_2O_3$ and the $(100)Si/(01\bar{1}2)A\ell_2O_3$ systems. These two Si planes are basically different in that the anisotropy in the (221) plane can be expected for any Si heteroepitaxial system, while that in the (100) Si plane results from the anisotropic thermal contraction of $A\ell_2O_3$ and would not be present, e.g., in the $Si/MgA\ell_2O_4$ system. The mobility anisotropy factor A, defined as the ratio of the difference between the maximum and minimum values of carrier mobility in the plane of the film to the average value of the mobility in that plane, was found to be about 40 percent for the (221) plane and about 9 percent for the (100) plane. Results of calculations (Subtask 1) based on the the piezoresistance effect in Si resulting from the difference in the thermal expansion coefficients for Si and $A\ell_2O_3$ agreed well with the experimental data. The calculations and the experimental results also indicate that (221) Si probably exhibits higher electron mobilities than other more commonly used orientations.

In the past six months further experimental studies of anisotropy in the electrical properties of $(111)Si/A\ell_2O_3$ have been in progress, using both $(10\bar{1}4)$- and $\sim(11\bar{2}0)$-oriented $A\ell_2O_3$ substrates. The observed anisotropies have not agreed with the predictions of the piezoresistance model for this Si orientation, for reasons which have not yet been established (Subtask 1); anisotropies as high as 30 to 40 percent have been observed, with an average of about 16 percent, while the stress model predicts values the order of 6 percent. These discrepancies are still under investigation, because these anisotropy effects — largely explained by the stress model — are highly significant to the entire technology of heteroepitaxial semiconductor devices. Preliminary measurements of the variation in anisotropy in $(221)Si/(11\bar{2}2)A\ell_2O_3$ films as a function of film thickness indicates there is a trend for the anisotropy effects to be larger for thinner films; further study is required to establish this, however.

During this same period the electrical evaluation of (111)Si films on $MgA\ell_2O_4$ has continued, with some evidence that the mobility decreases much more rapidly with film thickness (for thicknesses less than ~0.5μm) than it does in the $Si/A\ell_2O_3$ system. This indicates a need for a comparative study of the early stages of film growth in the two systems to assist in identifying the preferred substrate material for Si heteroepitaxial devices. The experimentally observed inhomogeneity in the donor concentration in a CVD $Si/A\ell_2O_3$ film from point to point over the film area has been investigated; there is evidence that a concentration gradient exists from the center of the susceptor radially outward, so that films will reflect this variation depending upon the placement of the substrate on the susceptor during the CVD growth. Gas flow characteristics or a non-uniform temperature of the rf-heated pedestal (susceptor) may account for the effect; investigations are continuing.

In other evaluation work, additional measurements have been made of the high-field transport characteristics of Si and GaAs films on Al_2O_3; although contact problems have continued to be troublesome, high-field data have been obtained (including some at 77K) with good consistency among the samples measured. The continuing study of photoelectric properties of Al_2O_3-based systems has concentrated on attempting to determine the nature of the dependence of the photoinjected current upon the condition and method of preparation of the Al_2O_3 surface.

7. SUBTASK 7. DESIGN AND FABRICATION OF DEVICES

In the first year of the contract apparatus for determining minority carrier lifetime by pulsed C-V measurement in MOS structures was designed and constructed and tests were begun. A special MOS structure was designed for measurement of channel conductance, high- and low-field transport properties, and various interface characteristics of heteroepitaxial films. Initial attempts to fabricate Schottky-barrier diodes in Si/Al_2O_3 films as a means of evaluating their electrical properties were not successful.

In the first half of the second year the preliminary design of a Schottky-barrier type of FET was completed for use in fabricating experimental FET structures in GaAs/insulator films for operation at 1 GHz. Preliminary results on carrier lifetime in Si/Al_2O_3 films were obtained, after initial development of the measurement technique on bulk single-crystal Si samples was completed and after impurity contamination problems encountered in the oxide growth process were solved.

During the second six months of the second year the device-oriented effort centered about the determination of carrier lifetimes using the MOS pulsed C-V technique and attempts to fabricate a Schottky-barrier FET in $GaAs/Al_2O_3$. Numerous processing difficulties were encountered in both of these investigations. An analysis was made to evaluate the effect of the impurity redistribution in the Si in the region near the oxide interface (resulting from the oxidation process used for making the MOS structures) on the interpretation of lifetime data obtained by this technique.

Lifetime measurements in both Si and GaAs films as a function of film thickness, carrier concentration, and crystallographic orientation have now been obtained on numerous samples, with thicknesses ranging from ~1 to ~10μm and resistivities from ~0.01 to ~1 ohm-cm. Analysis of the data for Si films has indicated lifetime values ranging from 9×10^{-12} to $\sim 5 \times 10^{-10}$ sec. Attempts are being made to find correlations between carrier lifetime and film resistivity and thickness, but no such correlations have yet been detected. Similar measurements on GaAs films on Al_2O_3 are now being carried out.

Recent device efforts have produced Schottky-barrier diodes (in n-type Si/Al_2O_3 samples) having good reverse but unsatisfactory forward characteristics; further improvements are being sought. The Schottky-barrier FET structures are still not satisfactory, with further work still in progress. Preliminary work on fabricating and evaluating Schottky-barrier photovoltic cells has begun, and work is about to begin on fabrication and test of charge-coupled devices in Si/Al_2O_3 composites.

REFERENCES

1. R. P. Ruth, "Fundamental Studies of Semiconductor Heteroepitaxy," First Semiannual Report, 28 January 1971, ARPA Order No. 1585, Contraet No. DAAH01-70-C-1311. Prepared by North Ameriean Rockwell, Autoneties Division, Anaheim, CA, for USAMICOM, Redstone Arsenal, AL.

2. R. P. Ruth, "Fundamental Studies of Semiconduetor Heteroepitaxy," Seeond Semiannual Report, July 1971, ARPA Order No. 1585, Contraet No. DAAH01-70-C-1311. Prepared by North American Rockwell, Autoneties Division, Anaheim, CA, for USAMICOM, Redstone Arsenal, AL.

3. R. P. Ruth, "Fundamental Studies of Semieonductor Heteroepitaxy," Third Semiannual Report, January 1972, ARPA Order No. 1585, Contract No. DAAH01-70-C-1311. Prepared by North Ameriean Roekwell Eleetronics Group, Research and Technology Division, Anaheim, CA, for USAMICOM, Redstone Arsenal, AL.

4. R. P. Ruth, A. J. Hughes, J. L. Kenty, H. M. Manasevit, and A. C. Thorsen, "Fundamental Studies of Semieonduetor Heteroepitaxy," Fourth Semiannual Report, July 1972, ARPA Order No. 1585, Contract No. DAAH01-70-C-1311. Prepared by North Ameriean Roekwell Eleetronics Group, Researeh and Technology Division, Anaheim, CA, for USAMICOM, Redstone Arsenal, AL.

5. A. C. Thorsen and A. J. Hughes, Appl. Phys. Lett. 21, 579 (1972).

6. A. J. Hughes and A. C. Thorsen, J. Appl. Phys. (to be published May 1973).

7. H. M. Manasevit, R. L. Nolder, and L. A. Moudy, Trans. Met. Soe. of AIME 242, 465 (1966).

8. J. L. Kenty, in 30th Ann. Proc. Eleetron Mieroseopy Soe. Amer., C. J. Arceneaux, ed. (Los Angeles, CA, 1972), p. 624.

9. D. K. Schroder and H. C. Nathanson, Solid-State Eleetronics 13, 577 (1970).

APPENDIX A†

ANISOTROPY IN THE ELECTRICAL PROPERTIES OF $\{001\}Si/\{01\bar{1}2\}A\ell_2O_3$*

A. J. Hughes and A. C. Thorsen
North American Rockwell Corporation
3370 Miraloma Avenue
Anaheim, California 92803

ABSTRACT

A detailed investigation of the Hall mobility has been carried out on a series of ~2μm thick n-type $\{001\}Si/\{01\bar{1}2\}A\ell_2O_3$ films. A specially designed Hall bridge pattern has been used to obtain independent measurements of mobility as a function of current direction in the plane of the film. The data show an anisotropy in the mobility of approximately 9%, with a maximum in mobility occurring along the <100> Si direction that is parallel to the $<2\bar{1}\bar{1}0>$ $A\ell_2O_3$ direction in the plane of the substrate. This behavior is found to be a consequence, through the piezoresistance effect, of the anisotropic thermal contraction of $A\ell_2O_3$ on cooling from the deposition temperature, which leads to an anisotropic thermally induced stress in the Si.

---

* Supported in part by ARPA under Order 1585, monitored by USAMICOM, Redstone Arsenal, AL, under contract DAAH01-70-C-1311

† See Reference 6, p. 75/76.

INTRODUCTION

The Hall mobility in epitaxial semiconductor films is usually considered to be a good criterion of film quality and has been used extensively in the optimization of the film growth process. It is therefore important that the properties of the film be homogeneous and uniform over the plane of the film if a realistic electrical parameter is to be deduced from a particular measurement. In most cases, it is tacitly assumed that the mobility is isotropic in the plane of the film and does not depend upon the direction in which the measurement is made. We present results in this paper of a detailed investigation of the electrical properties of n-type $\{001\}Si/\{01\bar{1}2\}Al_2O_3$ and show that for this system an assumption of isotropy is not justified.[1] The mobility is found to vary with current direction in the plane of the film and has a maximum value along the particular <100>Si direction that is parallel to the $<2\bar{1}\bar{1}0>Al_2O_3$ direction in the plane of the substrate.

The experimental anisotropy in mobility reported in this paper will be explained theoretically in terms of the piezoresistance effect and anisotropic substrate-induced thermal stresses. While we believe this to be the principal mechanism behind the observed mobility anisotropy, phenomena associated with surface electric fields and surface quantization can often play a role in current conduction in some other measurement or device situations.

Surface quantization and surface transport in semiconductor inversion and accumulation layers are reviewed briefly by Stern[2] and a number of recent references are listed. Sato et al [3] have investigated the mobility anisotropy of carriers in p-type and in n-type inversion layers on oxidized Si surfaces in MOSFET device configurations. These references compare field-

effect mobilities in each of two perpendicular orientations for a number of different surface plane orientations. For some orientations, sizable anisotropies were reported. However, for the (001)Si orientation, the field-effect mobility is isotropic because of symmetry considerations.

The work of Sato et al relates specifically to bulk Si and therefore did not consider any effects of substrate induced stresses on the mobility. If there were a surface perturbation in the electrical conductivity of heteroepitaxial (001)Si/$A\ell_2O_3$ films, induced by surface charge and/or oxide layer impurities and taking the form of an accumulation or inversion layer, the resulting surface component of mobility would also be isotropic, except for the fact that there is an anisotropy in the film stresses. The mobility of a surface layer would therefore exhibit a small anisotropic effect which would be similar in relative magnitude to that found in bulk Si under similarly stressed conditions. It is unlikely therefore, that a small component of surface conductivity could contribute substantially to the total mobility anisotropy that would be measured in (001)Si/$A\ell_2O_3$ films.

The mobility anisotropy to be discussed in the present paper is believed not to be associated with either surface quantization or self-accumulation or inversion effects. There is no applied electric field normal to the surface and the oxide film formed during the after-growth annealing sequence is removed prior to the measurement of film properties. In addition, the high donor concentrations in the films tend to mask contributions to the electrical conduction from surface effects. To numerically assess the magnitude of any possible surface effects present under these conditions, however, would require the measurement of electrical properties in a MOS device configuration, and this has not been done in this work.

Collectively, the above arguments form the basis for our assumption that the mobility anisotropy reported here is a bulk effect and is primarily to substrate-induced thermal stresses acting through the piezoresistance effect. The agreement between theory and experiment lends confidence to this interpretation.

THEORY

In order to explain the experimental observations discussed below, we have examined theoretically the effect of stress in the Si film on the electron transport properties of the film. As is well known, transport properties such as resistivity and mobility can be related to applied stresses through the piezoresistance effect. Numerous studies of the piezoresistance effect in bulk Si have been reported in the literature over a number of years. Much less attention has been paid to stress and its effect on the transport properties of epitaxial films.

Stress in Si films on sapphire (Al_2O_3) has been examined by Dumin[4], and in Si films on spinel substrates both by Schlötterer[5] and by Robinson and Dumin[6]. Schlötterer presents formulae for the fractional change in resistivity ($\Delta\rho/\rho_o$) in terms of piezoresistance coefficients π_{11}, π_{12}, π_{44} and an assumed isotropic stress σ_f in the Si film due to differential thermal contraction between film and substrate. Since he was dealing with spinel substrates, it was assumed that the thermal stress and the induced changes in resistivity were isotropic in the plane of the film. In this section of the present paper, we treat the anisotropy in stress and piezoresistivity and present formulae which are applicable to the anisotropic case.

Before presenting the theoretical results obtained, we will briefly sketch the method. A more detailed theoretical discussion will be given elsewhere[7]. The theoretical determination of the effect of thermally induced stresses on film resistivity and mobility can be divided into three parts: (1) calculation of the piezoresistance effect in terms of stresses; (2) calculation of these stresses in terms of the various

coefficients of thermal expansion; and (3) successive transformations of film and substrate coordinate systems to achieve the proper relative crystallographic orientation and to include anisotropy in the plane of the Si film.

The resistivity and stress are related through the equation[8] $E_i = \rho_{ij} J_j + \pi_{ijkl} J_j T_{kl}$, where E is the electric field, J the current density, ρ the zero-stress resistivity tensor, T the stress tensor and π the piezoresistance tensor. For cubic crystals such as Si, ρ_{ij} is both diagonal and isotropic and equal to $\rho_o \delta_{ij}$, where ρ_o is the zero-stress resistivity. This tensor equation is commonly contracted to a single-subscript notation for ρ and T and to a double-subscript notation for π[8]. In this notation, T can be written as a 6-component column vector and π as a 6 x 6 matrix. Referred to the Si crystal axes, π has only three independent coefficients π_{11}, π_{12}, and π_{44}; however, all 36 π coefficients may be non-zero when referred to a cartesian coordinate system having an arbitrary orientation with respect to the Si crystal axes.

We first consider the so-called longitudinal piezoresistance effect for the case in which there is only one component of current (J_1), and the field (E_1) is in the direction of the current flow. Then $(E_1/J_1) = \rho_o(1+\pi_{1k}T_k)$, where ρ_o is the zero-stress Si resistivity and k is summed from 1 to 6. Defining (E_1/J_1) as ρ_1, the longitudinal piezoresistance is then given by

$$\frac{\Delta\rho_1}{\rho_o} = \frac{\rho_1 - \rho_o}{\rho_o} = \left(\frac{E_1}{J_1\rho_o} - 1\right) = \pi_{1k}T_k. \qquad (1)$$

The longitudinal piezoresistance effect can thus be calculated if the π coefficients and the Si film stresses T_k are known. For a cartesian coordinate system with axes along the Si crystal axes, the π_{1k} are particularly simple and the sum involves only $\pi_{11} T_1 + \pi_{12} (T_2 + T_3)$. For an arbitrary orientation of axes, which is of primary interest to us here, "rotated" π coefficients are given by Pfann and Thurston[9]. These transformed π coefficients are given in terms of the direction cosines of the arbitrary coordinate system with respect to the Si crystal axes. The determination of π coefficients appropriate to an arbitrary coordinate system is straightforward but is laborious.

We next consider the determination of stresses in the Si film for the case of (001)Si on $(01\bar{1}2)Al_2O_3$. A state of compressive stress arises in the Si film due to the relative thermal contraction of the Si and the Al_2O_3 substrate. In order to calculate this stress, we consider the case of a thin film on a relatively (say 100-150 times) thicker substrate so that bending of the composite can be neglected, and assume that the strain induced in the Si is proportional to the difference in thermal contraction between the two materials. In addition, the thermal contraction is assumed to take place over a temperature range from room temperature to the growth temperature[10].

The cartesian coordinate system employed is defined as follows. The z axis is normal to the surface of the Si film and thus is $\perp$(001) Si and also $\perp (01\bar{1}2)$ Al_2O_3. The x and y axes are in the plane of the film with x || [100] Si and || $[2\bar{1}\bar{1}0]$ Al_2O_3. The y axis is || [010] Si and || $[01\bar{1}\bar{1}]Al_2O_3$.

The six stresses T_1, T_2, T_3, T_4, T_5, T_6 ($=T_{xx}$, T_{yy}, T_{zz}, T_{yz}, T_{xz}, T_{xy}, respectively) completely define the stress in the Si film. The stresses T_3, T_4, and T_5 are zero at the free surface of the Si film and if we further assume that the film is thin enough that all stresses are uniform in the z direction, then $T_3 = T_4 = T_5$ are zero everywhere in the film. T_6 is in general non-zero but for the relative orientation of film and substrate under consideration is identically zero. Thus only T_1 and T_2 are non-zero. Denoting the elastic constants of Si by C_{ij} and the stiffness coefficients by S_{ij}, we find the following implicit relations for the stresses T_1 and T_2:

$$\frac{T_1 + T_2}{2} = \frac{C_{11}^2 + C_{11} C_{12} - 2C_{12}^2}{2C_{11}} \left[1.287\,(\alpha_s - \alpha_1) + 0.713\,(\alpha_s - \alpha_2)\right] \Delta T$$

$$= \frac{1}{2\,(S_{11} + S_{12})} \left[1.287\,(\alpha_s - \alpha_1) + 0.713\,(\alpha_s - \alpha_2)\right] \Delta T\,, \tag{2}$$

and

$$\frac{T_1 - T_2}{2} = -0.713\,\frac{C_{11} - C_{12}}{2}\,(\alpha_1 - \alpha_2)\,\Delta T$$

$$= -0.713\,\frac{S_{11}}{2\,(S_{11} - S_{12})(S_{11} + 2S_{12})}\,(\alpha_1 - \alpha_2)\,\Delta T\,. \tag{3}$$

Here α_s is the (isotropic) Si thermal expansion coefficient and α_1 and α_2 are thermal expansion coefficients for the $A\ell_2O_3$ substrate, perpendicular to the c-axis of $A\ell_2O_3$ and parallel to the c-axis of $A\ell_2O_3$, respectively. ΔT is the temperature difference between growth and room temperatures and in Eqs. (2) and (3) is understood to be a positive number. In the limit

$\alpha_1 = \alpha_2$, T_1 and T_2 are equal, and Eq. (2) reduces to that given by Schlötterer[5]. The thermal stresses in the Si film due to the substrate and required for calculation of the piezoresistance effect have now been obtained.

We next return to the longitudinal piezoresistance effect and to Eq. (1). The stresses calculated above relate to the coordinate system and parallel Si/$A\ell_2O_3$ relations given. Using the results of Ref. 9 the π_{1k} coefficients in Eq. (1) are then transformed to the same coordinate systems used for the stress. The piezoresistance $(\Delta\rho'_1/\rho_o)$ thus obtained represents the change in resistivity due to stress for a current J_1 and field E_1 in the x direction || [100]Si. We are, however, interested in the piezoresistance as a function of angle in the plane of the film. A second transformation on both the π's and the stresses is then performed which represents a rotation about the z axis. The angle θ of this rotation is measured from the x axis and is positive toward the y axis. The longitudinal piezoresistance effect corresponding to current flow at an angle θ from the [100]Si direction then becomes

$$\frac{\Delta\rho_1}{\rho_o} = \left(\frac{E_1}{J_1\rho_o} - 1\right) = \left(\frac{T_1 + T_2}{2}\right)(\pi_{11} + \pi_{12}) + \left(\frac{T_1 - T_2}{2}\right)(\pi_{11} - \pi_{12}) \cos 2\theta, \quad (4)$$

where T_1 and T_2 are given in Eqs. (2) and (3). To avoid ambiguity in orientation, we repeat that the angle θ is measured from that <100> Si direction in the plane of the film that is parallel to the $<2\bar{1}\bar{1}0>A\ell_2O_3$ direction in the planeof the substrate. Note that the term depending on θ, which determines the amount of orientational anisotropy in resistivity and mobility, also depends

directly on $(\alpha_1 - \alpha_2)$. That is, the anisotropy in piezoresistance in the (001) Si plane depends directly on the anisotropy in thermal expansion coefficients of the $A\ell_2O_3$ substrate. Using $\alpha_s = 3.9 \times 10^{-6}/°C$[5], $\alpha_1 = 8.31 \times 10^{-6}/°C$, $\alpha_2 = 9.03 \times 10^{-6}/°C$[11], $\Delta T = 1100°C$, and the known elastic constants of Si[12], Eqs. (2) and (3) yield stresses of

$$\left.\begin{aligned} \frac{T_1 + T_2}{2} &= -0.9206 \times 10^{10} \text{ dynes/cm}^2 \text{ and} \\ \frac{T_1 - T_2}{2} &= +0.2852 \times 10^{9} \text{ dynes/cm}^2. \end{aligned}\right\} \qquad (5)$$

Substituting values of piezoresistance coefficients for n-type Si from Smith[13,14], Eq. (4) becomes

$$\frac{\Delta\rho_1}{\rho_o} = 0.44192 - 0.04449 \cos 2\theta. \qquad (6)$$

Since the mobility μ can be related to the resistivity ρ_1 by $\mu = R_H/\rho_1$, where R_H = the Hall constant, the theoretical anisotropy in mobility can be written

$$(\mu/\mu_o) = \frac{1}{1 + (\Delta\rho_1/\rho_o)} = [1.44192 - 0.04449 \cos 2\theta]^{-1}, \qquad (7)$$

where μ_o is the zero-stress mobility.
From Eq. (7), we note that the mobility will be a maximum along the [100]Si direction and will be a minimum 90° away along the [010] Si direction.

The amount of anisotropy can be described conveniently by a parameter A which we define as $A \equiv (\mu_{max} - \mu_{min})/\mu_A$, where $\mu_A \equiv (\mu_{max} + \mu_{min})/2$ is an

approximate average mobility in the plane[15]. The predicted mobility anisotropy is found to be A = 6.2% and the average mobility is found to be $\mu_A = 0.694\mu_o$. Thus we find a 6.2% anisotropy in mobility superimposed on a substantial 30% overall theoretical reduction in mobility for n-type Si.

The theory also predicts a transverse piezoresistance effect corresponding to an electric field (E_2) in the plane of the film and orthogonal to the current (J_1) direction. This transverse piezoresistance effect is also found to depend upon orientation and is given by

$$(E_2/J_1\rho_o) = -\left(\frac{T_1 - T_2}{2}\right)(\pi_{11} - \pi_{12}) \sin 2\theta = +0.04449 \sin 2\theta, \quad (8)$$

and is zero along the [100]Si direction and is of maximum magnitude along the [010]Si direction. The sign convention employed here is that E_2 is positive if $\bar{J}_1 \times \bar{E}_2$ is out of the plane of the film and is thus in the plus-z direction.

The transverse piezoresistance ($E_3/J_1\rho_o$) associated with a field E_3 normal to the Si film has also been examined and for (001)Si on $(01\bar{1}2)Al_2O_3$ is found to be identically zero.

Although the results described above were obtained explicitly for n-type Si, the formalism is also valid for p-type Si providing that appropriate values for the π coefficients are used. The quantity $(\pi_{11}-\pi_{12})$, which is important for the anisotropic effect, is found to be approximately a factor of twenty less for p-type Si. As a result, little anisotropy would be expected in the Si orientation under discussion, although other orientations can in general show pronounced effects.

EXPERIMENTAL

The films used for this study were grown by chemical vapor deposition techniques in two different reactor systems. One of these is a vertical system[16] and the other is a horizontal system. In both cases, the films were formed from the thermal decomposition of silane (SiH_4), with H_2 used as a carrier gas. Intentional doping to concentrations of $1\text{-}6 \times 10^{16} cm^{-3}$ was achieved with the use of arsine (AsH_3). Growth temperatures ranged from 955C in the horizontal system to 1075C in the vertical system, and film thicknesses varied from 1.5 to 1.8μm.

After growth the samples were annealed at 1100C in O_2 for 30 minutes followed by a N_2 anneal for 2 hours at 1100C in order to stabilize film properties and electrically neutralize any Aℓ impurities in the film[17]. The resulting oxide film was removed prior to making electrical measurements.

Measurements of resistivity and Hall effect were made on each film using a specially designed Hall bridge pattern etched in the epitaxial layers. This pattern, shown in Fig. 1, consists of two wheel-shaped bridges. The five arms of a single bridge are separated by 72 degrees from each other, and the arms of one bridge are rotated by 18 degrees with respect to those of the other bridge. This allows an independent measurement of electrical properties (Hall coefficient and resistivity) every 18 degrees in the plane of the film.

Electrical data were taken on eight samples of {001} Si/{01$\bar{1}$2} $Aℓ_2O_3$. For every sample, the orientation of each leg of the Hall pattern was determined with respect to one of the Si directions of the form <100> in the plane of the film. This was accomplished by obtaining a Laue back-reflection x-ray pattern for each substrate and from this locating a <2$\bar{1}\bar{1}$0> $Aℓ_2O_3$ direction in the plane of the substrate that is parallel to a <100> Si direction in the film plane. The mobility in each leg can then be plotted versus the angle θ between the current direction and that particular <1$\bar{0}\bar{0}$> Si axis. Typical room temperature mobility data from two samples are shown plotted in Fig. 2. The mobility

can be seen to vary with angle and appears to approach a maximum at $\Theta \approx 0$ degrees and a minimum at $\Theta \approx 90°$. This is consistent with the behavior predicted by Eq.(7) and suggests that the theoretical form of the mobility could be used to fit the experimental results.

The theory leading to Eq.(7) predicts that the mobility anisotropy should be of the form

$$(\mu/\mu_0) = [a - b \cos 2\Theta]^{-1} \tag{9}$$

where a and b are constants. Eq.(9) cannot be employed directly in analyzing the experimental results in that the zero-stress mobility μ_0 is not known and would be expected to be a function of growth conditions and to vary slightly from sample to sample or run to run. Accordingly, we have fitted the experimental results by the method of least squares to a theoretical curve of the form

$$\mu = [a' - b' \cos 2\Theta]^{-1}. \tag{10}$$

The numerical curves thus determined are shown by the two solid curves in Fig. 2 for two samples. The anisotropy parameter A is independent of μ_0 and is equal to $2b/a = 2b'/a'$.

The electrical data taken on the eight samples of $\{001\}Si/\{01\bar{1}2\}Al_2O_3$ were all fitted by least squares and analyzed in terms of Eq.(10). The maximum mobility (μ_{max}), minimum mobility (μ_{min}), average mobility (μ_A) and anisotropy parameter A were calculated. These four quantities are tabulated in Table I for the samples measured. It can be seen that the anisotropy A varies from approximately 7.6% to 11.7% with an average value of 9.5%.

The scatter in the mobility data, as evidenced by the results shown in Figure 2, is probably due primarily to inhomogeneities in film properties over the surface of the film For example, carrier concentrations measured on the separate areas of the Hall pattern on a given film are found to vary an average of ±7%. Even though these differences are taken into account in calculating the mobility in each arm of the bridge, slight errors may be introduced since the spatial extent over which the resistivity is measured is much larger than that over which the Hall constant (carrier concentration) is measured. (See configuration of bridge in Figure 1.)

The RMS error (in percent) between the experimental points and the fitted theoretical curve for each sample is shown in Table I. The error in all cases is sufficiently small compared with the anisotropy to indicate that the fit and hence the correlation between theory and experiment is statistically significant.

Measurements were taken at 77K on two selected samples and these results are also tabulated in Table I. Representative data for one sample are shown in Fig. 3 . The parameters deduced from the curve-fitting procedure for this data are also shown in Table I. The anisotropy A is found to increase in going from room temperature to 77K by roughly a factor of three for those samples measured. Correlation of this increase in anisotropy with theory would require information on the variation of the Si piezoresistance coefficients π_{11} and π_{12} with temperature. Data for π_{11} as a function of temperature is available in the literature[18] and indicates π_{11} increases by a factor close to three in going from room temperature to 77K. Data on π_{12} as a function of temperature does not appear to be available; however, it is not unreasonable to assume that the temperature dependence of both coefficients is the same. If this is the case, then the experimental increase in anisotropy at low temperature is consistent with theory.

The last column in Table I lists values of μ_o, the zero-stress mobility. As mentioned earlier, μ_o cannot directly be determined from experimental data but must be obtained from a combination of theory and experiment. The relationship between zero-stress mobility μ_o and the average mobility μ_A may be written as [15]

$$\mu_o = \mu_A \left(\frac{a^2 - b^2}{a} \right) = \mu_A \, a. \tag{11}$$

We then assume that Eq. (7) holds and that a = 1.44192. The values of μ_o thus determined are given in the last column of Table I and range from a high of 717 to a low of 584 with an average of 636.

The rather low value of μ_o compared with bulk mobilities in Si (>1000 $cm^2/V\text{-sec}$ at these carrier concentrations) should be noted and strongly suggests that a considerable mobility reduction results in these films from causes other than thermal stress.

We next consider the transverse piezoresistance effect described in Eq. (8). We have attempted to measure the transverse piezoresistance voltage appearing across appropriate terminals of the Hall bridge. However, the small size of the voltage makes this determination extremely difficult. The voltage is measured across the same terminals as the Hall voltage, with no magnetic field. As a consequence, any misalignment in the terminals would result in an "offset" voltage which would tend to mask the transverse voltage and introduce errors. In addition, inhomogeneities in bridge arm thickness and width also introduce some ambiguity.

Notwithstanding the above difficulties, some experimental transverse-effect data have been obtained. In obtaining these data, the sense of the transverse voltage must be properly accounted for since Eq. (8) predicts a negative voltage over some range of angles. The sign convention employed is that the transverse field is taken positive if the current direction crossed into the transverse field yields a vector out of the plane of the film.

Representative data on one sample taken at 300K are shown in Fig. 4. A least-squares fit of this data to a sin 2θ term as suggested by Eq. (8) is shown by the solid curve in Fig. 4. The resulting coefficient of the sin 2θ term is approximately equal to 0.08, which is larger than predicted from Eq. (8); however, the fit of the experimental points is not good. The value of ρ_o used in Eq. (8) is the value of ρ_o determined from the longitudinal mobility measurements described above.

The transverse voltage also becomes substantially larger at 77K, and low temperature data are also plotted in Fig. 4. The magnitude of the increase is a factor of between 2 and 3, similar to the increase found for the longitudinal effect. Note that the least-squares fit to a theoretical sin 2θ term is much better at 77K than at 300K, due probably to the larger signal.

SUMMARY AND CONCLUSIONS

Detailed studies of the electrical properties of {001} Si/{01$\bar{1}$2} Al_2O_3 have shown the existence of a significant anisotropy in mobility. This anisotropy can be accounted for through the piezoresistance effect in terms of a simple model of thermally induced stress taking into account the difference in thermal expansion coefficients of Al_2O_3 parallel and perpendicular to the c-axis. Both longitudinal and transverse piezoresistance effects were considered and theoretical formulae developed which account for the anisotropic effects.

The theory for the longitudinal piezoresistance effect predicts an anisotropy in mobility of about 6.2% and for the transverse piezoresistance effect predicts a sin 2θ anisotropy coefficient of about 0.044 for the normalized transverse electric field. The value of each of these quantities is strongly dependent upon the data used for the thermal expansion of Al_2O_3. Recent measurements[19] at this laboratory using a differential technique have given a difference in thermal expansion coefficients $(\alpha_1 - \alpha_2)$ of $(-1.08 \pm 0.12) \times 10^{-6}/°C$ for the Al_2O_3 substrate. Using this value for $(\alpha_1 - \alpha_2)$ leads to a predicted mobility anisotropy of 9.3%[20] and a transverse electric field anisotropy factor of 0.067 which are in good agreement with the experimental results.

A few concluding points suggested by our investigation of the electrical properties of {001} Si/{01$\bar{1}$2} Al_2O_3 should be mentioned. The first is simply that the anisotropy in mobility reported here must be taken into account in the evaluation and/or optimization of film growth processes. Previous practice has apparently been to ignore the orientation of current flow in the plane of the film, and thus mobility data for various {001} Si films could possess a built-in ≈10% scatter due to this anisotropy. Such scatter renders the task of definitively evaluating changes in film growth processes somewhat difficult.

Secondly, for some Si film applications in which the mobility is important it would be desirable to orient the current flow (along the <100> Si direction || <2$\bar{1}\bar{1}$0>Al_2O_3 direction) to obtain the maximum mobility.

The third and final point concerns the interpretation of the origin of the mechanisms determining mobility in these heteroepitaxial films. The excellent agreement between theory and experiment for the mobility anisotropy suggests that the anisotropy can be substantially accounted for in terms of thermal stresses induced by the Al_2O_3 substrate.

In principle, residual growth stresses in the Si due to lattice mismatch and effects of dislocation distributions in the films could also lead to anisotropies in carrier mobility. Our results, however, indicate that the anisotropy can be adequately explained without recourse to these effects. On the other hand, the rather low average value ($\simeq$636 cm^2/V-sec) deduced for the zero-stress mobility μ_o from analysis of the theoretical and experimental data indicates that thermally induced stress is not the dominant mechanism in lowering the overall average film mobility from bulk Si values. Thus, defect structures, such as dislocations, would appear to play an important role in determining heteroepitaxial Si film mobilities.

At any rate, these studies of mobility anisotropy have yielded more detailed information than has previously been available from studies of mobility. This also suggests that additional detailed investigations, which examine the variation of anisotropy with film thickness, growth conditions and temperature, may well prove valuable in better understanding and improving Si/Al_2O_3 films.

ACKNOWLEDGMENTS

The authors wish to thank H. M. Manasevit, F. M. Erdmann and R. Harada for providing the samples used for this study, J. P. Wendt for carrying out the electrical measurements, R. E. Johnson for performing the photolithographic processing, and R. P. Ruth for a critical review of the manuscript.

REFERENCES

1. Similar but larger anisotropic effects have also been observed in the $(221)Si/(11\bar{2}2)A\ell_2O_3$ system and are reported by A. C. Thorsen and A. J. Hughes, Appl. Phys. Letters 21, 579 (1972).
2. F. Stern, J. Vac. Sci. Tech. 9, 752 (1972).
3. H. Sato, Y. Takeishi, and H. Hara, Jap. J. Appl. Phys. 8, 588 (1969); Phys. Rev. B4, 1950 (1971).
4. D. J. Dumin, J. Appl. Phys. 36, 2700 (1965).
5. H. Schlötterer, Sol. St. Elect. 11, 947 (1968).
6. P. H. Robinson and D. J. Dumin, J. Electrochem. Soc. 115, 75 (1968).
7. A. J. Hughes (unpublished).
8. W. P. Mason and R. N. Thurston, J. Acoust. Soc. Amer. 29, 1096 (1957).
9. W. G. Pfann and R. N. Thurston, J. Appl. Phys. 32, 2008 (1961).
10. This procedure may overestimate the elastic stress at room temperature since it ignores plastic relaxation and generation of dislocations. On the other hand, the basic piezoresistance formula, Eq. (1), which is linear in the stress may, for large stresses, tend to underestimate the effect of stress on resistivity. For example, Schlötterer(5) included a term quadratic in the stress to calculate piezoresistivity in his isotropic calculations. Arguments for a numerical correction term of this nature have not been explored adequately and we believe inclusion of such a term would be largely illusory. For definiteness, we have therefore employed the model described above.
11. J. B. Austin, J. Am. Ceram. Soc. 14, 795 (1931).
12. R. F. S. Hearmon, Landolt-Börnstein Numerical Data and Functional Relationships in Science and Technology, New Series, edited by K. H. Hellwege (Springer-Verlag, New York, 1969), Vol. III/2, p. 3. The values of elastic constants employed in the text were $C_{11} = 16.5\times10^{11}$, $C_{12} = 6.4\times10^{11}$ and $C_{44} = 7.93\times10^{11}$ dynes/cm^2.

13. C. S. Smith, Phys. Rev. 94, 42 (1954).

14. The values of piezoresistance coefficients employed in the text for n-type Si were $\pi_{11} = -102\times10^{12}$, $\pi_{12} = +54\times10^{12}$, and $\pi_{44} = -14\times10^{12}$ cm^2/dyne. The assumption implicit here is that the bulk piezoresistance coefficients can be employed for these ~2μm-thick Si films. This is reasonable for this application but may be incorrect for narrow channel FET devices in which carrier quantization and altered piezoresistance coefficients would both have to be considered.

15. For a mobility variation of the form $(\mu/\mu_o) = (a + b\cos 2\theta)^{-1}$, it can be shown that the true rotational average value is $(\bar{\mu}/\mu_o) = (a^2 - b^2)^{-1/2}$, compared with $(\mu_A/\mu_o) = a/(a^2 - b^2)$. For the numerical parameters of Eq. (7), these two averages are identical to three significant figures.

16. H. M. Manasevit, D. H. Forbes, and I. B. Cadoff, Trans. AIME 236, 275 (1966).

17. E. C. Ross and G. Warfield, J. Appl. Phys. 40, 2339 (1969).

18. O. N. Tufte and E. L. Stelzer, Phys. Rev. 133, A1705 (1964); F. J. Morin, T. H. Geballe, and C. Herring, Phys. Rev. 105, 525 (1957).

19. S. B. Austerman (private communication).

20. In view of the approximations in the theoretical model, such close agreement for the mobility anisotropy between theory (9.3% for $(\alpha_1 - \alpha_2) = -1.08\times10^{-6}$/°C) and the average experimental value (9.5%) is fortuitous.

FIGURE CAPTIONS

FIGURE 1. Specially designed Hall-bridge pattern permitting an independent measurement of electrical properties every 18 degrees in the plane of the film.

FIGURE 2. Typical room temperature mobility data for two (001) Si/(01$\bar{1}$2) Al_2O_3 samples. The solid curves are least-squares theoretical fits to the experimental points. The maximum mobility is at $\theta = 0°$ and is along the [100] Si direction and the minimum is at $\theta = 90°$ along the [010] Si direction.

FIGURE 3. Low temperature (77K) mobility data for one (001)Si/(01$\bar{1}$2)Al_2O_3 sample and corresponding least-squares theoretical curve.

FIGURE 4. Plots of the normalized transverse field ($E_2/J_1\rho_o$) for one sample at 77K and at 300K. The transverse field E_2 is at right angles to the current flow J_1 and both are in the plane of the film. The least-squares theoretical fits to the data are shown as the solid curves.

TABLE I Anisotropy Data for $\{001\}Si/\{01\bar{1}2\}Al_2O_3$

Room Temperature Data

Sample	μ_{max}	μ_{min}	μ_A	A (%)	RMS Error (%)	μ_o
102	446	408	427	8.9	1.6	615
18-1	432	397	415	8.6	1.4	598
15	472	425	449	10.5	2.5	648
3412-3	513	472	493	8.2	1.9	711
3411-1	516	478	497	7.6	2.1	717
18-2	422	387	405	8.6	2.5	584
31	451	401	426	11.6	2.2	614
13	443	394	419	11.7	2.9	604
(average)	(462)	(420)	(441)	(9.5)		(636)

Liquid N_2 Temperature (77K) Data

18-1	1014	797	906	24	5.7	1305
31	1063	832	948	24	7.0	1367

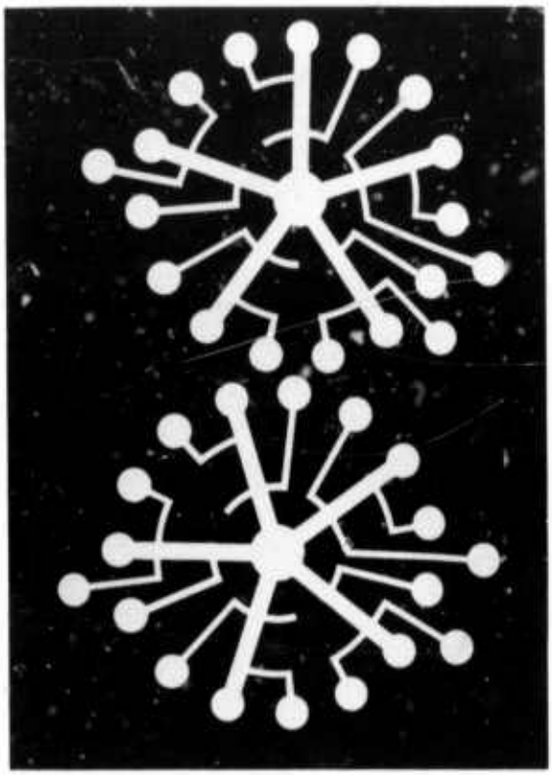

Figure 1

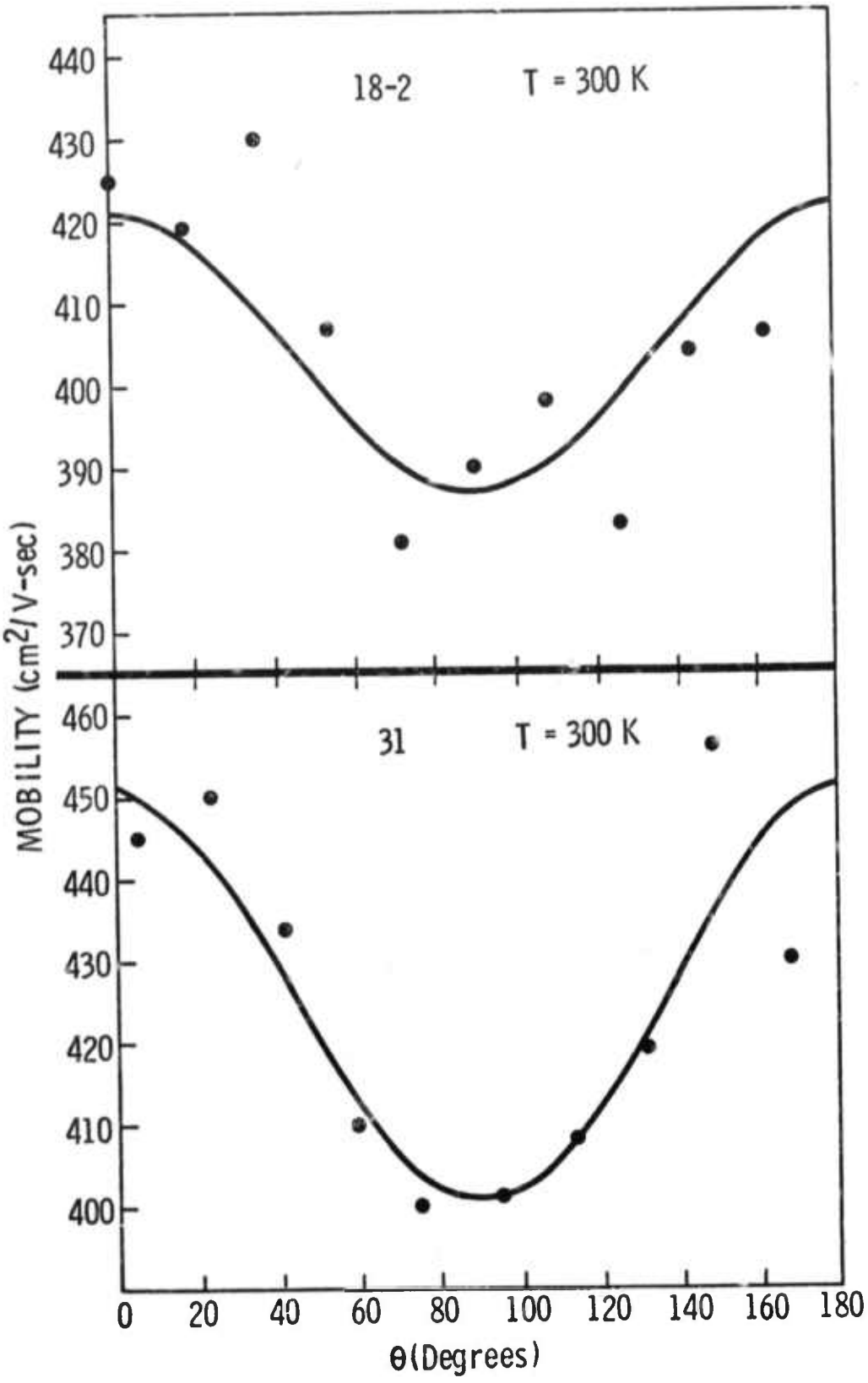
18-2
T = 300 K
31
T = 300 K
MOBILITY (cm²/V-sec)
440
430
420
410
400
390
380
370
460
450
440
430
420
410
400
0
20
40
60
80
100
120
140
160
180
θ(Degrees)

Figure 2

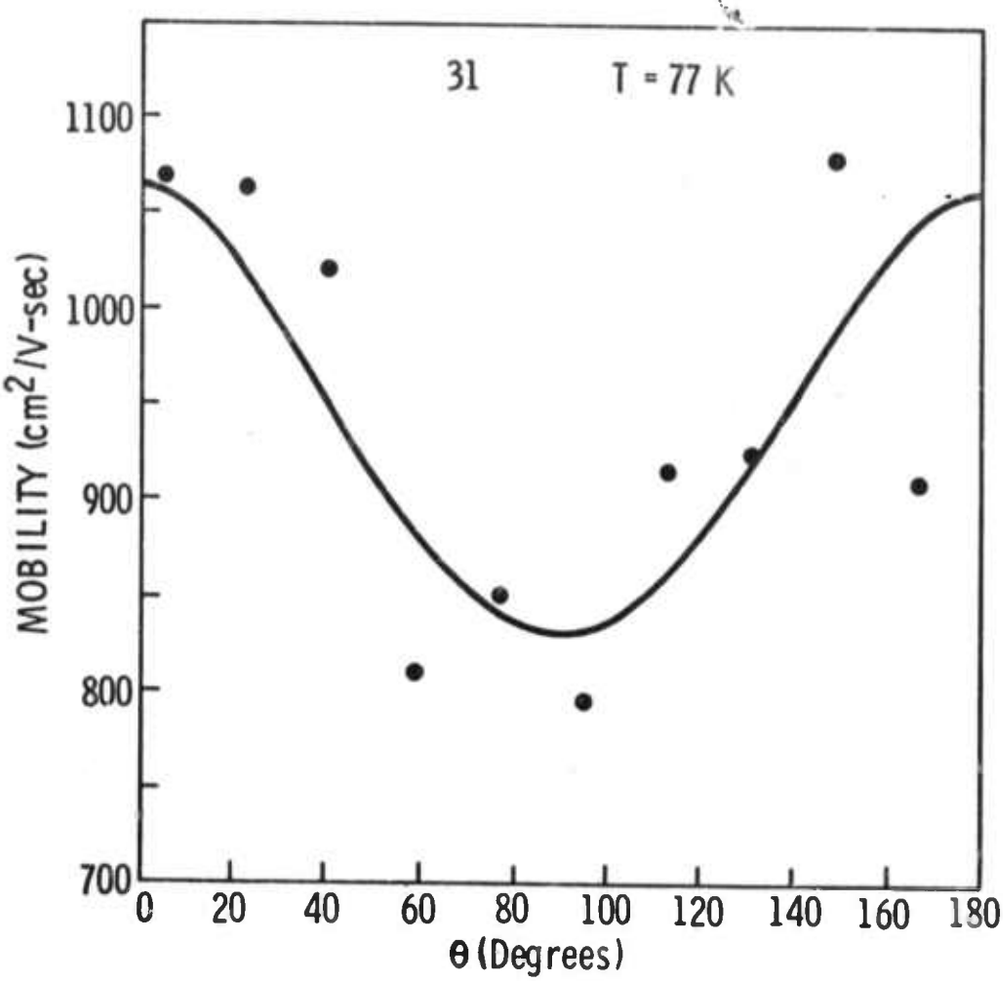
31
T = 77 K
1100
1000
900
800
700
MOBILITY (cm²/V-sec)
0
20
40
60
80
100
120
140
160
180
θ (Degrees)

Figure 3

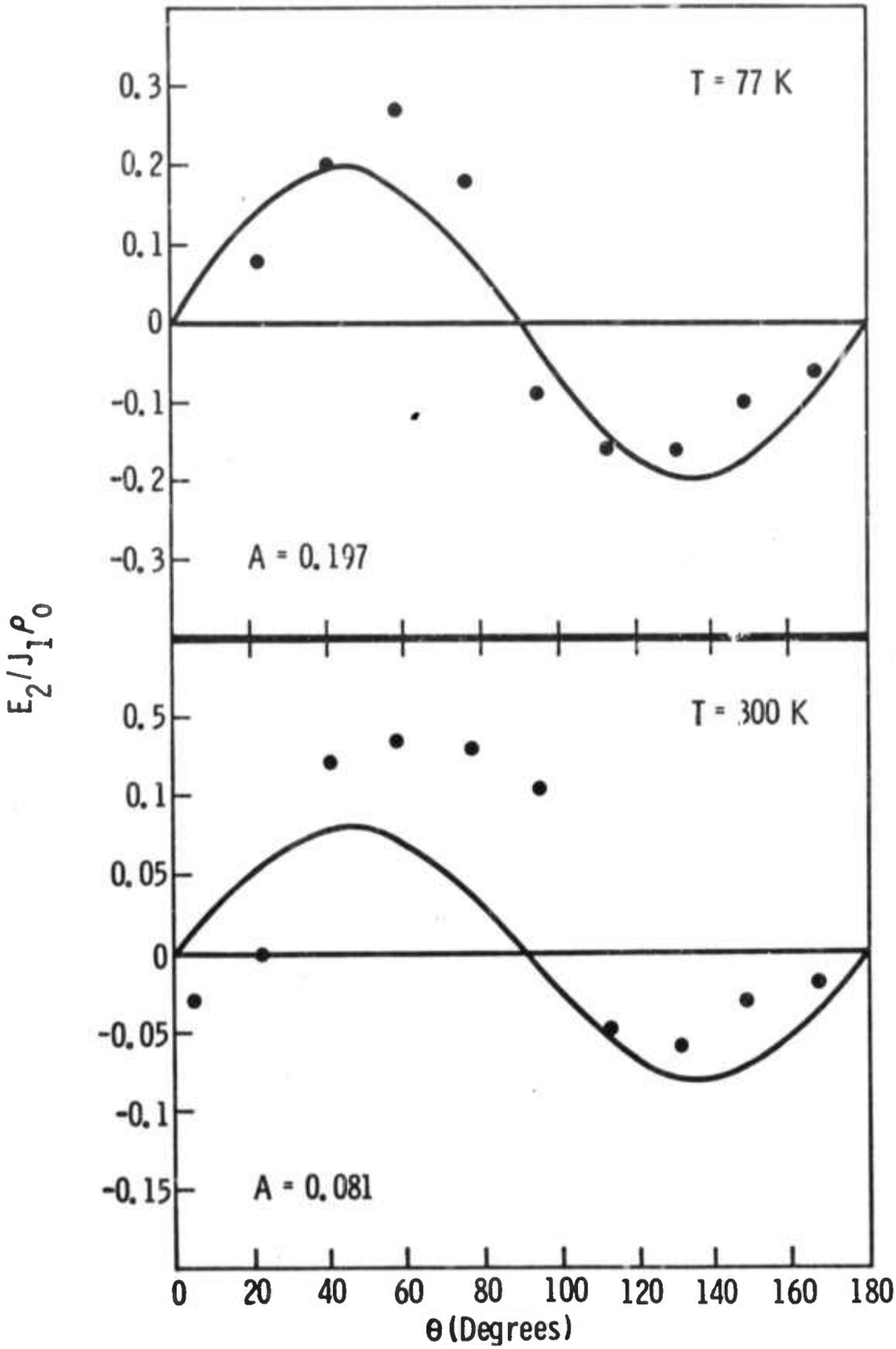
T = 77 K
A = 0.197
T = 300 K
A = 0.081
$E_2/J_1\rho_0$
θ (Degrees)
0.3
0.2
0.1
0
-0.1
-0.2
-0.3
0.5
0.1
0.05
0
-0.05
-0.1
-0.15
0
20
40
60
80
100
120
140
160
180

Figure 4

APPENDIX B †

Reprinted from:
"30th Ann. Proc. Electron Microscopy Soc. Amer."
Los Angeles, Calif., 1972. C. J. Arceneaux (ed.).

PRELIMINARY EM6 MODIFICATIONS FOR IN SITU CHEMICAL VAPOR DEPOSITION*

J. L. Kenty

North American Rockwell Corporation, Electronics Group, Anaheim, CA 92803

An AEI EM6 electron microscope is being modified for in situ chemical vapor deposition. The objective is to observe the nucleation and growth kinetics and structure of silicon deposited by SiH_4 gas pyrolysis on substrates of sapphire (single crystal α-$A\ell_2O_3$).

An Edwards DCB2 thermoelectrically cooled baffle has been installed using a simple adapter which permitted attachment without drilling or cutting of the EM6 frame or vacuum system. Prior to installation the measured contamination rate was 240Å/min; afterward the contamination rate was less than 100Å/min.

An auxiliary pumping system is mounted to the left rear of the column and attached by a special stainless steel flexible bellows to the pumping port at the rear of the specimen chamber. The auxiliary system has an ultimate presure $<1 \times 10^{-6}$ torr, but the measured pressure in the specimen chamber was no better than 1×10^{-5} torr, due primarily to the high outgassing rate of the beam deflector coil immediately above the specimen chamber. Future modifications planned include completion of the differential pumping system by addition of an impedance tube between the specimen chamber and beam deflector stage and a permanent aperture between the specimen chamber and objective lens.

The bottom of the plate camera has been modified to accept a transmission phosphor screen of aluminized P-11 phosphor material. A 16 mm motion picture camera has been mounted directly below this screen so that sequences of in situ growth may be photographed. Normal operation of the microscope is not affected.

A CVD microchamber, Figure 1, has been constructed which sits in the objective lens at the normal 4 mm focal length position. A new center post, brazed into the extensively modified base of a standard AEI specimen holder, acts as one electrode. The center post contains a 100μm dia. hole which serves as a gas limiting aperture. An outer cylindrical electrode is fastened by screws to a fired lava insulator, which is similarly fastened to the base. A gas-tight seal is obtained by lapping the insulator, base, and outer electrode base flat. Once assembled, the outer electrode need not be disassembled to load the specimen. A removable disc containing a 100μm dia. aperture is held tightly in place by a threaded cap. The specimen is held between two resistively heated 200-mesh stainless steel grids attached to the electrodes by two #80 NM screws. The holder is inverted for loading, permitting the specimen and removable aperture to be aligned with the fixed aperture. Gas is admitted to the microchamber through a flexible nickel bellows, flows through the annular space between the electrodes, and exhausts through the apertures. The space between apertures is 2 mm, which at a SiH_4 pressure of 2.9 torr corresponds to a mass thickness of 0.55 $\mu g/cm^2$, giving a 10% intensity loss assuming $\sigma = 2.5 \times 10^{-18} cm^2$.

---

*This research sponsored by ARPA under Order 1585, monitored by USAMICOM, Redstone Arsenal, AL, under Contract DAAH01-70-C-1311.

† See Reference 8, p. 75/76.

Reprinted from:
"30th Ann. Proc. Electron Microscopy Soc. Amer."
Los Angeles, Calif., 1972. C. J. Arceneaux (ed.).

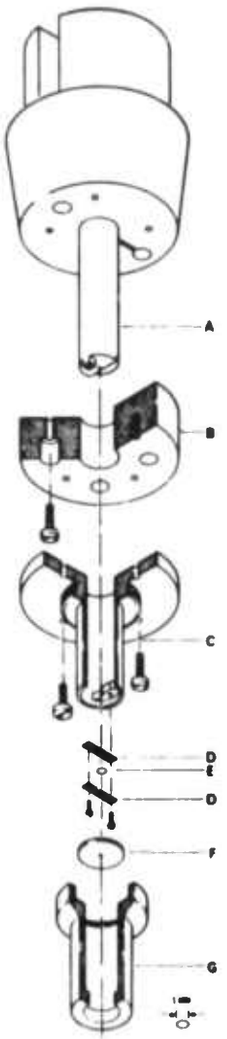

Figure 1. In Situ Chemical Vapor Deposition Microchamber. A, center electrode and gas limiting aperture; B, lava insulator; C, outer electrode; D, heating grids; E, sample; F, removable aperture; G, aperture cap.